NPS ARCHIVE
1969
HUNT, J.

TEMPERATURE DEPENDENCE OF THE ELECTRON SPIN RESONANCE SPECTRUM OF THE $CH_2CO_2^-$ RADICAL FORMED IN X-IRRADIATED ZINC ACETATE DIHYDRATE

by

John Woodrow Hunt

DUDLEY KNOX LIBRARY
NAVAL POSTGRADUATE SCHOOL
MONTEREY, CA 93943-5101

United States Naval Postgraduate School

THESIS

TEMPERATURE DEPENDENCE OF THE ELECTRON SPIN RESONANCE SPECTRUM OF THE $CH_2CO_2^-$ RADICAL FORMED IN X-IRRADIATED ZINC ACETATE DIHYDRATE

by

John Woodrow Hunt

June 1969

This document has been approved for public release and sale; its distribution is unlimited.

LIBRARY
NAVAL POSTGRADUATE SCHOOL
MONTEREY, CALIF. 93940

DUDLEY KNOX LIBRARY
NAVAL POSTGRADUATE SCHOOL
MONTEREY, CA 93943-5101

Temperature Dependence of the Electron Spin Resonance Spectrum of the $CH_2CO_2^-$ Radical Formed in X-Irradiated Zinc Acetate Dihydrate

by

John Woodrow Hunt
Major, United States Army
B. ChE., University of Florida, 1960

Submitted in partial fulfillment of the
requirements for the degree of

MASTER OF SCIENCE IN CHEMISTRY

from the

NAVAL POSTGRADUATE SCHOOL
June 1969

NPS ARCHIVE
1969
HUNT,J

THESIS
H945
c.1

ABSTRACT

A decrease of one to six gauss (depending on magnetic field orientation) in the coupling constants of the $CH_2CO_2^-$ radical formed in X-irradiated zinc acetate dihydrate has been observed over a temperature range of about -60°C to +30°C. Calculations of dipolar and Fermi contact interaction based on a model of internal rotation of the methylene group about the C-C bond have shown a small coupling constant decrease on the order of 0.19 gauss over a temperature range of -150°C to +90°C. The major effect has been shown to be due to a spin relaxation mechanism. The effect was calculated using Monte Carlo techniques, the results of which were confirmed by experimental data.

LIBRARY
NAVAL POSTGRADUATE SCHOOL
MONTEREY, CALIF. 93940

TABLE OF CONTENTS

I. INTRODUCTION---------- 11

II. BACKGROUND OF THE $CH_2CO_2^-$ RADICAL---------- 14

III. PROBLEM FORMULATION---------- 21

A. ROTATION OF THE METHYLENE GROUP---------- 24

1. The Restricted Rotor Model---------- 24

2. The Harmonic Oscillator Model---------- 26

3. Evaluation of Coupling Constants as a Function of Temperature---------- 28

a. Evaluation of A_ϕ, ---------- 30

(1) Subroutine HDCOS---------- 32

(2) Subroutine AXROT---------- 32

(3) Subroutine AXR---------- 33

(4) Subroutine REFH---------- 33

b. Evaluation of P_ϕ, and $\langle A \rangle_T$---------- 34

(1) Angular Dependence of Wave Functions---------- 34

(2) Temperature Dependence--------- 39

(3) Determination of $\langle A \rangle_T$---------- 40

B. HYPERCONJUGATION EFFECT ON COUPLING CONSTANTS 41

C. FLAP VIBRATIONAL MOTION---------- 43

D. SPIN RELAXATION EFFECT---------- 45

1. General Relaxation Theory---------- 45

2. Application of Relaxation Theory-------- 46

3. Calculation of Limiting Conditions------ 48

4. Calculation of Intermediate Conditions-- 49

5. The Monte Carlo Calculation---------- 52
6. Probability as a Function of Temperature 56
7. Fourier Representation of the Spectra--- 57
IV. EXPERIMENTAL PROCEDURES---------- 59
A. CRYSTAL GROWTH---------- 59
B. CRYSTAL IRRADIATION---------- 59
C. CRYSTAL ALIGNMENT---------- 60
D. THE ESR SPECTROMETER AND TEMPERATURE CONTROL UNIT---------- 62
V. RESULTS OF PROBLEM SOLUTION---------- 64
A. VERIFICATION OF SHIFT IN COUPLING CONSTANTS WITH TEMPERATURE---------- 64
B. MODEL DEVELOPMENT---------- 75
C. COUPLING CONSTANT SHIFT DUE TO DIPOLAR INTERACTION---------- 81
1. Test One for Proper Rotation---------- 83
2. Test Two for Proper Rotation---------- 84
D. COUPLING CONSTANT SHIFT DUE TO FERMI CONTACT INTERACTION---------- 88
E. COUPLING CONSTANT SHIFT DUE TO FLAP MOTION-- 95
F. COUPLING CONSTANT SHIFT DUE TO RELAXATION EFFECTS---------- 98
VI. CONCLUSION---------- 112
APPENDIX A---------- 115
APPENDIX B---------- 127
BIBLIOGRAPHY---------- 132
INITIAL DISTRIBUTION LIST---------- 134
FORM DD 1473---------- 135

LIST OF TABLES

Table		Page
I.	Experimental data----------	67
II.	Total coupling constant shifts observed experimentally----------	76
III.	Eigenvalues of the restricted rotor model------	78
IV.	Eigenvalues of the restricted rotor and the harmonic oscillator models----------	80
V.	Energy level populations in the harmonic oscillator model----------	81
VI.	Calculated coupling constant shift over temperature range of -150°C to +90°C due to dipolar coupling----------	85
VII.	Calculated hyperconjugation effect (Fermi contact interaction) on coupling constant shift----------	91
VIII.	Results of molecular orbital calculations for flap vibrational motion----------	96
IX.	Comparison of overall calculated coupling constant shift with experimentally observed shift----------	100
X.	Results of Monte Carlo calculations correlated to temperature----------	106

LIST OF FIGURES

Figure		Page
1.	Characteristic esr spectra at high and at low temperature----------	15
2.	Coalescence of absorption lines of esr spectra with increase of temperature----------	16
3.	The zinc acetate dihydrate crystal and the orthogonal crystal axis system (xyz or a*bc) and its relationship to the crystalline axis system (abc)----------	17
4.	Locations of the hyperfine axes in the $CH_2CO_2^-$ radical (planar configuration)----------	19
5.	Splitting of energy levels in a magnetic field due to electron and nuclei (H_1 and H_2) interaction for the $CH_2CO_2^-$ radical----------	22
6.	Comparison of restricted rotor and harmonic oscillator wave functions----------	37
7a.	CH_2 orbital configuration in the planar form of the $CH_2CO_2^-$ radical----------	42
7b.	CH_2 orbital configuration after rotation of the CH_2 group through angle ϕ' showing orbital overlap or mixing----------	42
8.	Out-of-plane flapping motion of the CH_2 group in the $CH_2CO_2^-$ radical----------	44
9.	Representation of the magnetic moments of nuclei H_1 and H_2 flipping from precession about one effective magnetic field to another due to rotation of the CH_2 group---------	47
10.	Pictorial representation of the trace of the magnetic moment of a proton as it flips from precession about effective field $\vec{h}_1$ to $\vec{h}_2$, back and forth----------	51
11a.	A decaying cosine function representative of the x component of magnetic moment----------	53
11b.	The Fourier transform of Figure 11a----------	53

12. Single crystal of zinc acetate dihydrate mounted on a quartz rod with the b axis coincident with the axis of the rod---------- 61

13. Characteristic experimental spectra---------- 65

14. Experimental results of the coupling constant dependence on temperature for selected magnetic field orientations---------- 71

15. Calculated coupling constants due to dipolar interaction as a function of ϕ'---------- 87

16. Results of molecular orbital calculation for Fermi contact (hyperconjugation) interaction compared to $f_{(\phi')} = A\sin^2 2\phi'$-------- 89

17. Dependence of coupling constants on temperature due to dipolar and hyperconjugation effects calculated---------- 93

18. Calculated dependence of coupling constants on temperature due to dipolar and hyperconjugation effects compared to experimentally observed temperature dependence---------- 94

19. Relative energy of the $CH_2CO_2^-$ radical at configurations caused by CH_2 group out-of-plane flapping motion---------- 97

20. Comparison of total coupling constant shift calculated with that observed experimentally---------- 102

21. Relative frequency as a function of correlation time---------- 104

22. Relative frequency as a function of temperature---------- 107

23. Comparison of calculated dependence of coupling constants upon temperature due to relaxation effects with experimentally observed dependence---------- 108

ACKNOWLEDGMENTS

The author expresses his sincere appreciation to Dr. William M. Tolles of the Naval Postgraduate School, Monterey, California, for his suggestion of and for his interest and assistance in this research project. In addition, appreciation is expressed to Mr. Robert Sanders of the Naval Postgraduate School for his invaluable assistance in technical problems.

I. INTRODUCTION

Study of the election spin resonance (esr) spectrum of single crystals damage by radiation have led researchers to the identification and structure of a number of paramagnetic species [Refs. 8, 11, 15, 13, 21, and 22]. Radicals may be generated by irradiation of single crystals at nearly any temperature where the crystal remains intact. However, irradiation at one temperature will not necessarily produce the same radical or combination of radicals as that at another temperature. Hence, by selection of the appropriate temperature, it is possible to selectively study several radicals which may be generated in the same system.

A considerably lesser amount of research has been done concerning the temperature dependence of the observed esr spectra for given paramagnetic species. Crawford [Ref. 4], in his study of the zinc acetate dihydrate crystal and the paramagnetic species, $CH_2CO_2^-$, formed therein, noted a marked temperature effect in the sum of the coupling constants. The effect ranged from a one to six gauss change (for an average coupling constant of about 45 gauss) over a temperature range of 298°K to 133°K depending on the external magnetic field orientation. Moss [Ref. 14] calculated the temperature effect in the esr spectrum of methyl radicals by attributing the effect to out-of-plane vibrations. However, he was unable to account for the magnitude of temperature coefficient by applying his method to the benzene anion. In a study of the

hydrazine positive ion, $N_2H_4^+$, Falle [Ref. 7] observed an increase in the ratio of nitrogen hyperfine splitting to proton hyperfine splitting, $|a_n/a_h|$, with increase in temperature. The effect was attributed primarily to a decrease in the proton hyperfine splitting, a_h, as caused by torsional (rotational) displacement of an amino group about the N-N bond. This torsional motion causes an introduction of positive spin density at the protons leading to an increase in proton hyperfine coupling, a_h, with increased torsional motion as experienced with increasing temperature. Schrader [Ref. 17] has theoretically (based on the procedure of Schrader and Karplus [Ref. 18]) predicted the coupling constants for the methyl radical over a wide range of temperature from zero to 500 degrees Kelvin, and has assigned temperature coefficients thusly which are in good agreement with Moss' results [Ref. 14]. Zlochower, Miller, and Fraenkel [Ref. 23] also applied the theory of Schrader and Karplus [Ref. 18] to the methyl radical and observed experimentally a dependence of the proton hyperfine splitting with temperature on the order of 0.002 gauss/degree in a 50°C range extending above and below room temperature. Work done on the isotropic proton hyperfine interaction in the esr study of π-electron free radicals has shown that out-of-plane vibrations should have a contribution to the splitting as a result of direct overlap between the proton and the unpaired electron in the π orbital [Refs. 13 and 14]. This contribution would be expected to increase with

increasing temperature leading to a corresponding decrease in the coupling constants with increasing temperature.

Crawford [Ref. 4] gave no detailed explanation of the marked shift in coupling constants observed for the $CH_2CO_2^-$ radical of zinc acetate. It becomes the dual purpose of this work to verify the effect observed and then to develop a model by which the phenomena may be explained.

II. BACKGROUND OF THE $CH_2CO_2^-$ RADICAL

Tolles, Crawford, and Valenti [Ref. 21] have recently published work on the epr (esr) study of zinc acetate dihydrate single crystals. Almost simultaneously, Ohigashi and Kurita [Ref. 15] published a similar work.

Both groups of authors have identified the $CH_2CO_2^-$ radical to exist in X-irradiated single crystals of zinc acetate. The radical is stable for hours at room temperature with a half life of about ten minutes at 80°C. Figure 1 shows typical esr spectra generated by the irradiated zinc acetate system. Coalescence of the typical four absorption line spectrum observed at low temperatures into the typical 1:2:1 three line spectrum at high temperatures as indicated in Figure 2 is evidence of internal rotation of the methylene group, CH_2, about the C-C bond of the radical. This phenomena and determination of the barrier to internal rotation is discussed by Tolles et. al. [Ref. 21] and Ohigashi and Kurita (Ref. 15].

The crystal structure of zinc acetate dihydrate and the a, b, c cell axis system as related to an a*, b, c (x,y,z) orthogonal axis system within the crystal is shown in Figure 3. The relationship between the two axis systems is given by the transformations

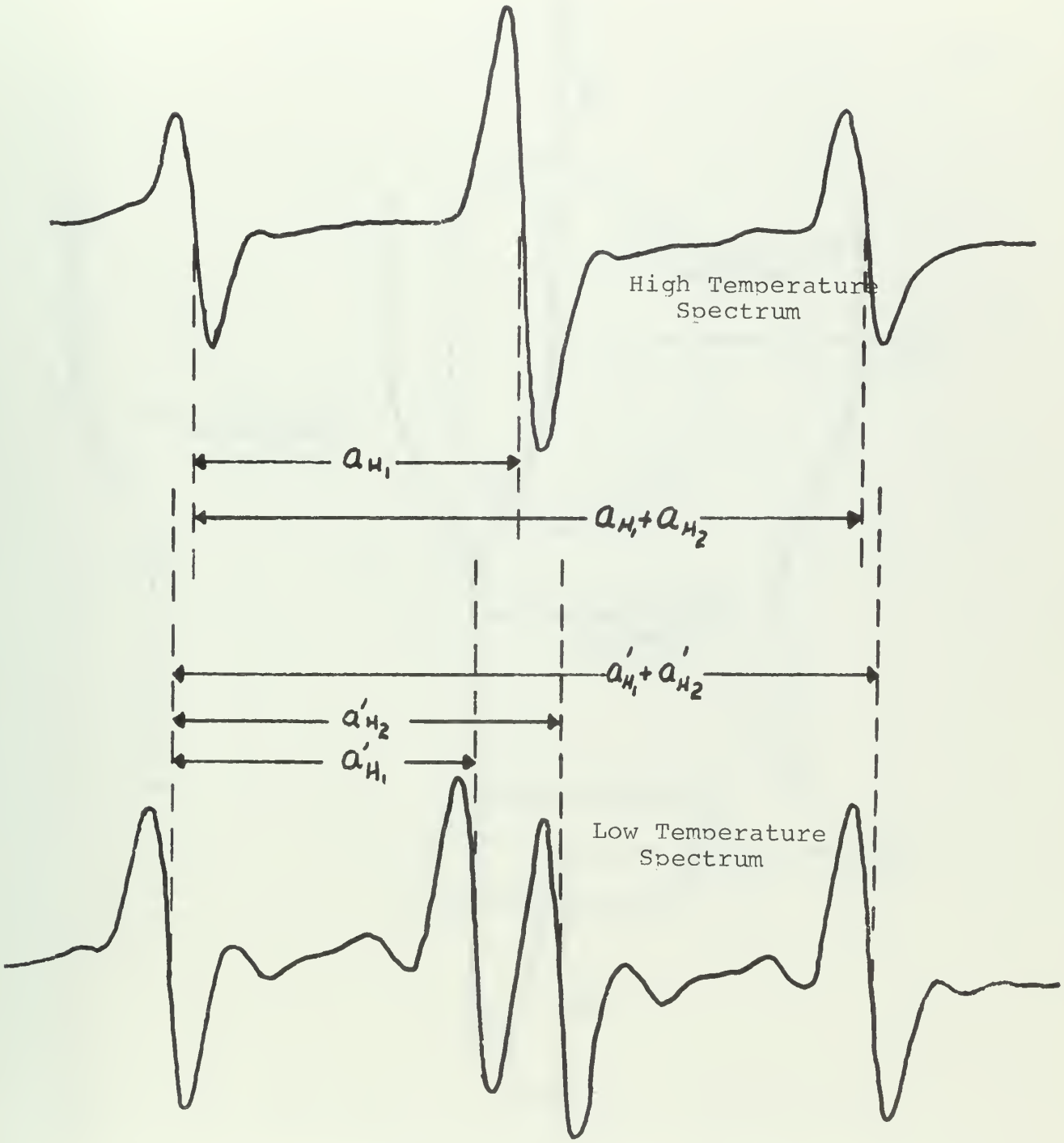

Figure 1. Characteristic esr spectra at high and at low temperature.

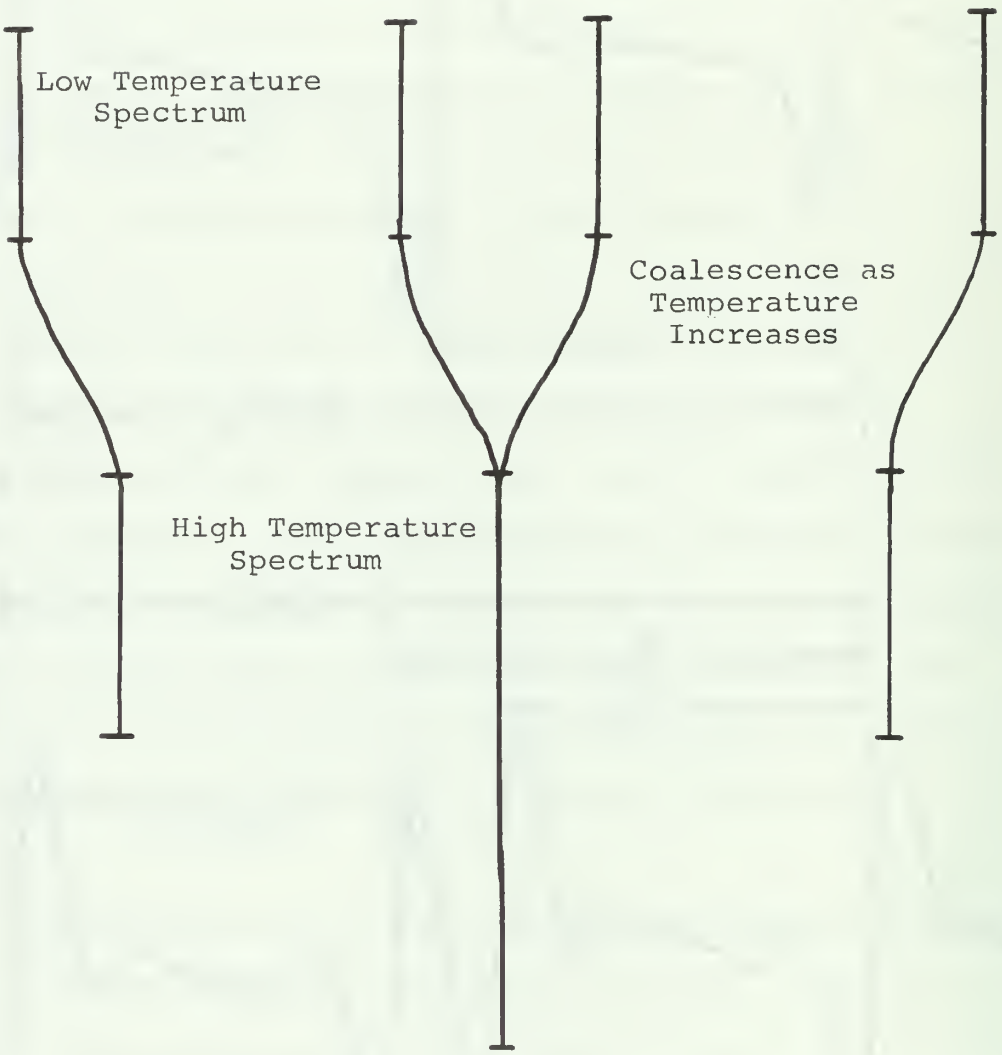

Figure 2. Coalescence of absorption lines of esr spectra with increase of temperature.

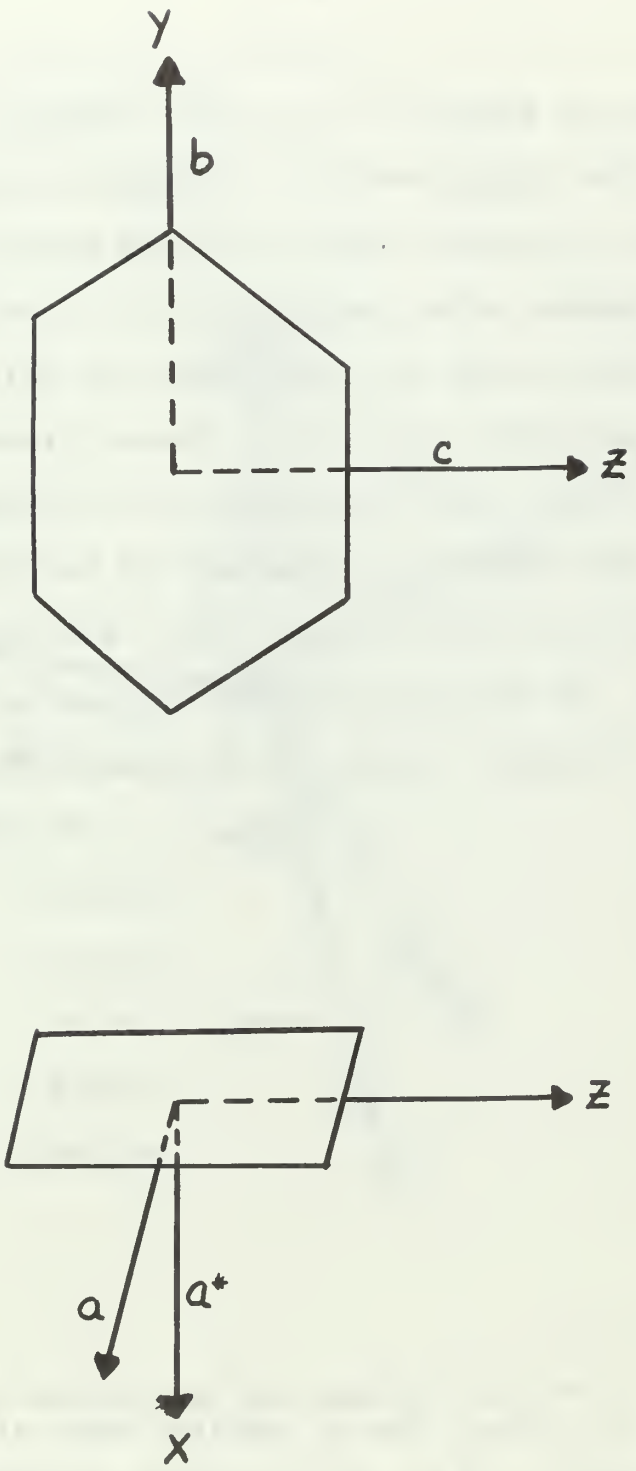

Figure 3. The zinc acetate dihydrate crystal and the orthogonal crystal axis system (xyz or a*bc) and its relationship to the crystalline axis system (abc) [Ref. 4].

$$a = \sin\beta x + \cos\beta z$$

$$b = y$$

$$c = z$$

where in Figure 3, x is also referred to as a*.

The $CH_2CO_2^-$ radical is shown in Figure 4. The orientation shown is planar, each C-H group having assigned to it an orthogonal axis system X_1, Y_1, Z_1, or X_2, Y_2, Z_2 wherein the Y_1 and Y_2 axes are coincident and fall along the p_z orbital of the carbon (C_2) atom. These directions correspond to vectors $\vec{u}$, $\vec{v}$, and $\vec{w}$ in the a*, b, c crystal axis system.

The following parameters of the $CH_2CO_2^-$ radical as presented by Tolles et. al. [Ref. 21] and Ohigashi and Kurita [Ref. 15] are pertinent to studies in this paper.

Principal values of the hyperfine coupling tensors[1]

H_1 tensor	-26.80 MHz
	-59.59
	-92.15
H_2 tensor	-26.41
	-58.98
	-92.78

---

[1]Principal values are designated to lie along the respective C-H_n bond, the p_z orbital axis of the carbon atom in the CH_2 group, and in the CH_2 plane perpendicular to the respective C-H_n bond as shown in Figure 4.

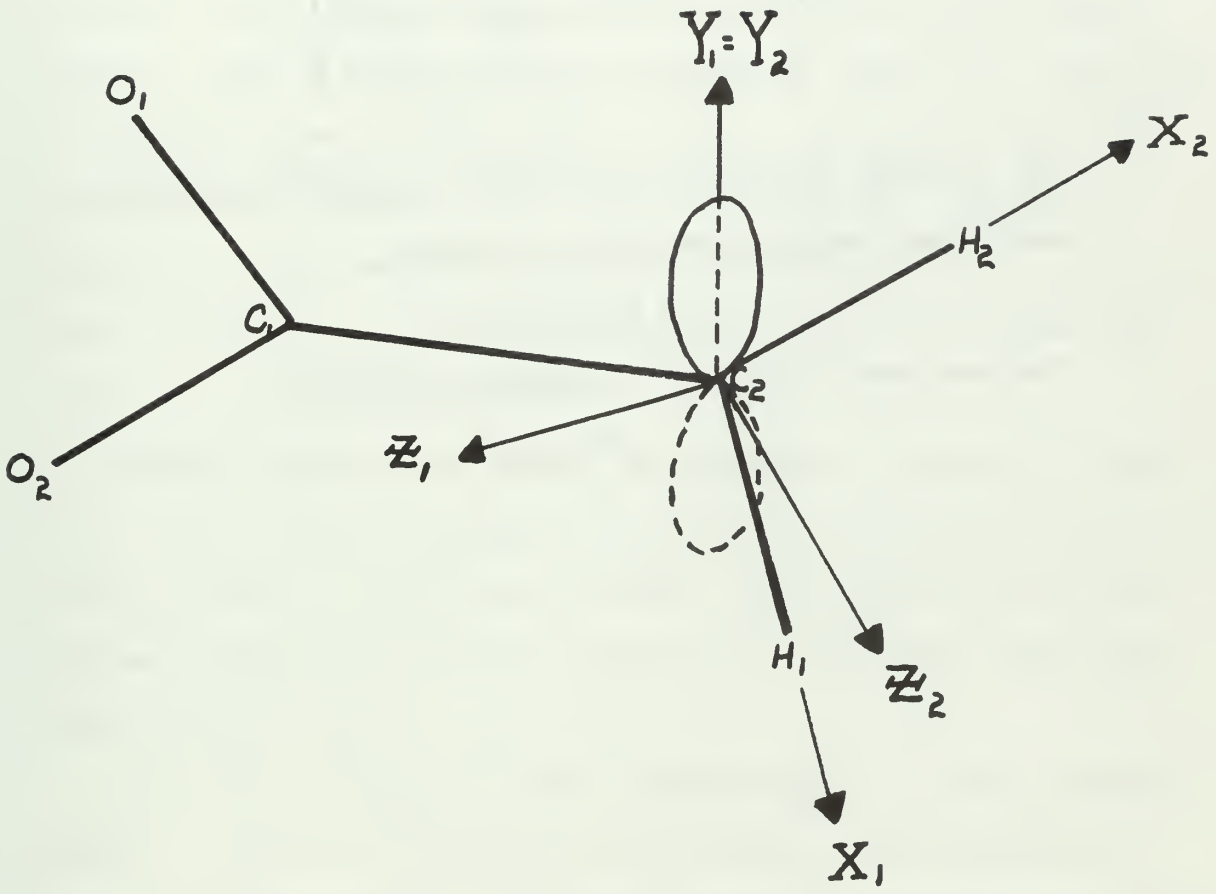

Figure 4. Locations of the hyperfine axes in the $CH_2CO_2^-$ radical (planar configuration) [Ref. 4].

Direction cosines with respect to the crystal axis system[1]

$$H_1 \begin{pmatrix} 0.547 & 0.722 & 0.423 \\ 0.768 & -0.634 & 0.088 \\ -0.332 & -0.276 & 0.902 \end{pmatrix}$$

$$H_2 \begin{pmatrix} 0.048 & -0.081 & -0.996 \\ 0.768 & -0.634 & 0.088 \\ 0.638 & 0.769 & -0.032 \end{pmatrix}$$

The barrier potential to internal rotation of the methylene group about the C-C bond

$$5.8 \text{ kcal/mol}$$

The average rotational frequency factor

$$4.4 \times 10^{12} \text{ sec}^{-1} \quad .$$

---

[1] The direction cosines are expressed as row vectors.

III. PROBLEM FORMULATION

To qualitatively understand the effect being studied, reference is made to Figure 1, page 15 which shows a typical first derivative esr spectrum of the $CH_2CO_2^-$ radical at high temperature and at low temperature respectively. The esr experiment basically measures the interaction of the election magnetic moment with an applied magnetic field, H. Hyperfine structure is due to the free election interacting with the two methylene protons. The coupling constant, a_H, is a property of the radical dependent on orientation in the magnetic field and reflects the magnetic field of a given nucleus, H_i, experienced by the electron.

Figure 5 shows the splitting of energy levels in a magnetic field due to electron and nuclei interactions for the $CH_2CO_2^-$ radical. The four vertical lines represent allowed energy transitions giving rise to the basic four line spectrum of Figure 1.

When an oscillating field perpendicular to the external magnetic field H is applied, transitions are induced provided the frequency, ν, is such that the resonance condition

$$h\nu = g\beta H$$

is satisfied, where g is the spectroscopic splitting term and β is the Bohr magneton. Hence it can be said

$$\Delta E_i = h\nu_i = g\beta H_i$$

or

$$H_i \propto \Delta E_i \quad .$$

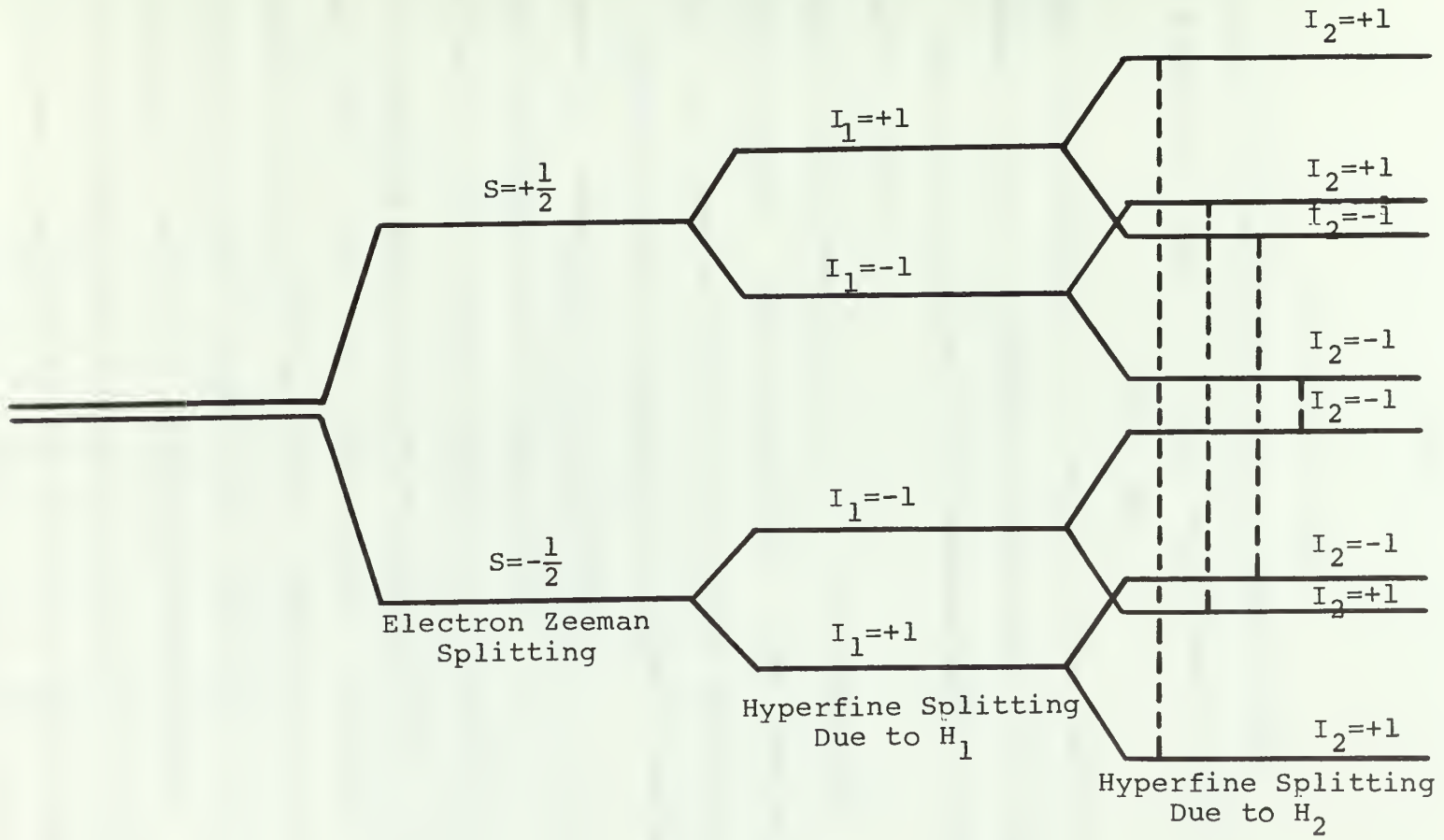

Figure 5. Splitting of energy levels in a magnetic field due to electron and nuclei (H_1 and H_2) interaction in the $CH_2CO_2^-$ radical.

Each resonance (absorption) line of the spectrum is a representation of a transition energy ΔE_1 proportional to the magnetic field, H_1, causing resonance. Hence, the difference between two spectral lines in gauss is a representation of the difference in transition energy which itself is a measure of the hyperfine interaction and is called the coupling constant. Experimentally the "distance" between absorption lines is directly measured in gauss to determine the relative coupling constants, a_{H_1} and a_{H_2}, or the sum of the coupling constants, $a_{H_1} + a_{H_2}$ seen in Figure 1.

As previously mentioned, Crawford [Ref. 4] in his work on zinc acetate dihydrate noted that at a given orientation of magnetic field, the esr spectrum showed a one to six gauss decrease in the sum of the coupling constants as the temperature was increased from 133°K to room temperature (Figures 1 and 2). In section I studies of temperature dependence of radical spectra have been discussed. These studies have contributed similar temperature effects to out-of-plane vibrations. Studies by Horsfield [Ref. 12] and Heller [Ref. 10] of methyl groups have shown internal rotations of the group to occur about a C-C bond. The temperature dependence of the $CH_2CO_2^-$ radical has been attributed to motion of the CH_2 group consisting of rapid reorientation around the C-C bond above room temperatures being quenched at low temperature [Refs. 15 and 21].

It is the purpose of this work to develop a mathematical model, consistent with experimental data, by which the temperature effect in the $CH_2CO_2^-$ radical may be predicted for any given orientation of the zinc acetate crystal in a magnetic field.

It will be seen in the discussion of results that the observed effect does not depend solely on one particular phenomenon but rather is due to a combination of several phenomena. Hence the problem is formulated into four effects, rotation of the methylene group, hyperconjugation, flap or vibrations perpendicular to the plane of the radical, and nuclear spin relaxation.

A. ROTATION OF THE METHYLENE GROUP

1. The Restricted Rotor Model

The CH_2 (methylene group) acting as an internally restricted rotor representing the exchanging of the two protons is the model used in explaining the temperature effect.

The Hamiltonian for a restricted rotor is

$$H = BL_z^2 + \frac{V}{2}(1-\cos 2\phi')$$

assuming the radical to be planar and the angular momentum, L_z, to be quantized along the Z axis (the C-C bond). In the Hamiltonian equation, B is a constant of the system, V is the activation energy or barrier to internal rotation, and ϕ' is the angle of rotation of the CH_2 rotor about the C-C bond.

The Schroedinger wave equation for the restricted rotor may be solved by such standard procedures as given in

Eyring, Walter and Kimble [Ref. 6], page 358, to yield wave functions which in the limit of the free rotor become:

$$\psi_{\phi'} = Ae^{im\phi'}$$

where A is a normalization constant equal to $\frac{1}{\sqrt{2\pi}}$.

The set of basis functions are chosen to be

$$|m\rangle = Ae^{im\phi'} = (\frac{1}{\sqrt{2\pi}})e^{im\phi'}$$

where m runs from minus to plus infinity.

Eigenvalues of the Hamiltonian yield the possible quantum mechanical energy levels of the system. These values are established by diagonalization of the Hamiltonian matrix, the diagonal values being the eigenvalues.

The Hamiltonian matrix elements are determined through the following operations:

On-diagonal matrix elements are represented as

$$\langle m'|BL_z^2+\frac{V}{2}|m\rangle = \langle m'|H'|m\rangle = (Bm^2+\frac{V}{2})\delta_{mm'}$$

where $\delta = 0$ unless $m = m'$.

The diagonal elements are numerically evaluated from the knowledge of V, the barrier potential, and B, where

V = 5.8 Kcal/mol

$B = \frac{h^2}{8\pi^2 I}$

h = Planck's constant

I = the moment of inertia of the rotating CH_2 group.

For convenience of calculation,

$$\frac{B}{h} = \frac{h}{8\pi^2 I}$$

where

$$\frac{h}{8\pi^2} = 5.05538 \times 10^5 \text{ MHz amu } \mathring{A}^2 .$$

Off-diagonal elements of the Hamiltonian matrix result from the perturbation term

$$-\frac{V}{2}\cos\phi'$$

and are represented by

$$\langle m'|-\frac{V}{2}\cos\phi'|m\rangle .$$

Evaluation of these integrals shows that the value is zero unless

$$m' = m+2 \text{ or } m-2 .$$

The non-zero off-diagonal elements are then expressed in terms of the basis function as

$$-\frac{V}{2}\int_0^{2\pi} \frac{e^{-im\phi'}}{\sqrt{2\pi}} \cos 2\phi' \frac{e^{im\phi'}}{\sqrt{2\pi}} d\phi' .$$

Using the identity

$$\cos 2\phi' = \frac{1}{2}(e^{i2\phi'}+e^{-i2\phi'})$$

the integral is evaluated to yield

$$-\frac{V}{8\pi}(2\pi\delta_{(m-m'+2)} + 2\pi\delta_{(m-m'-2)})$$

or when $m' = m+2$ or $m' = m-2$ the off-diagonal values become

$$-\frac{V}{4} .$$

The calculated matrix elements are placed into the secular determinant which is diagonalized to yield the eigenvalues and eigenvectors of the system. Solution of the determinant was performed by IBM 360 computer.

2. The Harmonic Oscillator Model

The limits of a restricted rotor model are the free rotor at one extreme and the harmonic oscillator at the other. Considering the first several excited states above ground to be significantly populated at the temperatures used in this study, an approximately constant difference between levels of the restricted rotor was seen to exist (Section V-B).

The nearly constant difference in energy levels suggests the approximation that the system can be represented by a harmonic oscillator model, the energy levels of which are represented by

$$E = (n+\frac{1}{2})h\nu \qquad \text{(A2-1)}$$

where n runs from zero to infinity. If this approximation were to prove valid, further system analysis would be made easier.

The restricted rotor model yields eigenvalues in units of E/h, hence some rearrangement of equation A2-1 is necessary to compare the two models. A solution of the Schroedinger equation for the harmonic oscillator by procedures of Eisberg [Ref. 5] shows

$$\nu = \frac{1}{\pi}\sqrt{\frac{V}{2I}} \quad . \qquad \text{(A2-2)}$$

Equation A2-1 may then be rewritten

$$E = (n+\frac{1}{2})h\sqrt{(\frac{V}{h})(4)\frac{h}{8\pi^2 I}} \quad . \qquad \text{(A2-3)}$$

Direct substitution with proper units as used in section A 1 yields

$$E/h = 2(n+\frac{1}{2})\sqrt{18.159208} \qquad \text{(A2-4)}$$

from which eigenvalues may be determined in units of terahertz (THz) consistent with the units of the restricted rotor model. (One THz equals 10^{12} Hz.)

3. Evaluation of Coupling Constants as a Function of Temperature

The harmonic oscillator model was used to develop the values of coupling constants expected to be seen experimentally at any given temperature due to rotation of the CH_2 group.

The effective spin Hamiltonian for the interaction of an electron and two nuclear spins in a magnetic field for the case of quenched angular momentum is

$$\mathcal{H} = B\vec{H}\cdot\vec{g}\cdot\vec{S} - \sum_{i=1,2} g_n\beta_n\vec{I}_i\cdot\vec{H} + \sum_{i=1,2}\vec{S}\cdot\vec{T}_i\cdot\vec{I}_i \ . \qquad \text{(A3-1)}$$

The first term represents the electron Zeeman energy, the interaction of an unpaired electron with the external magnetic field $\vec{H}$. β is the Bohr magneton, $\vec{S}$ is the electronic spin equal to $\pm\frac{1}{2}$ and $\vec{g}$ is the spectroscopic splitting tensor. The second term is the summation of the nuclear Zeeman energies where g_n is the nuclear g factor, β_n is the nuclear magneton, and $\vec{I}_i$ is the spin of the i^{th} proton. The third term represents the energy of hyperfine interaction between electron spin, $\vec{S}$, and nuclear spin, $\vec{I}_i$. $\vec{T}_i$ is the hyperfine interaction tensor. Equation A3-1 may be rewritten

$$H = \beta\vec{H}\cdot\vec{g}\cdot\vec{S} - g_n\beta_n \sum_{i=1,2} (\vec{H} - \frac{1}{g_n\beta_n}\vec{S}\cdot\vec{T}_i)\cdot\vec{I}_i \qquad \text{(A3-2)}$$

where the parenthetical term is the effective magnetic field seen by the i^{th} proton. Solution of equation A3-2 leads to (among other parameters) the coupling constants of the spin system.

When an electron and a proton are placed in the influence of a magnetic field, the spins of each tend to line up parallel to the field creating dipolar coupling which is represented in the effective magnetic field term of equation A3-2. If the orientation of the magnetic field is changed relative to the proton and electron as caused by the rotation of the CH_2 group, different dipolar coupling occurs, and the Hamiltonian solution yields different values of the coupling constants. Hence, the coupling constants are a function of the CH_2 angle of rotation, ϕ'.

The Hamiltonian is a representation of the energy of the spin system. There will be a certain probability $P_{\phi'}$, that a given energy level will be found at a given angle of CH_2 rotation, ϕ'. In addition, there will be a statistical distribution of electron spin population in the existing energy levels as determined by Boltzman distribution factors.

Based on the foregoing considerations the general relation to be solved to yield the average coupling constants for a given temperature is

$$\langle A \rangle_T = \int_{-\infty}^{\infty} A_{\phi'} P_{\phi'} W_n d\phi' \qquad \text{(A3-3)}$$

where $\langle A \rangle_T$ is the coupling constant averaged over all orientations for a given magnetic field orientation at a given temperature, T. A_ϕ, is the coupling constant as a function of angle of rotation, ϕ', of the methylene group about the C-C bond axis. P_ϕ, is the probability distribution factor, W_n is the Boltzman statistical weighting factor.

a. Evaluation of A_ϕ,

An existing computer program, SSESR (Solid State Spectrum ESR), was used as a starting point to calculate values of A_ϕ,. As originally written by Crawford [Ref. 4], SSESR computes the esr spectrum of a radical trapped in the solid state assuming the angle ϕ' to be zero, i.e. the planar model.

The theory behind the SSESR program is based on the development of Box et. at [Ref. 2]. If the components of $\vec{S}$ perpendicular to $\vec{H}$ are ignored in equation A3-1 (a good approximation [Ref. 2]) the energy levels of the spin system can be written as

$$E = \beta g H S_H - g_n \beta_n \Sigma_i I_{ih} |h_i| \qquad \text{(A3-4)}$$

where g is the observed g value, S_H is the electron spin component along $\vec{H}$, and I_{ih} is the component of nuclear spin along $\vec{h}_i$, the vector along which the nuclear spin is quantized. The vector $\vec{h}_i$ may be written

$$\vec{h}_i = \vec{H} - S_H(\vec{u}_i A_i \alpha_i + \vec{v}_i B_i \beta_i + w_i C_i \gamma_i) \frac{1}{g_n \beta_n} . \qquad \text{(A3-5)}$$

In A3-5, A_i, B_i and C_i are principal values of the hyperfine coupling tensors, $\vec{\vec{T}}_i$. The vectors $\vec{u}_i$, $\vec{v}_i$, and $\vec{w}_i$, are unit

vectors denoting the direction of the two sets of principal axes corresponding to A_i, B_i, and C_i respectively, as seen in Figure 4. The terms α_i, β_i, and γ_i are the direction cosines of the external field, $\vec{H}$, with respect to these axes. For the $CH_2CO_2^-$ radical S_H, I_{1h}, and I_{2h}, are each $\pm\frac{1}{2}$.

Incorporating all allowed combinations of spin states, solution of equation A3-4 yields 16 electron transitions in terms of $2\Delta Hg\beta_0/g_n\beta_n$, represented by

$$\pm|h_{1(+)}| \pm |h_{1(-)}| \pm |h_{2(+)}| \pm |h_{2(-)}| \qquad \text{(A3-6)}$$

where the 16 transitions are seen by the 2^4 choices of sign and where $|h_{i(+)}|$ and $|h_{i(-)}|$ are the magnitudes of the vectors $\vec{h}_i$ corresponding to $S_H = +\frac{1}{2}$ and $-\frac{1}{2}$ respectively. The computer program, SSESR, calculates the relative intensities and frequencies for the 16 transitions of the planar radical.

Basic input data include the number of nuclei in the molecule or radical, magnetic field magnitude, direction cosines relating the nuclei principal axes to the crystal axis system, the principal values of the coupling tensors for each nucleus, the direction cosines of the magnetic field, and the nuclear Zeeman frequency. Output yielded transition frequencies, transition intensities, and transitions in gauss from the center of the spectrum, all assuming an isotropic g tensor [Ref. 4] or a value of g = 2.0023, that for a free electron.

Several modifications to the existing program were made to incorporate the harmonic oscillator model. The

complete program, PREDICT II, appears in Appendix A. All computations were performed in double precision.

(1) Subroutine HDCOS. The first modification involved an additional subroutine to compute the three direction cosines of the magnetic field for a given input of θ and ϕ, the angles through which the crystal would be rotated in the magnetic field. This subroutine was called HDCOS and was based on the relations

$$u_1 = -\cos\theta$$
$$u_2 = -\sin\theta \sin\phi$$
$$u_3 = \sin\theta \cos\phi \quad .$$

(2) Subroutine AXROT. A second modification involved the subroutine AXROT, which computed the normalized direction cosines of the C-C bond axis using values of the direction cosines which relate the nuclei to the crystal axis system as listed in section II.

The vector, $\vec{CH}_1$, representing that vector along the C-H, bond is expressed from values of the H_1 tensor (Section II) as

$$x_1 = 0.547$$
$$y_1 = 0.722$$
$$z_1 = 0.423 \quad .$$

Likewise the vector $\vec{CH}_2$ is represented by values of the H_2 tensor

$$x_2 = 0.048$$
$$y_2 = -0.081$$
$$z_2 = -0.996 \quad .$$

Addition and normalization of these vector components yielded the direction cosines of the C-C bond with respect to the crystal axis system a*, b, c.

(3) Subroutine AXR. As the methylene group rotates through angle ϕ', the hyperfine coupling tensors, H_1 and H_2 must change as a function of ϕ'. Hence, a further modification by the inclusion of subroutine AXR was required. The rotation of any vector a number of degrees ϕ' about a vector (a,b,c) is represented by the transformation matrix resulting from evaluation of the following matrix multiplications:

$$\begin{pmatrix} \frac{b}{d} & \frac{ac}{d} & a \\ -\frac{a}{d} & \frac{bc}{d} & b \\ 0 & -d & c \end{pmatrix} \begin{pmatrix} \cos\phi' & \sin\phi' & 0 \\ -\sin\phi' & \cos\phi' & 0 \\ 0 & 0 & 1 \end{pmatrix} \begin{pmatrix} \frac{b}{d} & -\frac{a}{d} & 0 \\ \frac{ac}{d} & \frac{bc}{d} & -d \\ a & b & c \end{pmatrix}$$

where $d = (1-c^2)^{1/2}$ and $a^2 + b^2 + c^2 = 1$.

Assigning a, b, and c the values of the vector components of the C-C bond axis as computed in AXROT, the resulting transformation matrix was applied to the H_1 and H_2 hyperfine tensors to yield the adjusted tensors as a function of ϕ'. These values then became input to the basic SSESR program.

(4) Subroutine REFH. As a final refinement, subroutine REFH was written to insure orthonormality of tensor values, the result of which became input to the AXR subroutine.

With the modifications described it was possible to calculate the stick spectra for any magnetic field

orientation and any desired angle of rotation, ϕ'. From the stick spectra the coupling constants for any angle, ϕ', could be readily calculated by differences in the proper transition values.

b. Evaluation of $P_{\phi'}$ and $\langle A \rangle_T$

Two additional modifications of SSESR were required for the evaluation of the average coupling constants as a function of temperature.

(1) Angular Dependence of Wave Functions. The solution of Schroedinger's equation for the harmonic oscillator as basically presented by Eisberg [Ref. 5] along with a Lagrangian formulation was used to find the system's eigenfunctions, but the displacement variable was ϕ' rather than x as presented by Eisberg.

The time independent Schroedinger wave equation may be expressed as

$$-\frac{\hbar^2}{2I}\frac{\partial^2\psi(\phi')}{\partial\phi'^2} + V\psi_{(\phi')} = E\psi_{(\phi')} \qquad \text{(A3-7)}$$

where V is the potential energy term, and I is the moment of inertia of the CH_2 group.

The potential energy may be expressed as

$$V = \frac{1}{2}K\phi'^2. \qquad \text{(A3-8)}$$

The kinetic energy as

$$KE = \frac{1}{2}mr^2\omega^2 = \frac{1}{2}mr^2\left(\frac{\partial\phi'}{\partial t}\right)^2 = \frac{I}{2}(\dot{\phi}')^2 \ . \qquad \text{(A3-9)}$$

Therefore, the Lagrangian (L) for the system is

$$L = \frac{I}{2}(\dot{\phi}')^2 + \frac{K}{2}(\phi')^2 \ . \qquad \text{(A3-10)}$$

Solution of the Lagrangian yields the equation of motion

$$\ddot{\phi}' - \frac{K}{I}\phi' = 0 \qquad \text{(A3-11)}$$

which upon solution yields the frequency, ν, as

$$\nu = \frac{1}{2\pi}\sqrt{\frac{K}{I}} \quad . \qquad \text{(A3-12)}$$

To determine the actual value of the frequency, ν, the following Hamiltonian was studied,

$$H = \frac{L^2}{2I}\phi' + \frac{K}{2}\phi^{2\prime} \qquad \text{(A3-13)}$$

where $\frac{L^2}{2I}\phi'$ is derived directly from the classical mechanics expression for kinetic energy,

$$KE = \frac{1}{2}mv^2$$

and L is angular momentum.

Considering the angular momentum quantum mechanical operator,

$$L_z = -\hbar^2 \frac{\partial^2}{\partial\phi'^2}$$

the Hamiltonian may be rewritten as

$$H = -\frac{\hbar^2}{2I}\frac{\partial^2}{\partial\phi'^2} + \frac{K}{2}\phi'^2 \qquad \text{(A3-14)}$$

which may be further rewritten using equation A3-12 as

$$H = -\frac{\hbar^2\partial^2}{2I\partial\phi'^2} + \nu^2 2\pi^2 I\phi'^2 \quad . \qquad \text{(A3-15)}$$

Operating on the wave function, ψ, with this Hamiltonian gives

$$-\frac{\hbar^2}{2I}\frac{\partial^2\psi_{(\phi')}}{\partial\phi'^2} + (\nu^2 2\pi^2 I\phi'^2)\psi_{(\phi')} = E\psi_{(\phi')} \qquad \text{(A3-16)}$$

which is an identity with equation A3-14. Hence, rather than determine the frequency, ν, by such means as, say the IR

frequency between energy levels, it was possible to calculate K (and hence ν) from equation A3-12 directly.

The potential energy of the restricted rotor is expressed as

$$V = \frac{V_2}{2} (1-\cos 2\phi') \qquad \text{(A3-17)}$$

where V_2 is the barrier potential observed experimentally as 5.8 kcal/mol. Expanding the cosine term as a series yields

$$V = \frac{V_2}{2} - \frac{V_2}{2} + \frac{V_2}{2} \frac{(2\phi')^2}{2!}$$

$$+ \text{higher terms.}$$

Neglecting higher terms,

$$V = V_2\phi'^2$$

which is just the potential energy of the harmonic oscillator, so that

$$V = V_2\phi'^2 = \frac{1}{2}K\phi'^2 \qquad \text{(A3-18)}$$

and

$$\frac{1}{2}K = V_2 = 5.8 \text{ kcal/mol.} \qquad \text{(A3-19)}$$

In dropping higher terms and approximating the harmonic oscillator the assumption has been made that significant values of energy will occur only with a few degrees either side of $\phi' = 0$ and that as ϕ' approaches infinity, V approaches infinity as shown in Figure 6.

Combining the results of equations A3-18 and A3-19, equation A3-7 is rewritten and transformed to give

$$\frac{\partial^2\psi(\phi')}{\partial\phi^2} + [\frac{2IE}{\hbar^2} - \frac{2I}{\hbar^2}V_2\phi'^2]\psi_{(\phi')} = 0 \; . \qquad \text{(A3-20)}$$

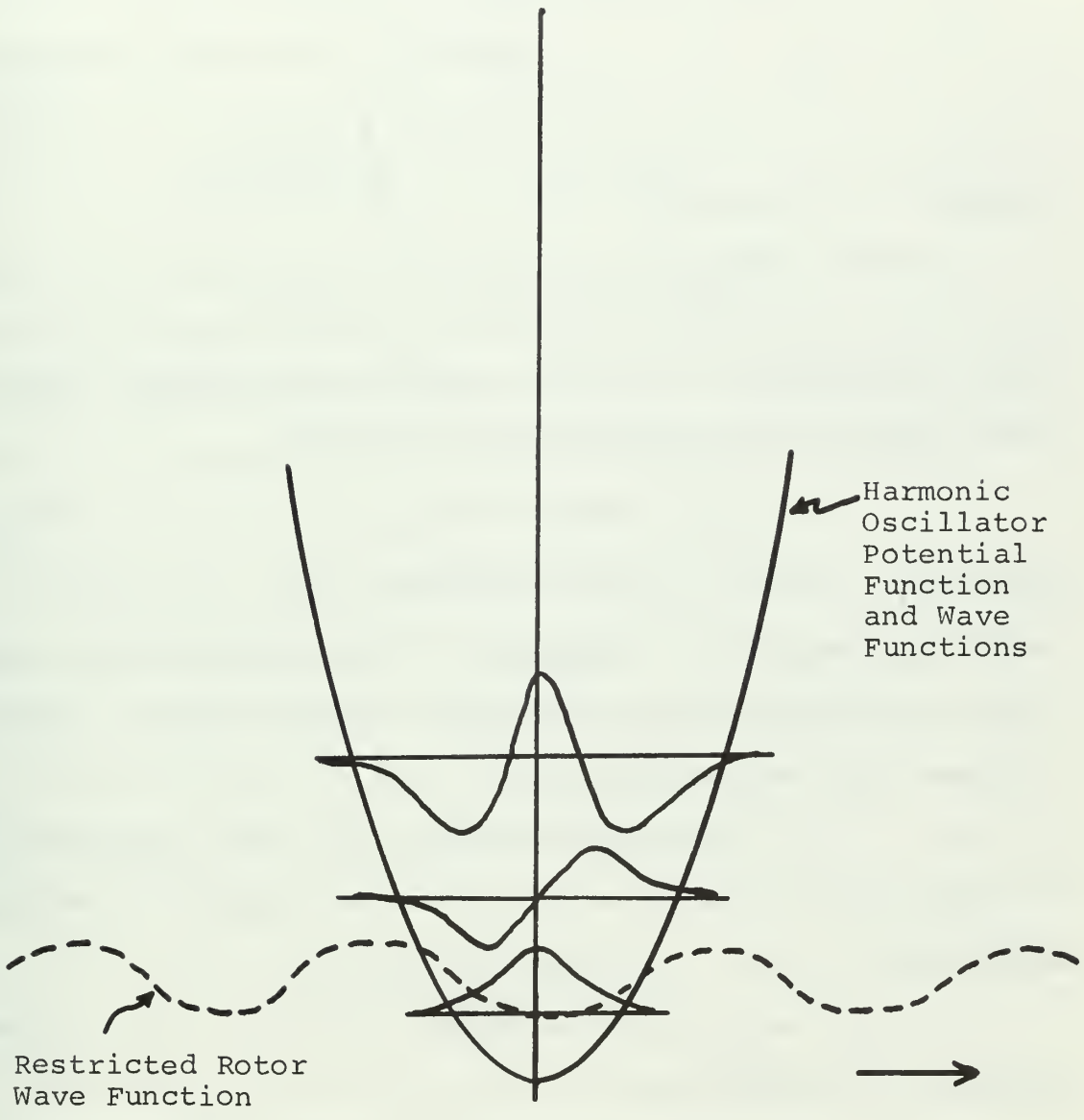

Figure 6. Comparison of restricted rotor and harmonic oscillator wave functions.

Defining the terms

$$\alpha = \left(\frac{2IV_2}{\hbar^2}\right)^{1/2} \tag{A3-21}$$

$$\beta = \frac{2IE}{\hbar^2} \tag{A3-22}$$

$$\text{and} \quad \zeta = \sqrt{\alpha}\ \phi' \tag{A3-23}$$

equation A3-20 becomes

$$\frac{\partial^2 \psi_{(\phi')}}{\partial \phi'^2} + (\beta - \alpha\ \zeta^2)\psi_{(\phi')} = 0$$

which with boundary conditions applied per Eisberg's procedures leads to the eigenfunction solutions

$$\psi_{(\zeta)} = \exp(-\zeta^2/2) H_{n(\zeta)} \tag{A3-24}$$

where $H_{n(\zeta)}$ are the Hermite polynomials for the respective levels n = zero to n = infinity, n = zero representing ground state. It can be shown that these functions form an orthogonal set over all space [Ref. 5].

Combining equation A3-21 with equation A3-23, and applying the proper units conversion factors, ζ was determined to be

$$\zeta = 3.77629\phi' \tag{A3-25}$$

where ϕ' is in radians.

The probability, P_n, that a given state n will be found at an angle of CH_2 rotation, ϕ', is

$$P_{n(\zeta)} = \psi^*_{n(\zeta)} \psi_{n(\zeta)}$$

where $\psi^*_{(\zeta)}$ is the complex conjugate of $\psi_{(\zeta)}$, but since real wave functions are involved,

$$P_{(\zeta)} = e^{-\zeta^2} H^2_{n(\zeta)}$$

and the integral of equation A3-3 takes the form

$$\langle A \rangle_T = 3.77629 \int_{-\infty}^{\infty} A_{\phi'} e^{-\zeta^2} H^2_{n(\zeta)} W_n d\phi'$$

which when normalized, becomes

$$\frac{3.77629}{2^n n! \pi^{1/2}} \int_{-90}^{90} e^{-\zeta^2} H^2_{n(\zeta)} W_n d\phi' \qquad \text{(A3-26)}$$

Limits of integration were chosen based on the assumption previously mentioned that significant values occur only within a few degrees either side of $\phi' = 0$. This assumption was justified by considering that for the ground state where $H_{0(\zeta)} = 1$,

$$P_{(\zeta)} = e^{-\zeta^2} = e^{-\alpha \phi'^2} .$$

After about 0.27 radians or 16 degrees, $P_{(z)}$ has decayed to $\frac{1}{e}$ of its original value. After 64° it is expected that $P_{(z)}$ will have negligible values, hence integration over the limits of -90° to +90° was considered suitably close to those of minus to plus infinity.

(2) Temperature Dependence. As yet, no calculation has been developed concerning temperature explicitly. The probability term derived above merely states the probability that a state n will be found at a given angle of CH_2 rotation ϕ'. Boltzman statistics, however, when applied, show the statistical distribution of electrons between the possible energy levels, the greatest percentage population occurring normally in the ground state level and decreasing exponentially with higher excited levels.

The population distribution in each energy level is expressed by the Boltzman weighting factor

$$W_n = \frac{g_n e^{-E_n/kT}}{\sum_n g_n e^{-E_n/kT}} = \frac{g_n e^{-E_n/kT}}{Z} \qquad \text{(A3-27)}$$

where g_n is the degeneracy factor, E_n is the difference between zero energy and the n^{th} state energy, k is the Boltzman constant and Z is the partition function. Since all levels in the model are doubly degenerate, (Section V-B) g_n cancels in the equation.

(3) Combining Coupling Constants, Angular and Temperature Dependence to Determine $\langle A \rangle_T$

Equation A3-3 may now be rewritten

$$\langle A \rangle_T = \int_{-90}^{90} 3.77629 A_{\phi'} \sum_{n=0} e^{-\zeta^2} H_{n(\zeta)} \frac{e^{-E_n/kT}}{Z} d\phi' \qquad \text{(A3-28)}$$

Two subroutines were added to PREDICT II to perform the calculation. The first, AVGCC, evaluated the integral by numerical integration to yield the average coupling constants for each energy level, n, assuming 100% population of each level. The second subroutine, AVBZM, applied the statistical factor to yield the average coupling constants as a function of temperature, $\langle A \rangle_T$. These two subroutines appear in Appendix A as an integral part of PREDICT II.

B. HYPERCONJUGATION EFFECT ON COUPLING CONSTANTS

Hydrogen atoms attached to β carbon atoms (carbon atoms adjacent to the carbon atom having unpaired spin) undergo interaction with the unpaired spin. This interaction is usually termed hyperconjugation and is a maximum when the carbon-hydrogen bond and electron orbital are coplanar. Hydrogen atoms attached to an α carbon atom with an unpaired electron in a hybrid orbital also undergo interaction due to orbital overlap. This can be loosely considered a type of hyperconjugation and is the effect to be analyzed in this work.

When the proton 2s orbital overlaps the carbon p_z orbital there becomes a finite probability that the free electron will come in direct contact with the proton. This phenomenon is known as Fermi contact interaction and its effect is seen in the effective magnetic field term of equation A3-2. The Fermi contact interaction again changes the Hamiltonian values and hence the coupling constants of the system.

If the planar form of the $CH_2CO_2^-$ radical is considered, a plane of symmetry exists and there will be no direct interaction of the α carbon p_z orbital and the hydrogen 2s orbital as seen in Figure 7a. Spin-spin is the sole interaction in this configuration. At any other angle we expect direct orbital interactions as seen in Figure 7b, the amount of Fermi contact interaction being determined by the electron density on the protons.

The input coupling constants used in SSESR were those for the planar model. In order to adjust these values for Fermi

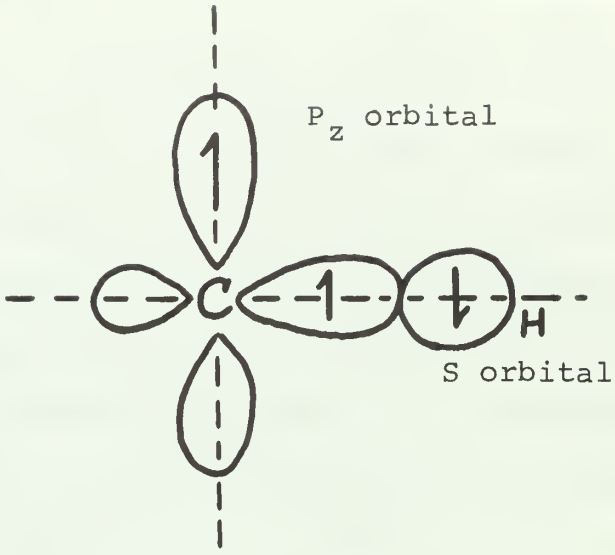

Figure 7a. CH_2 orbital configuration in the planar form of the $CH_2CO_2^-$ radical

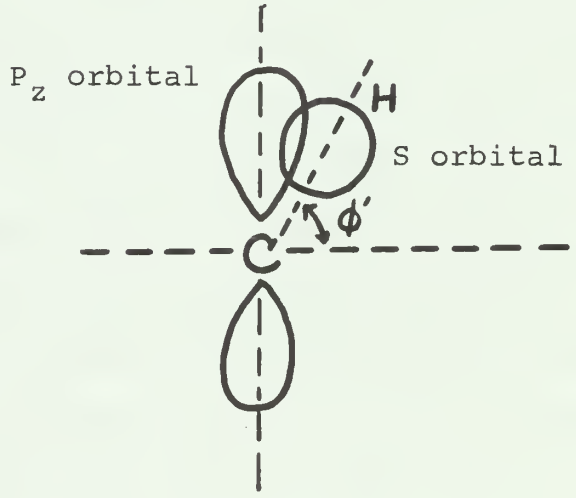

Figure 7b. CH_2 orbital configuration after rotation of the CH_2 group through angle ϕ' showing orbital overlap or mixing.

contact interaction (hyperconjugation), a molecular orbital calculation [Refs. 4 and 19] using the CNDO approximation of Pople et.al [Ref. 16] was made to determine spin densities on the two protons for various angles of rotation, ϕ'. As seen in Section V, a plot of spin density versus angle of rotation yielded a hyperconjugation effect expressed by

$$A_{\phi'_i} = A_i + B(0.273 \times 10^{-2} \sin^2 2\phi')$$

where B = 1,420.4058 MHz, the hyperfine splitting constant of a hydrogen atom with a complete electron in the 2s orbital.

This relationship was incorporated into the SSESR basic program as subroutine CCCA and used to adjust the computation of equation A3-3 for hyperconjugation as well as to determine the magnitude of the effect. CCCA appears as an integral part of PREDICT II in Appendix A.

C. FLAP VIBRATIONAL MOTION

An additional type of motion which can be termed as out-of-plane flapping motion of the CH_2 group may be considered as a possible source of contribution to the temperature dependence of the coupling constants, (Figure 8).

The effects of this type motion would be expected to act very similar to that discussed under the subject of hyperconjugation except that in the flap motion, "bending" of the CH_2 group through an angle γ is of interest. This action can be considered a further type of hyperconjugation effect leading to mixing of the α carbon p_z orbital with the hydrogen 2s orbitals but under a different mathematical relationship than

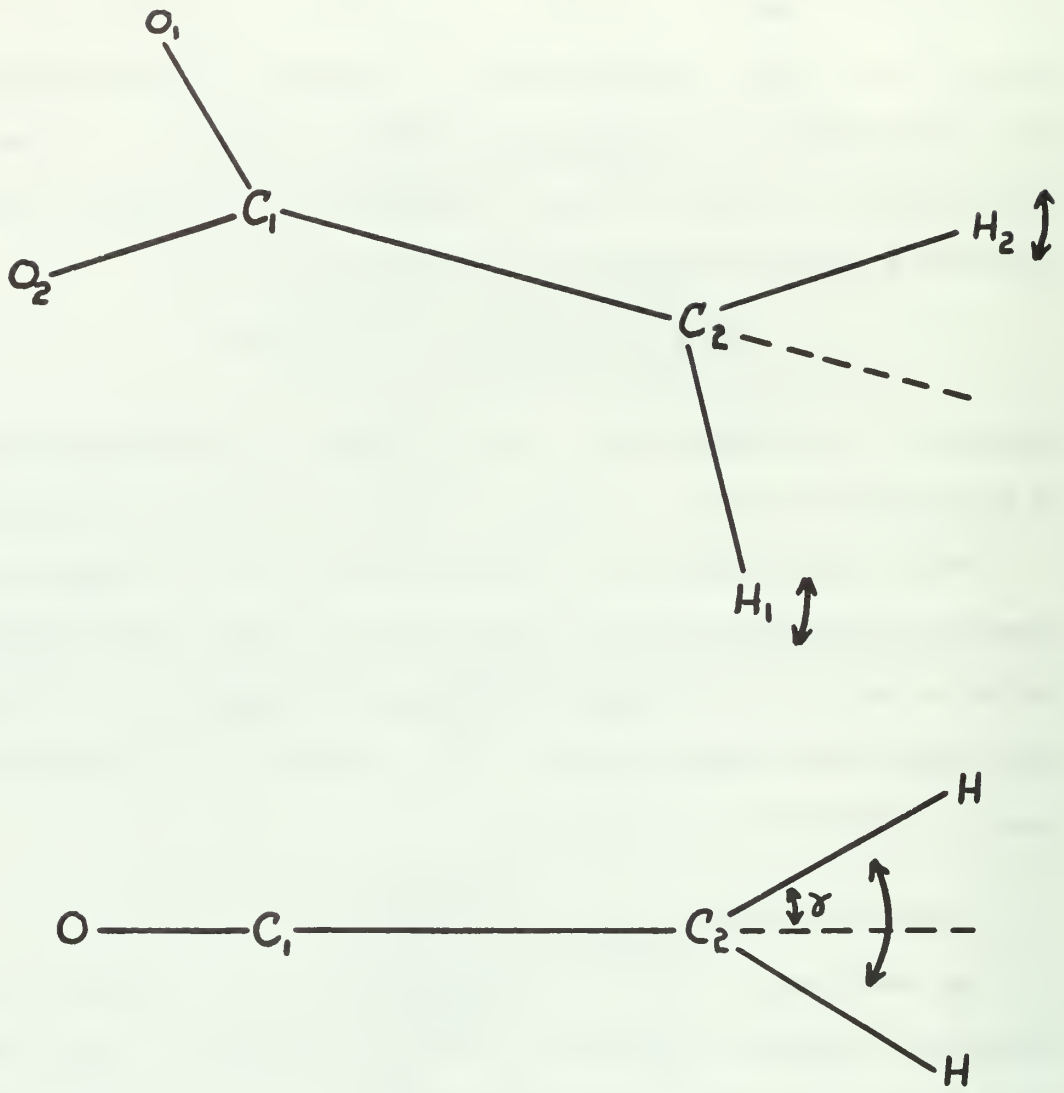

Figure 8. Out-of-plane flapping motion of the CH_2 group in the $CH_2CO_2^-$ radical.

that due to rotational motion. As with rotational motion, an increase of electron density on the protons (Fermi contact interaction) and a corresponding change in the coupling constants due to mixing of orbitals is expected for flap motion.

Molecular orbital calculations based on the CNDO approximation (as used for rotational motion) were utilized to calculate the electron density for any angle of flap, γ. From the results of the calculations, molecular energy values were used to test the feasibility of this type motion and electron spin density values to determine the functional dependence of the coupling constants upon the effect.

D. SPIN RELAXATION EFFECT

1. General Relaxation Theory

To observe electron spin resonance absorption there must be a population difference between the two spin levels between which transition occurs. Carrington and McLachlan [Ref. 3] discuss this criteria in rather easy to understand terms.

The rate of absorption of energy from the radiation field (power) is

$$\frac{\partial E}{\partial t} = N_\alpha P_{\alpha\beta}(E_\beta - E_\alpha) + N_\beta P_{\beta\alpha}(E_\alpha - E_\beta) = nP\Delta E \qquad (D1\text{-}1)$$

where N is the population of energy states E_α or E_β. $P_{\alpha\beta}$ is the probability of transition from state α to β ($\alpha\beta$) and is approximately equal to P. The difference in state population is $n = N_\alpha - N_\beta$ and follows a time dependent exponentially decaying function

$$n = n_0 e^{-2Pt} \qquad (D1\text{-}2)$$

Equations D1-1 and D1-2 show that resonance absorption disappears at equilibrium.

Since $N_\alpha = N_\beta$ in the absence of a magnetic field, application of a field must inevitably require interactions between nuclei and their surroundings as thermal equilibrium is approached. This interaction is called spin-lattice relaxation and results from changing spin orientation as magnetic energy is transferred to other degrees of freedom.

In addition, other processes are known to exist in spin systems due to nuclei-surroundings interaction which cause energy level shifts and hence an expected shift in coupling constants through solution of the effective spin Hamiltonian of equation A3-1. These effects are called spin-spin relaxation, and through solutions of the Bloch equations yield correlation times representative of time the spin system remains in a given energy configuration.

2. Application of Relaxation Theory

Through a qualitative analysis of the physical picture of the rotating methylene group, a relaxation effect was postulated.

Consider as in Figure 9a the CH_2 methylene group oriented in a position having the magnetic moments of protons H_1 and H_2 precessing about effective magnetic fields represented by vectors $\vec{h}_{\pm 1}$ and $\vec{h}_{\pm 2}$ consistent with the notation of Section A-3-a. When the two protons exchange sites as in Figure 9b, each will see a different effective magnetic field. There is then a finite probability that the protons will

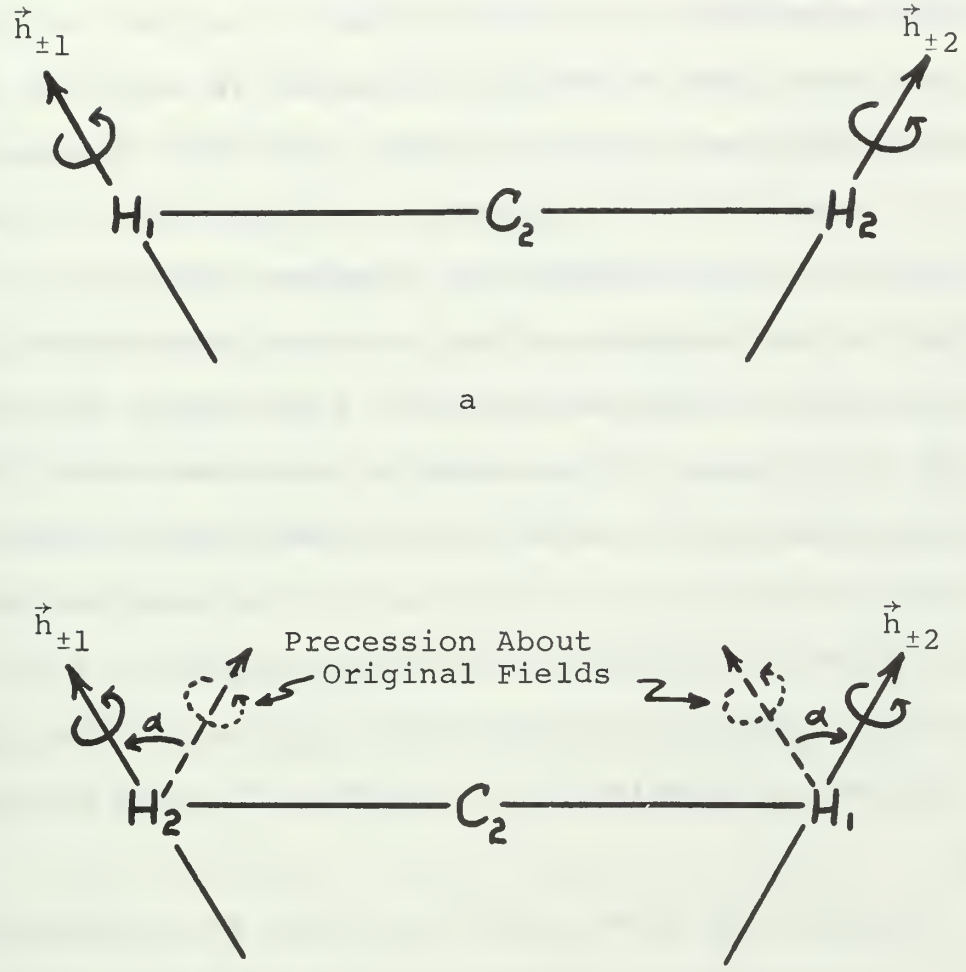

Figure 9. Representation of the magnetic moments of nuclei H_1 and H_2 flipping from precession about one effective magnetic field to another due to rotation of the CH_2 group.

reorient or "flip" through an angle α into precession from about the original effective field to about the effective field now constituting their environment. The two limiting conditions occur when rotational frequency is very high corresponding to high temperature and when rotational frequency is very low - essentially nonexistant - corresponding to quenching of motion at low temperature. Alternatively, it may be said that at high temperature the frequency of rotation being fast will yield a high probability of flip (rapid flip) between the two states. At low temperatures, the probability of making a flip will be small, and approach zero at the point where rotation can be considered to be quenched. When the flip probability is low, significant relaxation effect is not expected. Hence a correspondingly greater average coupling constant is expected over that when flip probability is high.

It should be noted that Figure 9 is only intended to present a representative picture of the relaxation effect. In a real system, the probability of flip or reorientation of the magnetic moment must be considered at every increment of CH_2 rotation.

3. Calculation of Limiting Conditions

In Section A-3-a Box's development for solution of the spin Hamiltonian was seen to yield transition frequencies and hence coupling constants for the $CH_2CO_2^-$ radical. As derived from Box's relations the transition frequencies and hence coupling constant for low flip probability (low temperature

limit), are expressed by

$$-|h_{1(+)}| - |h_{2(+)}| + |h_{1(-)}| + |h_{2(-)}| \qquad \text{(D3-1)}$$

where the results of both fields are assumed oriented in the same direction at quenched rotation. Solution of this relation was obtained by a slight modification to Crawford's [Ref. 4] SSESR computer program.

Coupling constants were obtained for the rapid flip (high temperature) limit through an approximation that at rapid flip conditions, the effective field experienced by each of the protons is an average of the two fields $\vec{h}_1$ and $\vec{h}_2$ experienced at quenched rotation. This approximation was expressed as

$$-|h_{1(+)}+h_{2(+)}| + |h_{1(-)}+h_{2(-)}| \qquad \text{(D3-2)}$$

which was solved, again, by the modification of SSESR to yield the coupling constants for the rapid flip limit.

The difference between the limiting values yielded a relative shift in coupling constants for the relaxation effect at any given orientation of external magnetic field.

4. Calculation of Intermediate Conditions

Anderson [Ref. 1] has calculated frequency shift over a range of temperature but his calculations are based on an approximation that the motional Hamiltonian commutes with the time independent Hamiltonian, an approximation that does not apply to the model under consideration. To date a rigorous calculation without using Anderson's or other approximations has not been developed (Freed and Fraenkel [Ref. 9]).

As a result, a modified solution of the Bloch equations in the presence of a random field using Monte Carlo techniques was used to calculate the frequency and hence, coupling constant shift for intermediate values of flip probability (temperature).

A simple physical picture of the phenomenon calculated by the Monte Carlo technique is depicted in Figure 10 which represents a sphere with an orthogonal axis system X, Y, Z having its origin at the center of the sphere. At the origin is placed a proton. Vectors $\vec{h}_1$ and $\vec{h}_2$ lie in the YZ plane at an angle α either side of the Z axis and represent the effective magnetic fields $\vec{h}_1$ and $\vec{h}_2$ depicted in Figure 9. Assume, as an arbitrary starting point, that at the instant a magnetic field is turned on, the magnetic moment vector, $\vec{M}$, of the proton lies along the X axis with its tip falling on the surface of the sphere at polar coordinates (θ_0, ϕ_0). Let classical mechanics theory show that in the influence of a magnetic field, the vector $\vec{M}$ will precess about $\vec{h}_1$, tracing a path along the sphere's surface from point one to point two. Finally, designate an increment of precession, Δ, such that after each increment a random decision as to whether or not to flip from precession about $\vec{h}_1$ to precession about $\vec{h}_2$ is made. The random decision is correlated to a selected probability of no flip, P_n, which upon problem solution becomes correlated with a value of temperature. As time progresses, the magnetic moment will first flip from precession about $\vec{h}_1$ to $\vec{h}_2$ to $\vec{h}_1$ back and forth as shown after increment two, four,

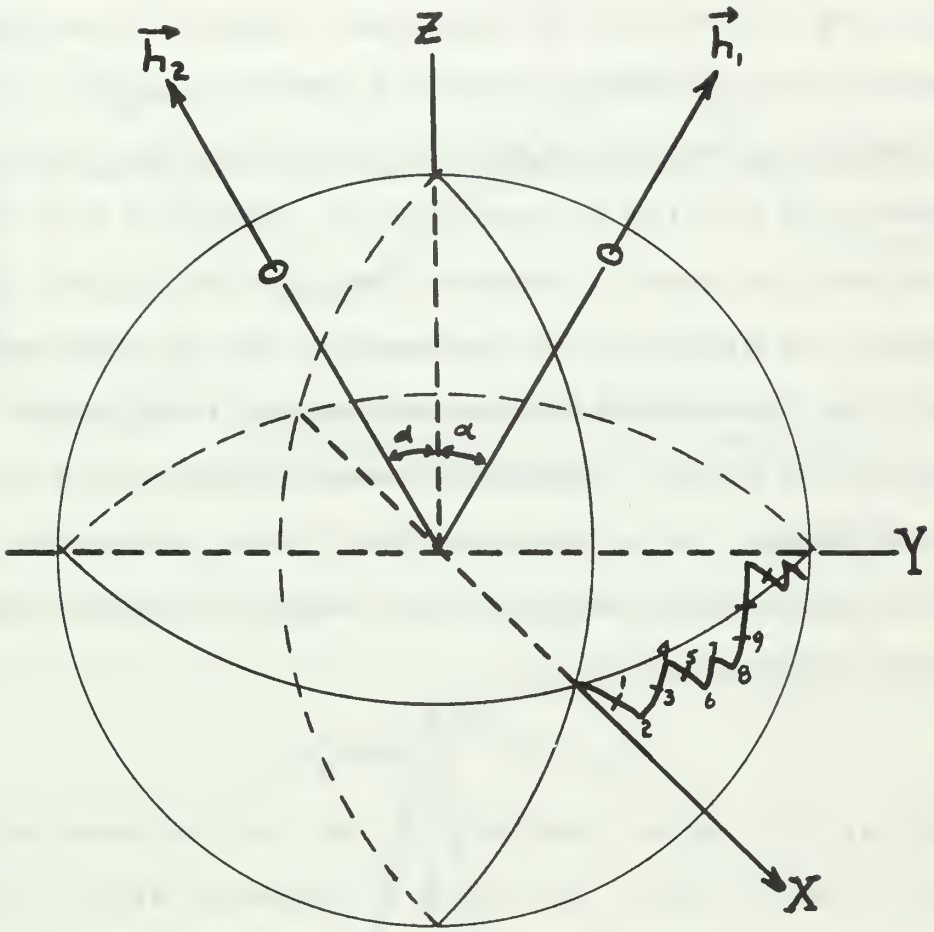

Figure 10. Pictorial representation of the trace of the magnetic moment of a proton as it flips from precession about effective magnetic field $\vec{h}_1$ to $\vec{h}_2$, back and forth.

six, seven, eight, etc. The result is a random path traced on the surface of the sphere.

In the esr experiment an oscillating magnetic field along the X direction is observed. Hence, motion of the M_X component of the proton magnetic moment changing with time is the factor to be determined in the relaxation effect. If the probability of flip is zero, the M_X component will trace out a cosine-like curve. However, when a flip occurs and M changes its direction of precession, the M_X component deviates also from its original trace and begins tracing out a new cosine-like curve. As the $\vec{M}$ trace spreads over the surface of the sphere, it is expected that the M_x component will follow an approximate exponentially decaying cosine curve which can be represented by

$$f_{(t)} = e^{-a_1 t} \cos\omega_o a_2 t \qquad \text{(D4-1)}$$

where a_1 is a decay constant, ω_0 is the frequency with zero probability of flip, and a_2 is a frequency shift factor.

Figure 11 is representative of the function, $f_{(t)}$. The Fourier transform of equation D4-1 (Figure 11b) yields a single peak of frequency $\omega = \omega_0 a_2$ characteristic of the flip probability and hence temperature. Plots of flip probability versus ω may then be made for a given orientation of magnetic field from which coupling constant shift may be correlated with temperature.

5. Monte Carlo Calculation

To calculate this effect, a random (Monte Carlo) technique of generating the most probable function, f'(t),

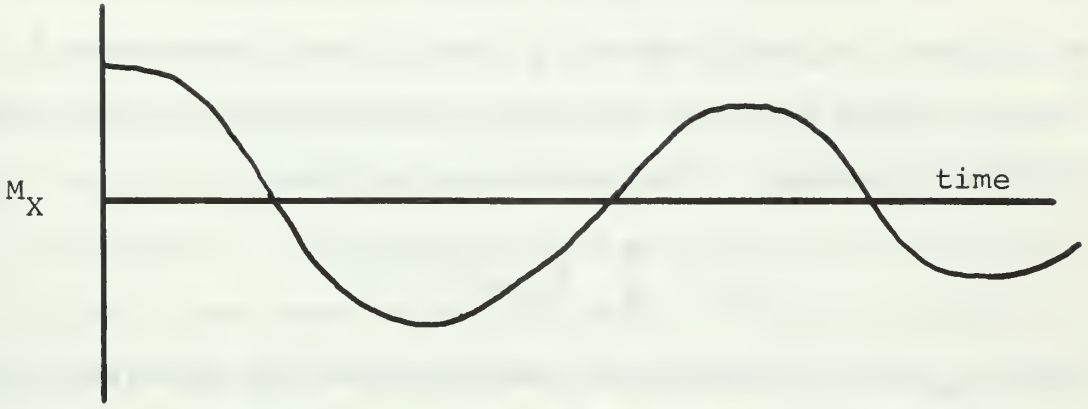

Figure 11a. A decaying cosine function representative of the X component of magnetic moment.

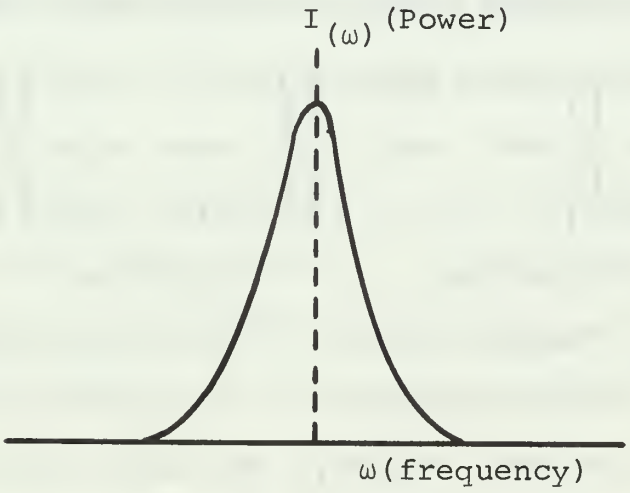

Figure 11b. The Fourier transform of Figure 11a.

approximating that of Figure 11a was used. The computer program was written by Tolles [Ref. 20] and appears in Appendix B.

The magnetic moment $\vec{M}$ initially positioned at (θ_0,ϕ_0) was rotated initially about $\vec{h}_1$ then flipped from about $\vec{h}_1$ to rotation about $\vec{h}_2$, back and forth according to a first order Markoffian process. The problem is to find

$$I_{(\omega)} = \int_0^{\infty} M_{x(t)} e^{i\omega t} dt$$

where $I_{(\omega)}$ is a function of frequency and the integral is a Fourier integral giving the spectral density.

Let Δ be an angle through which the magnetic moment, M, rotates about $\vec{h}_1$ prior to having the opportunity to flip from state $\vec{h}_1$ to $\vec{h}_2$. The position of $\vec{M}$ after rotation by Δ about $\vec{h}_1$ is expressed by the rotation matrix manipulations:

$$\begin{pmatrix} 1 & 0 & 0 \\ 0 & \cos\alpha & \sin\alpha \\ 0 & -\sin\alpha & \cos\alpha \end{pmatrix} \begin{pmatrix} \cos\Delta & -\sin\Delta & 0 \\ \sin\Delta & \cos\Delta & 0 \\ 0 & 0 & 1 \end{pmatrix} \begin{pmatrix} 1 & 0 & 0 \\ 0 & \cos\alpha & -\sin\alpha \\ 0 & \sin\alpha & \cos\alpha \end{pmatrix} \begin{pmatrix} \sin\theta\cos\phi \\ \sin\theta\sin\phi \\ \cos\theta \end{pmatrix} =$$

$$\begin{pmatrix} \cos\Delta & -\sin\Delta\cos\alpha & \sin\Delta\sin\alpha \\ \sin\Delta\cos\alpha & \cos\Delta\cos^2\alpha+\sin^2\alpha & (-\cos\Delta+1)\sin\alpha\cos\alpha \\ -\sin\Delta\sin\alpha & (-\cos\Delta+1)\sin\alpha\cos\alpha & \cos\Delta\sin^2\alpha+\cos^2\alpha \end{pmatrix} \begin{pmatrix} \sin\theta\cos\phi \\ \sin\theta\sin\phi \\ \cos\theta \end{pmatrix}$$

which yield a new point (θ_1,ϕ_1) and hence a new value of the M_x component.

After a flip, rotation of Δ about $\vec{h}_2$ yields another point (θ_n,ϕ_n) expressed as above with each $\sin\alpha$ replaced by $-\sin\alpha$. The rotational transformation is made after each increment of rotation, Δ.

To perform the Monte Carlo calculation a selected number of points along the M_x trace separated by the value of Δ were chosen. For example, 36 points each separated by a Δ of 10° would represent one cycle or one revolution of $\vec{M}$ about $\vec{h}$, 72 points would represent two cycles. A probability, d, of having no spin flip after each increment Δ was chosen, a value of, for example d = 2 representing one chance out of two that the flip will not occur after increment Δ (rapid flipping), a value of d = 100 representing 99 chances out of 100 that no flip will occur (slow flipping). A random number chosen completely arbitrarily was fed to a random number generator (RANDU) which produced in turn another completely random number representing a condition of either "yes flip" or "no flip". RANDU was correlated to randomly permit the system to flip in accordance with the desired flip probability ... 2 or 100, etc.

Starting with a point M_0 (θ_0, ϕ_0), rotation through Δ was calculated and a new value (θ_1, ϕ_1) was determined. At Δ the random number generated by RANDU indicated the system flipped or did not flip. If flip occurred, another value of (θ, ϕ) was calculated based on rotation about $\vec{h}_2$. If no flip occurred, rotation was continued about $\vec{h}_1$. After each increment Δ, the decision was randomly made until the selected number of points was covered. Note that, especially for large probability factors, such as 100, due to randomness of the generated yes/no decision, all points may be covered without any flip while on the other hand, several flips may have

occurred. To obtain a most probable picture of the true physical phenomena, the calculation over the selected number of points was run over and over a selected number of times, the random number generator providing an ever increasing number of adjusted points along the $M_x(f'_{(t)})$ curve. The final point values were then fitted to the damped cosine function $f_{(t)}$, equation D4-1, by a method of least squares.

Output from the Monte Carlo calculation yields a trace of the damped cosine curve, the relative frequency, $\omega_0 a_2$, the exponential decay constant a_1 for the best fitting $f_{(t)}$, and a listing of deviations of the calculated $f'_{(t)}$ curve from the best fitting $f_{(t)}$ curve.

6. Probability as a Function of Temperature

At the time, t, when the first flip decision is made (after Δ_1) the probability, P_n, of no flip is

$$1 - \frac{1}{d} .$$

After $\frac{2\pi}{\Delta}$ decisions, one cycle has elapsed and time

$$t = \frac{1}{\nu} \text{ seconds.}$$

The probability, P_n, of no flip has exponentially decayed to

$$P_n = D^{2\pi/\Delta} \qquad \text{(D6-1)}$$

where

$$D \equiv 1-\frac{1}{d} .$$

Hence equation D6-1 may be rewritten as

$$P_n = e^{-t/\tau_c} \qquad \text{(D6-2)}$$

where t is the time progressed and τ_c is a correlation time

representing the lifetime in a particular state before flipping to the alternate state. Using the relation

$$D = e^{\ln D}$$

the probability of no flip, at $t = \frac{1}{\nu}$ is

$$P_n = \exp(\frac{2\pi}{\Delta} \ln D) = \exp(-1/\nu\tau_c) = \exp(-1/\tau_c).$$

Hence,

$$\tau_c = \frac{-\Delta}{2\pi \ln D} \qquad \text{(D6-4)}$$

where a basis of frequency of 1 Hz has been used.

The results of Tolles et.al. [Ref. 21] and Ohigashi and Kurita [Ref. 15] show

$$\frac{1}{\tau_c} = f_0 e^{-V/RT} \qquad \text{(D6-5)}$$

where f_0 and V are the frequency factor and activation energy for the rotation of the CH_2 group.

For given values of input parameters, Δ and d, τ_c may be calculated by equation D6-4. From these values, temperatures are determined by equation D6-5 resulting in a correlation between flip probability, temperature, and frequency shift as calculated by the Monte Carlo computer program.

7. Fourier Representation of the Spectra

The results of the Monte Carlo calculation yields valuable information about the predicted experimental spectrum representing the system.

The symmetric Fourier integral of the curve, $f_{(t)}$, best fitting the calculated points of $f'_{(t)}$ is

$$F_{(t)} = \int_{-\infty}^{\infty} e^{-i\omega t} e^{-a_1 t} \cos\omega_0 a_2 t dt \quad .$$

Solution of this integral yields,

$$F_{(t)} = \frac{-a_1}{a_1^2+(\omega-\omega_0 a_2)^2} = \frac{-\frac{1}{a_1}}{1+\frac{1}{a_1^2}(\omega-\omega_0 a_2)^2} \quad . \qquad \text{(D7-1)}$$

The Lorentzian line shape function, characteristic of damped oscillatory motion and characteristic of esr absorption spectra, is

$$g_{(\omega)} = \frac{T_2}{1+T_2^2(\omega-\omega_0)^2} \qquad \text{(D7-2)}$$

where T_2 represents relaxation effects. Comparing equations D7-1 and D7-2 the esr line shape parameters become

$$\text{Center frequency} = \omega_0 a_2$$

$$\text{Half height} = \frac{2}{T_2} = 2a_1$$

$$\text{Line width} = \frac{1}{T_2} = a_1 \quad .$$

These factors were used in analyses of the results of Section V-F.

IV. EXPERIMENTAL PROCEDURES

A. CRYSTAL GROWTH

As described by Crawford [Ref. 4] single crystals of zinc acetate dihydrate were grown by slow evaporation of aqueous solutions. A mass ratio of about 2.5:1 water to zinc acetate dihydrate was used to form a nearly saturated solution, aliquots of which were allowed to evaporate from watch glasses. Single crystals formed in 12 to 16 hours.

B. CRYSTAL IRRADIATION

Prior to irradiating a crystal, it was examined under a microscope to determine that the b axis (Figure 3) could be readily identified for proper orientation later in the esr spectrometer. A single crystal was placed on scotch tape and mounted in the open window of an X-ray diffractometer. Three such crystals could be irradiated simultaneously. Exposure was made typically for about two hours at room temperature using 50 KV, 25 ma, and a copper target. Immediately after irradiation, the crystals were placed in closed containers and refrigerated until use. The acetate radicals formed by the X-irradiation remained stable under refrigeration of zero degrees Centigrade up to one month. The signal may remain even longer, but no irradiated crystals were kept longer than this before study.

C. CRYSTAL ALIGNMENT IN THE MAGNETIC FIELD

In order to vary the orientation of the magnetic field, a crystal was rotated through angles θ and ϕ as shown in Figure 12. The angles θ and ϕ are converted to the direction cosines of the magnetic field with respect to a*, b, c axis system through the transformations:

Axis	Direction Cosine
a*	$-\cos\theta$
b	$-\sin\theta \sin\phi$
c	$\sin\theta \cos\phi$.

Using these two angles it was then possible to describe any orientation in a three dimensional system. Since a slight change in the magnetic field orientation will produce significant change in the esr spectrum, precise orientation was necessary.

A crystal to be studied in the esr spectrometer was placed on a quartz rod having both ends ground flat and parallel to each other, one end for crystal mounting, the other for clamping to an extension rod connected above the resonance cavity to an angle indicator for determining the angle θ. The crystal was held on the quartz rod by a spot of stopcock grease acting as a glue. This procedure held the crystal in place over the entire temperature range studied, -150°C to +100°C.

Prior to placing the crystal into the spectrometer, the angle ϕ was established. As mentioned, careful orientation was critical. To establish ϕ, a Bausch and Lomb microscope having a crosshair eyepiece over a calibrated revolving

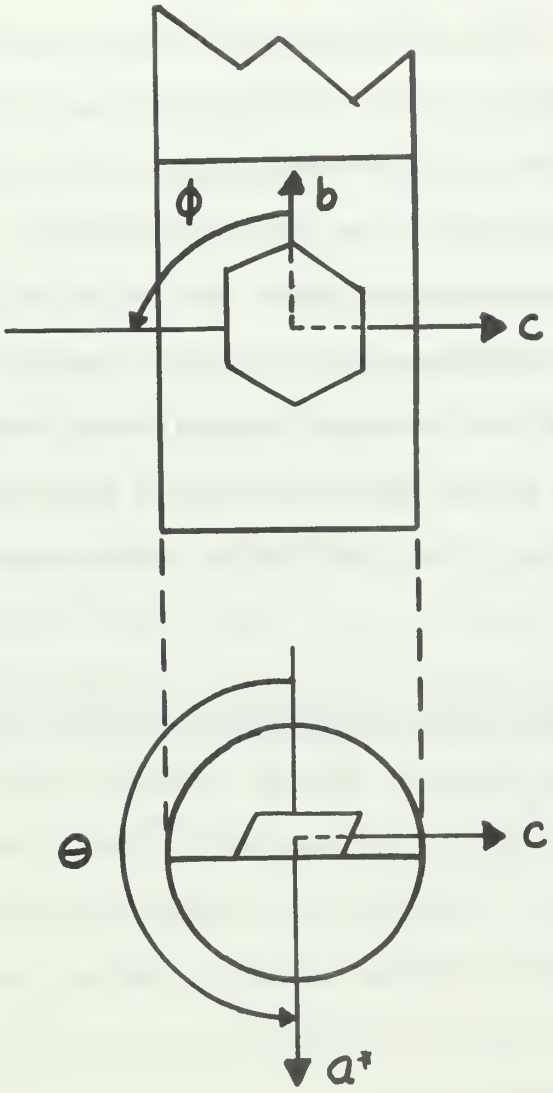

Figure 12. Single crystal of zinc acetate dihydrate mounted on a quartz rod with the b axis coincident with the axis of the rod. Crystal is rotated by ϕ and rod by θ to establish magnetic field orientations. [Ref. 4].

platform was used. The quartz rod was placed on the revolving platform and one crosshair was aligned parallel to the long axis of the rod. The platform (and rod) was rotated through the desired angle ϕ and the crystal was then aligned with the b axis parallel to the crosshair. The angle ϕ could be established to within ±0.5° by this procedure.

The angle θ was established after the crystal and rod were placed into the spectrometer resonance cavity. The end of the rod opposite to the mounted crystal was clamped to the extension rod leading to an angle indicator positioned directly above the cavity. This indicator established angles to within ±1.0°.

D. THE ESR SPECTROMETER AND TEMPERATURE CONTROL UNIT

All data was taken using a Varian V-4502-13 esr spectrometer having a Fieldial V-Fr 2503 magnetic field regulator, a nine inch magnet, and a conventional reflection type cavity. Temperature control was attained using a Varian variable temperature control unit which had been calibrated for proper nitrogen flow to within ±1.5°C.

During warmup and stabilization of the equipment, the angles ϕ and θ were established. With both angles set, the spectrometer was fine tuned at a magnetic field of (3210 + 40.00) gauss, the 40.00 being the initial setting of the Fieldial. The desired temperature was established using liquid nitrogen and nitrogen gas per operating characteristics of the temperature control unit. Ten minutes or longer was allowed for the crystal and cavity to reach temperature equilibrium.

Most data runs were taken at a set orientation of θ and ϕ, annotated as $(^{\theta}_{\phi})$, starting at a given temperature and varying the temperature for each succeeding spectrum. Each time the temperature was changed, thermal equilibrium was allowed to be established prior to recording the spectrum.

With all factors stabilized, first derivative spectra were recorded on an X-Y recorder over a 2.5 minute, 100 gauss sweep of magnetic field. Each absorption line of a spectrum was then determined and labeled using the field dial of the spectrometer. To avoid backlash error of the field dial, all lines were approached from the low magnetic field side when identifications were made. Line values were read to 0.01 gauss. Measurements could be repeated to within ± 0.03 gauss.

V. RESULTS OF PROBLEM SOLUTION

A. VERIFICATION OF SHIFT IN COUPLING CONSTANTS WITH TEMPERATURE

The first objective in this investigation was to confirm the extraordinary shift in coupling constants with temperature observed by Crawford [Ref. 4]. In Section IV, the method of recording experimental data was discussed. Generally, data was taken at a fixed orientation of magnetic field (θ_ϕ) while the temperature was initially set at -150°C and then raised by increments of ten or twenty degrees, spectra being recorded at each temperature increment up to about 90°C. Above 90°C the crystal began to dehydrate and the esr signal due to the $CH_2CO_2^-$ radical rapidly broadened, decreased in intensity, and finally disappeared, no signal being observed at 100°C. This effect was probably due to molecular reorientation upon dehydration leading to destruction of the $CH_2CO_2^-$ radical.

Figure 13 shows characteristic spectra obtained over the temperature range of -150° to +90°C. The particular spectra shown is that for a magnetic field orientation giving rise to two magnetically observable sites within the crystal. Two sets of coupling constants are obtained from spectra of this type, one for orientation (θ_ϕ), the other for orientation ($_{-\phi}^{\theta}$). When ϕ is zero, the two magnetic sites are indistinguishable and spectra characteristic of that in Figure 1 are observed.

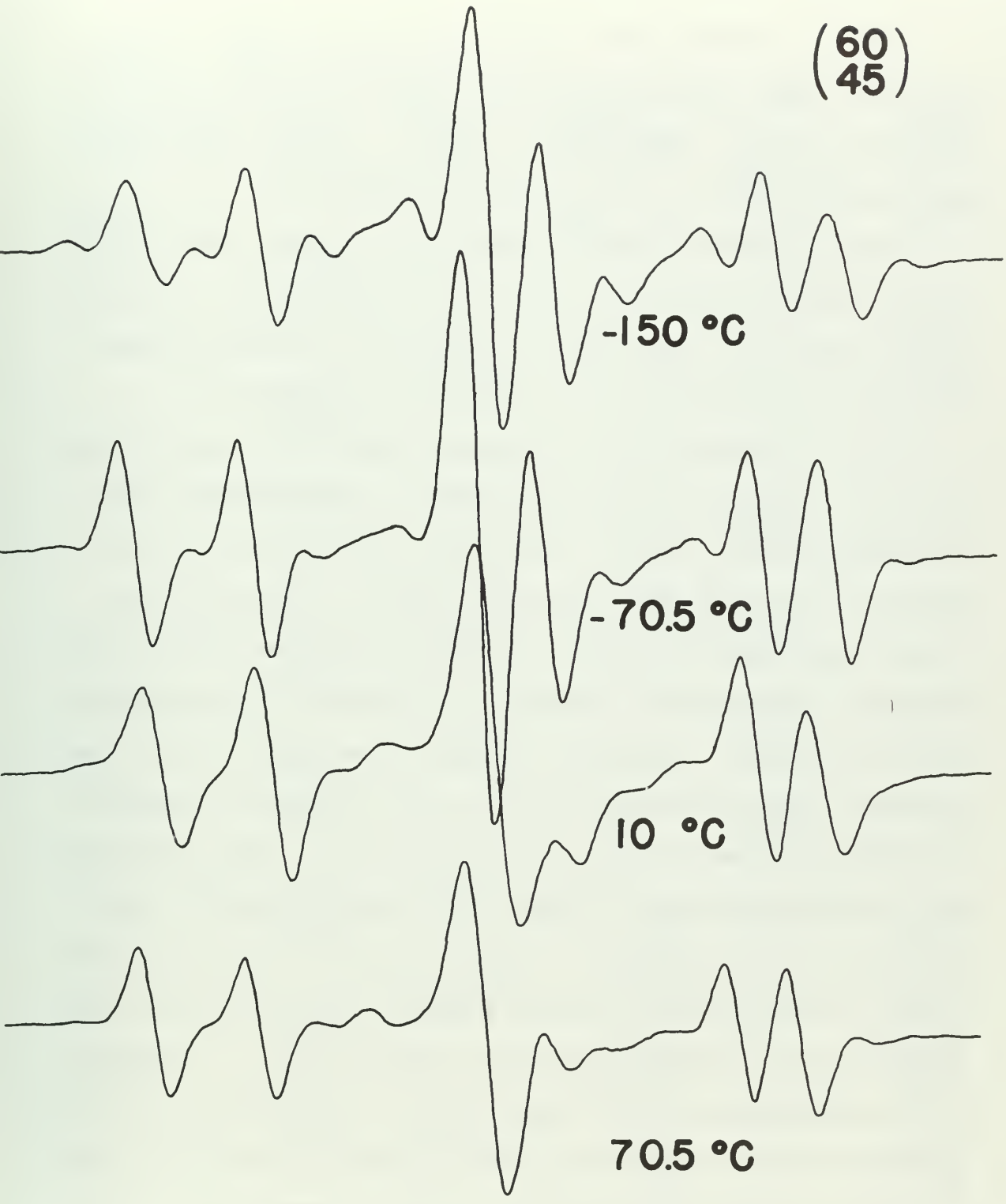

FIGURE 13

Data as recorded from the esr spectra is tabulated in Table I. From the difference in values (in gauss) of the absorption lines, experimental coupling constants were extracted for a corresponding temperature.

Figure 14 shows characteristic plots of the coupling constants versus temperature for given orientations of magnetic field, while the total shift in coupling constants between low and high temperature are tabulated in Table II.

For all orientations of magnetic field, the total observed shift in coupling constants was in close agreement with that observed by Crawford, verifying that the large shift does in fact occur for the $CH_2CO_2^-$ radical. Several additional and very interesting phenomena were observed when the coupling constants were studied at increments of temperature as in Figure 14. Crawford's cursory observation of the temperature effect was based solely on the coupling constants determined at two points, + 25°C and -140°C. This investigation confirms Crawford's observation but in addition shows that for all orientations of magnetic field, the temperature effect is confined to a narrow range of about +30°C to -60°C as seen by the characteristic "S" shaped plots. A decrease in the temperature coefficient was to be expected at low temperatures as the system approached quenched rotation of the CH_2 group, however the decrease at high temperatures above +30°C was totally unexpected and eventually led to formulation of the relaxation model described in Section III. Initially it was thought that the decrease in temperature coefficient

TABLE I. Experimental data.

Field Orien.	Temp (°C)	Field Dial Reading[1]	Diff. Taken	Field Orien.	Temp (°C)	Field Dial Reading[1]	Diff. Taken
(90 / 0)	-150	21.56	39.81	(90 / 0)	+ 8	21.18	40.14
		31.91				*	
		51.12				*	
		61.37				61.32	
	-130	21.55	39.93		+27	21.12	40.16
		31.95				*	
		51.19				*	
		61.48				61.29	
	-110	21.47	40.01		+46	21.08	40.11
		31.88				41.21	
		51.13				61.19	
		61.48					
					+60.5	21.02	40.10
	- 90	21.41	40.08			41.13	
		31.89				61.12	
		51.08					
		61.49			+81	20.98	39.99
						41.01	
	- 70.5	21.34	40.14			60.97	
		31.95					
		50.96			+90.5	20.94	39.95
		61.48				40.96	
						60.89	
	- 50	21.30	40.18	(120 / 0)[3]			
		32.00			-90	Footnote[2]	40.50
		50.88			-70		40.44
		61.48			-63		40.35
					-50		40.25
	- 30.5	21.25	40.23		-43		40.15
		32.61			-33		39.85
		*			-23		39.31
		61.48			-13		38.30
					-11		37.98
	- 11	21.21	40.19		- 3		37.65
		*			+ 8		37.20
		*			+17		36.75
		61.40			+27		36.59
					+51		36.30

[1]Gauss field dial on spectrometer.

[2]Field dial readings will not be listed for remaining data.

[3]Data as corrected for Temperature recalibration.

*Unresolvable.

Field Orien.	Temp. (°C)	Differences Taken
$\binom{120}{0}$	+60.5	36.39
	+67	36.25
	+75	36.25
	+90	36.35
$\binom{135}{0}$ [1]		
	-140	40.86
	-90	40.78
	-70	40.67
	-50	40.50
	-31	39.60
	-20	38.80
	-11	38.15
	- 9	37.95
	1	37.15
	+10	36.90
	+27	36.60
	+42	36.48
	+60.5	36.41
	+80	36.31
$\binom{150}{0}$		
	-150	41.29
	-140	41.29
	-100	41.21
	- 60	41.08
	- 40	40.79
	- 20	40.00
	- 11	39.54
	+ 8	38.86
	+ 27	38.51
	+ 37	38.48
	+ 60.5	38.42
$\binom{165}{0}$ [1]		
	-140	43.14
	-100	43.14
	- 90	43.12
	- 72	43.10
	- 50	43.00
	- 33	42.70
	- 11	42.15
	+ 3	41.86
	+ 27	41.62
	+ 60.5	41.55

Field Orien.	Temp. (°C)	Differences Taken
$\binom{180}{0}$ [1]		
	-90	46.58
	-50	46.41
	-43	46.20
	-33	46.00
	-23	45.81
	-11	45.53
	+ 8	45.05
	+17	44.93
	+27	44.84
	+38	44.72
	+47	44.71
	+60.5	44.69
	+70	44.69
$\binom{45}{30}$		
	-150	54.67
	-130	54.96
	-110	55.32
	- 90	55.46
	- 70.5	55.43
	- 50	55.33
	- 30.5	54.84
	- 11	53.50
	+ 8	52.20
	+ 27	51.61
	+ 46	51.25
	+ 60.5	50.88
	+ 70.5	50.81
	+ 81	50.86
	+ 90.5	50.89
$\binom{45}{-30}$		
	-150	45.35
	-130	45.45
	-110	45.66
	- 90	45.66
	- 70.5	45.62
	- 50	45.65
	- 30.5	45.34
	- 11	45.00
	+ 8	44.40
	+ 27	44.15
	+ 46	44.05
	+ 60.5	43.80
	+ 70.5	43.85

[1] Data as corrected for Temperature recalibration.

Field Orien.	Temp. (°C)	Differences Taken
(45 / -30)	+ 81	43.88
	+ 90.5	43.84
(55.3 / 48.2)	-150	55.91
	-140	55.97
	-130	56.02
	-120	56.12
	-110	56.20
	-100	56.34
	- 90	56.44
	- 80	56.60
	- 70	56.76
	- 50	56.88
	- 40	56.85
	- 30	56.83
	- 20	56.69
	- 10	56.52
	0	55.89
	+ 5	55.66
	+ 20	54.84
	+ 40	53.92
	+ 60	52.99
	+ 70	52.96
(55.3 / -48.2)	-150	42.37
	-140	42.27
	-130	42.22
	-120	42.13
	-110	42.09
	-100	42.04
	- 90	41.99
	- 80	41.90
	- 70	41.81
	- 50	41.67
	- 40	41.63
	- 30	41.59
	- 20	41.48
	- 10	41.37
	0	40.96
	+ 5	40.82
	+ 20	40.39
	+ 40	39.90
	+ 60	39.34
	+ 70	39.35

Field Orien.	Temp. (°C)	Differences Taken
(60 / 45)	-150	41.88
	-130	41.78
	-110	41.72
	- 90	41.65
	- 70.5	41.59
	- 50	41.42
	- 30.5	41.05
	- 11	40.35
	+ 8	39.81
	+ 18	39.61
	+ 27	39.42
	+ 46	39.26
	+ 60.5	39.25
	+ 70.5	39.24
	+ 81	39.36
(60 / 45)	-150	56.76
	-130	56.97
	-110	57.08
	- 90	57.06
	- 70.5	57.00
	- 50	56.85
	- 30.5	56.49
	- 11	55.47
	+ 8	54.19
	+ 18	53.70
	+ 27	53.39
	+ 46	53.04
	+ 60.5	52.91
	+ 70.5	52.85
	+ 81	52.73
(90 / 45)	-150	52.32
	-130	52.33
	-110	52.27
	- 90	52.22
	- 70.5	52.18
	- 50	51.99
	- 30.5	51.60
	- 11	50.71
	+ 8	49.59
	+ 27	49.00
	+ 46	48.75
	+ 60.5	48.62
	+ 70.5	48.47
	+ 81	48.40

Field Orien.	Temp. (°C)	Differences Taken
(90, -45)	-150	40.85
	-130	40.45
	-110	40.27
	- 90	40.24
	- 70.5	40.20
	- 50	40.14
	- 30.5	39.39
	- 11	37.04
	+ 8	35.51
	+ 27	34.89
	+ 46	34.63
	+ 60.5	34.55
	+ 70.5	34.55
	+ 81	34.55
	+ 90.5	34.54
(90, 90)	-150	47.14
	-130	47.01
	-110	46.86
	- 90	46.79
	- 70.5	46.65
	- 50	46.44
	- 30.5	46.03
	- 11	45.38
	+ 8	44.82
	+ 27	44.47
	+ 46	44.29
	+ 60.5	44.16
	+ 70.5	44.13
	+ 81	44.05
	+ 90.5	44.00

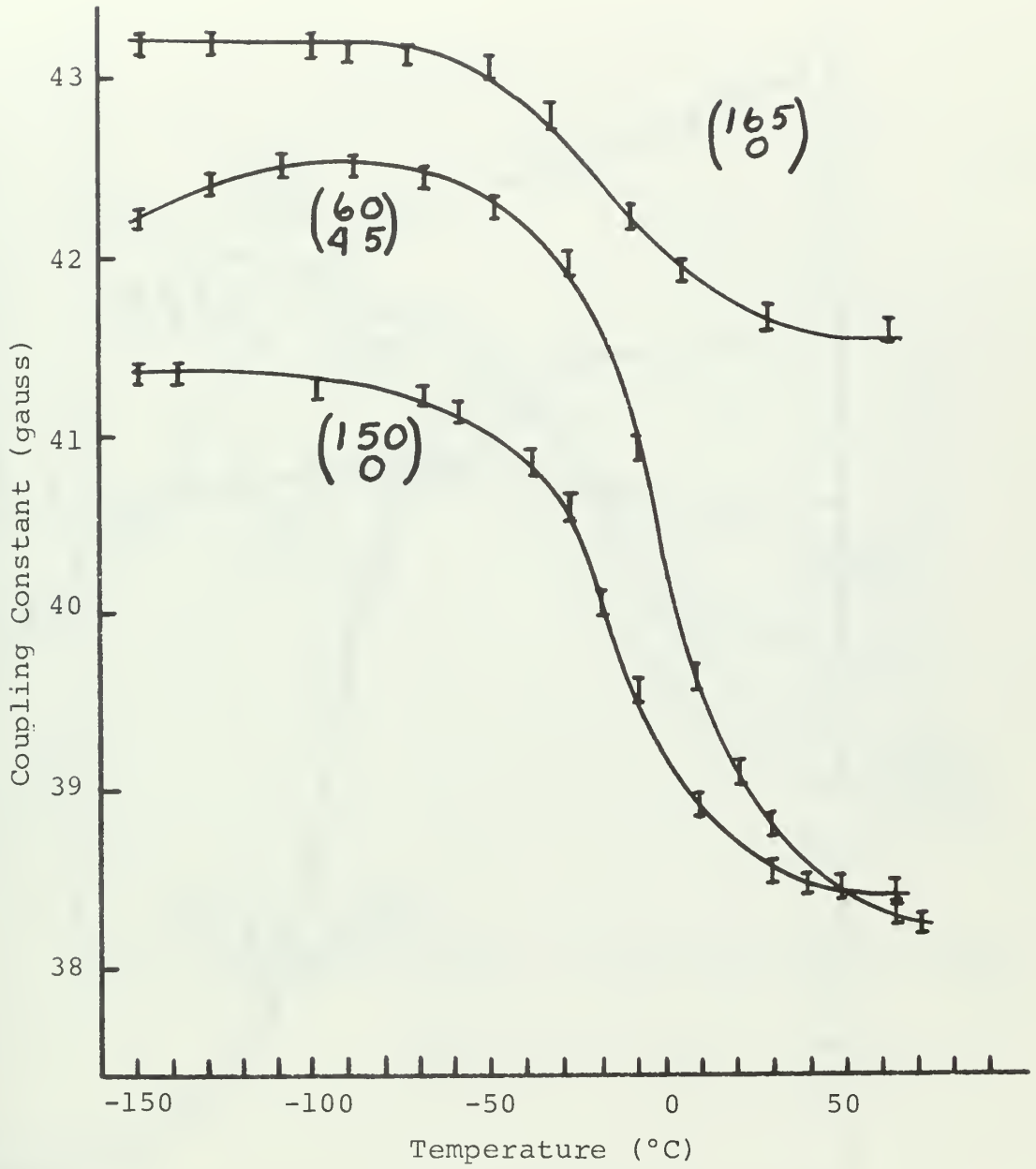

Figure 14a. Experimental results of the coupling constant dependence on temperature for selected magnetic field orientations, $\binom{\theta}{\phi}$

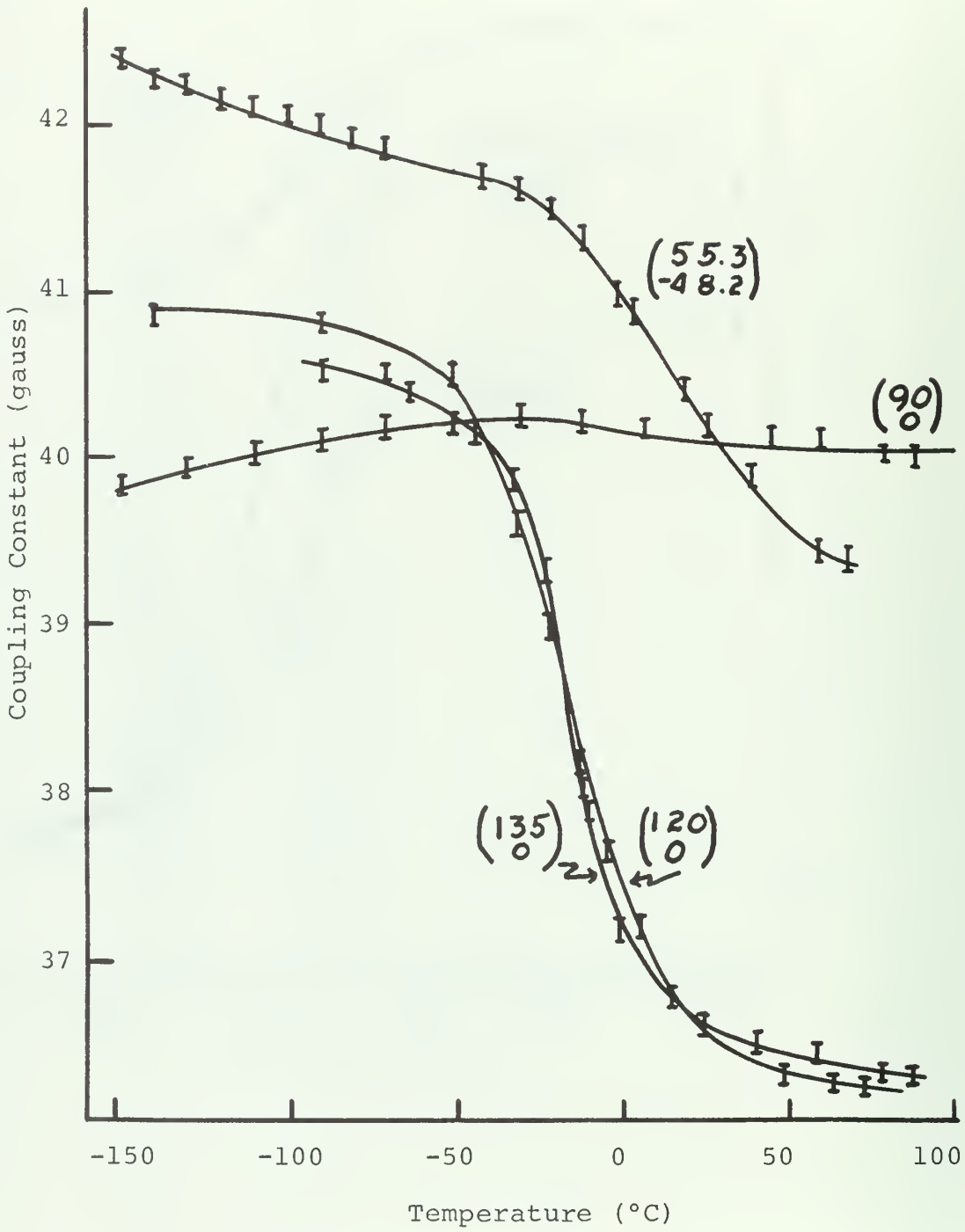

Figure 14b. Experimental results of the coupling constant dependence on temperature for selected magnetic field orientations, $\binom{\theta}{\phi}$

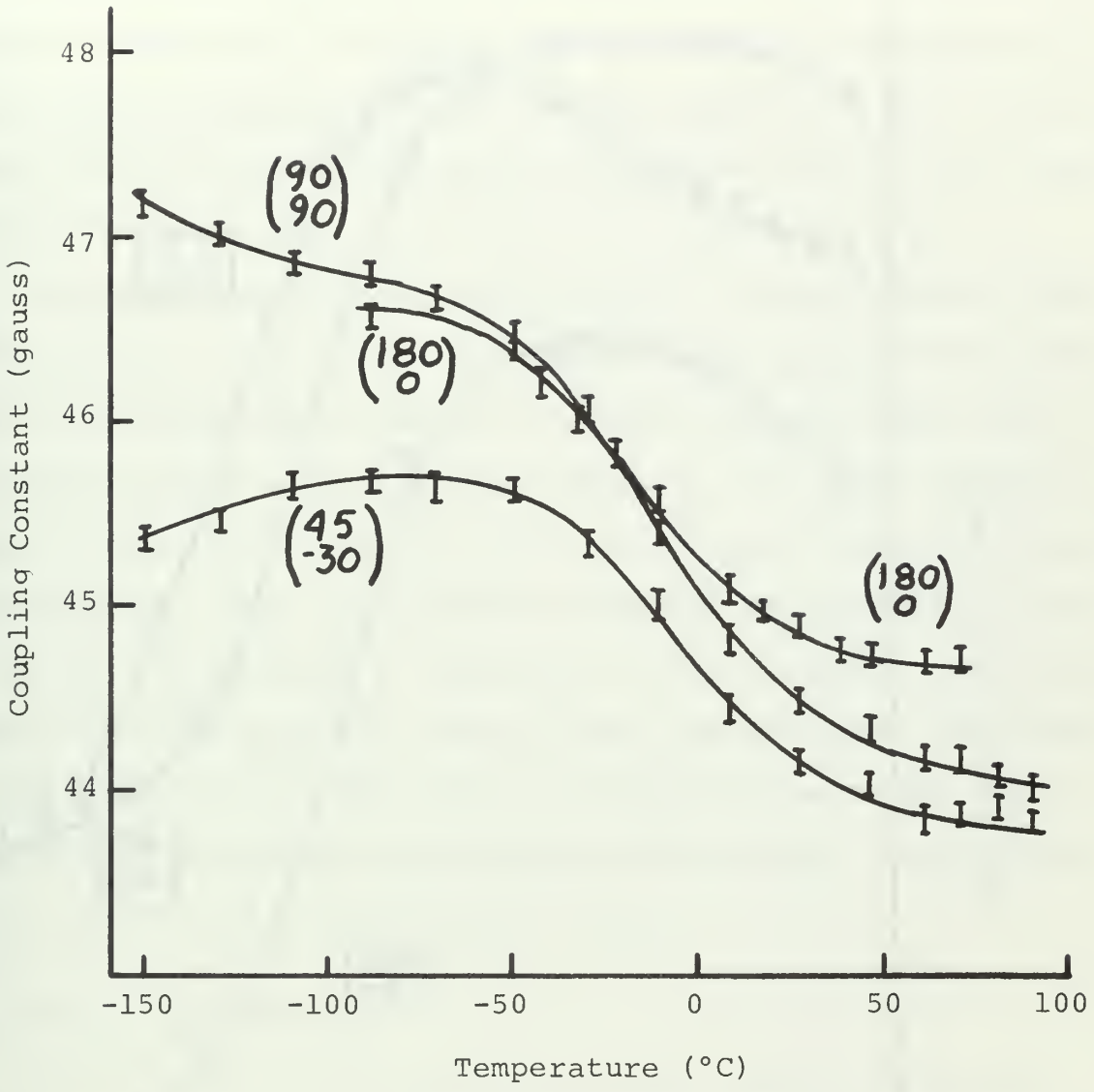

Figure 14c. Experimental results of the coupling constant dependence on temperature for selected magnetic field orientations, $\binom{\theta}{\phi}$.

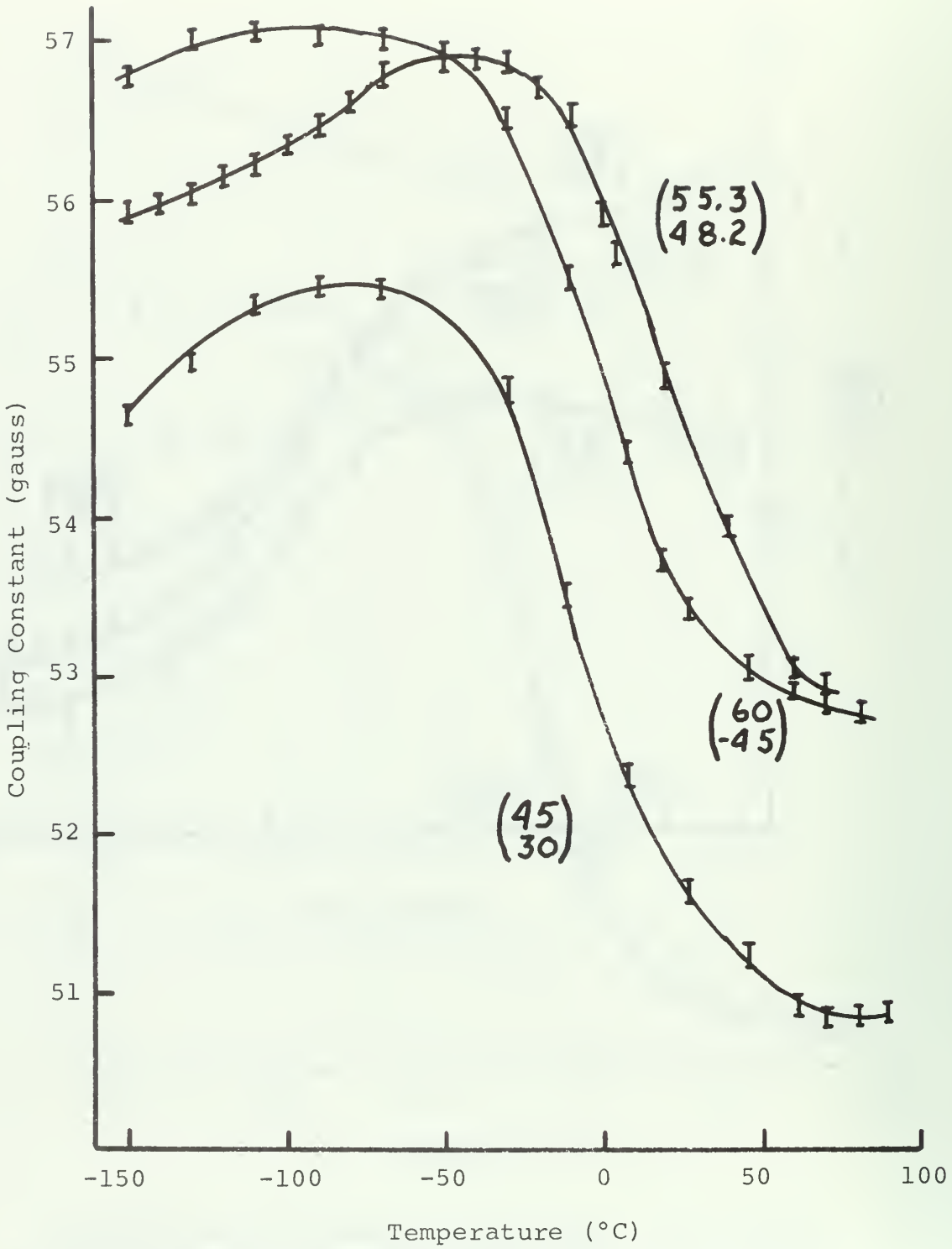

Figure 14d. Experimental results of the coupling constant dependence on temperature for selected magnetic field orientations, $\binom{\theta}{\phi}$.

may be due to a crystallographic change in the system occurring at about 30°C. However, X ray diffraction patterns of the crystal compared at approximately liquid nitrogen temperatures and at temperatures above 30°C showed that no such phase change had occurred.

The experimental data shows that for those magnetic field orientations at which the two magnetically inequivalent sites can be distinguished there is a characteristic rise or drop in the coupling constants after leveling off as the temperature is lowered. This drift of the coupling constants remains unexplained. The total shift in coupling constants tabulated in Table II are based on the shift observed between the points where leveling occurs at low and high temperatures, the noted drift being disregarded. This procedure proved to be justified based on calculations of the overall shift to be discussed under the relaxation effect results.

B. MODEL DEVELOPMENT

Experimental proof of the coupling constant dependence upon temperature led to development of a model by which the effect could be explained. The work of Tolles et.al [Ref. 21] and Ohigashi and Kurita [Ref. 15] showed rotation of the CH_2 group about the C-C bond; hence the restricted rotor was chosen as the initial model to be studied.

The Hamiltonian for the restricted rotor has been discussed in Section III and was seen to be

$$H = BL_z^2 + \frac{\nu}{2}(1-\cos 2\phi')$$

TABLE II. Total coupling constant shifts observed experimentally

Field Orientation	Total Shift[1] (gauss)
$\begin{pmatrix} 90 \\ 0 \end{pmatrix}$	0.35
$\begin{pmatrix} 120 \\ 0 \end{pmatrix}$	1.25
$\begin{pmatrix} 135 \\ 0 \end{pmatrix}$	4.48
$\begin{pmatrix} 150 \\ 0 \end{pmatrix}$	2.90
$\begin{pmatrix} 165 \\ 0 \end{pmatrix}$	1.60
$\begin{pmatrix} 180 \\ 0 \end{pmatrix}$	1.86
$\begin{pmatrix} 45 \\ 30 \end{pmatrix}$	4.61
$\begin{pmatrix} 45 \\ -30 \end{pmatrix}$	1.80
$\begin{pmatrix} 55.3 \\ 48.2 \end{pmatrix}$	3.95
$\begin{pmatrix} 55.3 \\ -48.2 \end{pmatrix}$	2.34
$\begin{pmatrix} 60 \\ 45 \end{pmatrix}$	4.28
$\begin{pmatrix} 60 \\ -45 \end{pmatrix}$	2.50
$\begin{pmatrix} 90 \\ 45 \end{pmatrix}$	3.70
$\begin{pmatrix} 90 \\ -45 \end{pmatrix}$	5.69
$\begin{pmatrix} 90 \\ 90 \end{pmatrix}$	2.70

[1]Measured by the difference in extreme absorption lines.

where solution of the Hamiltonian matrix elements and computerized diagonalization of the resulting secular determinant led to the eigenvalues characteristic of the restricted rotor system. Using the results of Tolles et.al. [Ref. 21] for an H-C-H angle of 116.9° and a C-H bond length of 1.08Å, the moment of inertia, I, of the CH_2 rotation about the C-C bond was calculated to be 1.69408Å. The barrier potential, V, of 5.8 kcal/mol was converted to units of V/H and found to be 60.8524 THz (terahertz). Knowing I, B was calculated to be 0.298414 THz in units of B/h. From these values, the Hamiltonian matrix elements were readily calculated for integer values of m.

As it was obviously impossible to work with a determinant of infinite size corresponding to the range of m values of minus to plus infinity, several determinants of increasingly larger size were solved until the variance in eigenvalues from one size to the next larger size was within 0.2% or approximately 0.1 THz. It was found that a 29 x 29 determinant (m having values -14 to +14) was the smallest to meet these requirements. Tabulation of the eigenvalues for the 29 x 29 determinant appear in Table III.

Examination of the resulting eigenvalues for the restricted rotor shown in Table III showed each energy level to be doubly degenerate as expected from the solution of Schroedinger's equation which yields energy values

$$E = \frac{m^2h^2}{2I}$$

so that a -m or +m value yields the same eigenvalue.

TABLE III. Eigenvalues of the restricted rotor model.

Energy Level	Restricted Rotor Eigenvalues[1] THz)
0	4.1853
	4.1853
1	12.3979
	12.3981
2	20.2843
	20.2861
3	27.8221
	27.8318
4	34.9854
	35.0223
5	41.7450
	41.8451
6	48.0342
	48.2856
7	53.9234
	54.0146
8	58.1838
	60.0289

[1]Values obtained using a barrier to internal rotation of 5.8 kcal/mol.

Further examination showed that for the first four levels above ground state there was an approximately 8 THz difference between levels and that the ground state level itself was 4.19 THz which is approximately half of the energy level differences. This observation suggested immediately that the restricted rotor system might well be approximated by an harmonic oscillator which has energy levels represented by

$$E = (n+\frac{1}{2})h\nu \qquad \text{(equation III-A2-1)}$$

and which in itself is one limit of a restricted rotor. The harmonic oscillator approximation was applied to the restricted rotor, and energy levels were calculated by using equation III-A2-1 as rearranged to obtain the eigenvalues in units consistent with those of the restricted rotor. (Equation III-A2-3, Page 27). Values of n equal zero to eight were used in the calculation, the results of which were compared to the restricted rotor results and appear in Table IV. Examination of Table IV shows that there is good agreement between the two models in the first four levels above ground state, but that at higher energy levels, the oscillator model yields increasingly higher results.

A Boltzman distribution calculation to obtain approximate population of energy levels in the harmonic oscillator is shown in Table V.

Based on negligible population of energy levels higher than the fourth excited state, the harmonic oscillator was assumed to be a good approximation to the restricted rotor and subsequent calculations were based on this approximation.

TABLE IV. Eigenvalues of the restricted rotor and the harmonic oscillator model

Energy Level	Restricted Rotor Eigenvalues (THz)	Harmonic Oscillator Eigenvalues (THz)
0	4.1853 4.1853	4.2614
1	12.3979 12.3981	12.7842
2	20.2843 20.2861	21.3070
3	27.8221 27.8318	29.8298
4	34.9854 35.0223	38.3526
5	41.7450 41.8451	46.8574
6	48.0342 48.2856	55.3982
7	53.9234 54.0146	63.9210
8	58.1838 60.0289	72.4438

1. Values obtained using a barrier to internal rotation of 5.8 kcal/mol.

TABLE V. Energy level populations in the harmonic oscillator model.

Energy Level	Percentage Population At 273°K	Percentage Population At 133°K
0	68.9	94.54
1	23.5	5.15
2	5.8	0.29
3	1.6	0.02
4	0.2	0.00043

C. SHIFT OF COUPLING CONSTANTS DUE TO DIPOLAR INTERACTION

In Section III development of the calculation used to determine the average coupling constant as a function of temperature ($\langle A \rangle_T$) based on the effect of dipolar interaction was discussed. It was seen that the relation to be solved was

$$\langle A \rangle_T = \int_{-90}^{+90} 3.77629 A_{\phi'} \sum_n e^{-\zeta^2} H_{n(\zeta)} \frac{e^{-E_n/KT}}{Z} d\phi' \ .$$

(equation III A-3-27)

In the development of this equation, a number of computerized subroutines were written to the basic computer program SSESR to yield program PREDICT II which appears in Appendix A. Not considering hyperconjugation effects (Subroutine CCCA) which will be considered in the next section of this work, equation III-A3-27 was solved by PREDICT II to yield the shift in coupling constants for selected magnetic field orientations

over a temperature range of +90°C to -150°C. The overall shifts are tabulated in Table VI.

Before considering the significance of the results, the manner in which PREDICT II was utilized will be discussed.

The theoretical development of each of the individual subroutines was discussed in Section III-A-3. Basic input data to the main program consisted of those parameters which Tolles et.al [Ref. 21] determined for the planar form of the $CH_2CO_2^-$ radical plus parameters determined in this work to include,

The number of protons in the radical = 2.

The magnitude of the magnetic field or the nuclear Zeeman frequency = 13.8 THz.

The principal values of the coupling tensors (coupling constants) as listed on page 18 of this work.

The orientation of external magnetic field, $\binom{\theta}{\phi}$.

The direction cosines of the H tensor as listed on page 20 of this work.

The first five eigenvalues of the harmonic oscillator as developed in section V-2 and appearing in Table IV.

The temperatures at which the coupling constants were to be calculated.

The limits of integration, -90° to +90°.

The increments of $d\phi'$ used in the numerical integration, 3°.

Miscellaneous constants as appropriate.

The output yielded the esr spectrum at any given angle of rotation, ϕ', in terms of transition frequencies and intensities as intermediate results. The coupling constants were then determined by frequency differences and automatically fed back into the program to yield the average coupling constants $\langle A \rangle_T$ at given values of input temperatures for dipolar coupling effects.

It was of prime concern to insure that PREDICT II was rotating (operating) properly and yielding reliable results. Hence, two operational tests were devised and used as checks.

1. Test One for Proper Rotation

The spectra computed at +90° rotation might be expected to be coincident with that at -90°, and this would make an ideal check for proper rotation. Initially the results of the two rotations did not agree which led to incorporation of subroutine REFH which insured orthonormality of the coupling tensors H_1 and H_2. It must be noted, in addition, however, that the input coupling constants for proton one are not exactly the same as those for proton two, hence the dipolar effect cannot be expected to yield identical results for +90° and -90° of rotation. To check for proper rotation, both sets of input coupling constants were made identical (arbitrarily, identical to those of proton one) and rotation by PREDICT II was found to yield identical spectra at +90° and -90° of rotation. This procedure gave one good confirmation that PREDICT II was operating properly. For all future calculations except where indicated, input coupling constants were assigned their original values.

2. Test Two for Proper Rotation

Using the transformation

$$\left(M \right) \begin{vmatrix} \cos\phi & \sin\phi & 0 \\ -\sin\phi & \cos\phi & 0 \\ 0 & 0 & 1 \end{vmatrix} \left(M^{-1} \right)$$

an orientation of magnetic field $\binom{180}{0}$ was rotated through an angle ϕ of 90°, where the matrix M is that for the direction cosines of magnetic field $\binom{180}{0}$. This transformation was performed with aid of a desk calculator and yielded new direction cosines for the magnetic field of

0.323832

0.896897

0.301199 .

These direction cosines were then fed to PREDICT II as input direction cosines for the magnetic field while also setting the input coupling constants identical as in test one, and the spectra were computed for angles of CH_2 rotation of -90° and +90°. If the program was rotating properly, the resulting spectra were expected to correspond to that spectrum for an input of magnetic field orientation $\binom{180}{0}$ at 0° rotation of the CH_2 group. Agreement was excellent and it was concluded that PREDICT II was rotating properly.

Table VI shows that a shift in coupling constants between -150°C and +90°C did occur due to dipolar coupling, however the magnitude of the effect in no instance was that observed experimentally. The direction of the dipolar coupling effect was seen to be dependent on the external magnetic

TABLE VI. Calculated coupling constant shift over temperature range of -150°C to +90°C due to dipolar coupling.[1]

Field Orientation	Shift (gauss)
$\binom{45}{30}$	-0.013
$\binom{45}{60}$	+0.006
$\binom{60}{60}$	0.000
$\binom{75}{30}$	+0.033
$\binom{75}{60}$	-0.035
$\binom{90}{45}$	-0.054
$\binom{90}{-45}$	+0.045
$\binom{90}{75}$	-0.091
$\binom{90}{90}$	-0.079
$\binom{120}{0}$	+0.048
$\binom{135}{0}$	+0.013
$\binom{150}{0}$	-0.013
$\binom{165}{0}$	-0.079
$\binom{180}{0}$	-0.119

[1]All shifts are determined by subtracting the coupling constant at -150°C from that at +90°C.

field. Table VI shows that some magnetic fields caused an effect which led to an increase of coupling constants with increasing temperature (dipolar coupling values positive) while others led to a decrease in coupling constant with increasing temperature (dipolar coupling values negative), the general effect observed experimentally. This effect was also observed graphically with plots as shown in Figure 15 where the calculated coupling constants due to dipolar interaction have been plotted against angle of CH_2 rotation, ϕ', for several magnetic field orientations.

As the temperature is raised, greater angles of ϕ' are attained. Hence, analysis of Figure 15 showed that increasing temperature would be expected to cause an increase in coupling constants for those plots having positive curvature at ϕ' equal zero (e.g. the $\binom{120}{0}$ plot) and a decrease in coupling constants for those plots with negative curvature at ϕ' equal zero (e.g. the $\binom{90}{75}$ plot). The curvature of the plots and the direction of coupling constant shift in Table VI agreed. The $\binom{150}{0}$ orientation showed curvature of nearly zero and this too agreed with the nearly zero value seen in Table VI.

These results showed that although some shift in coupling constants occurred due to dipolar interaction, the direction of shift was not always consistent with that observed experimentally and hence dipolar interaction was not the primary cause of the effect.

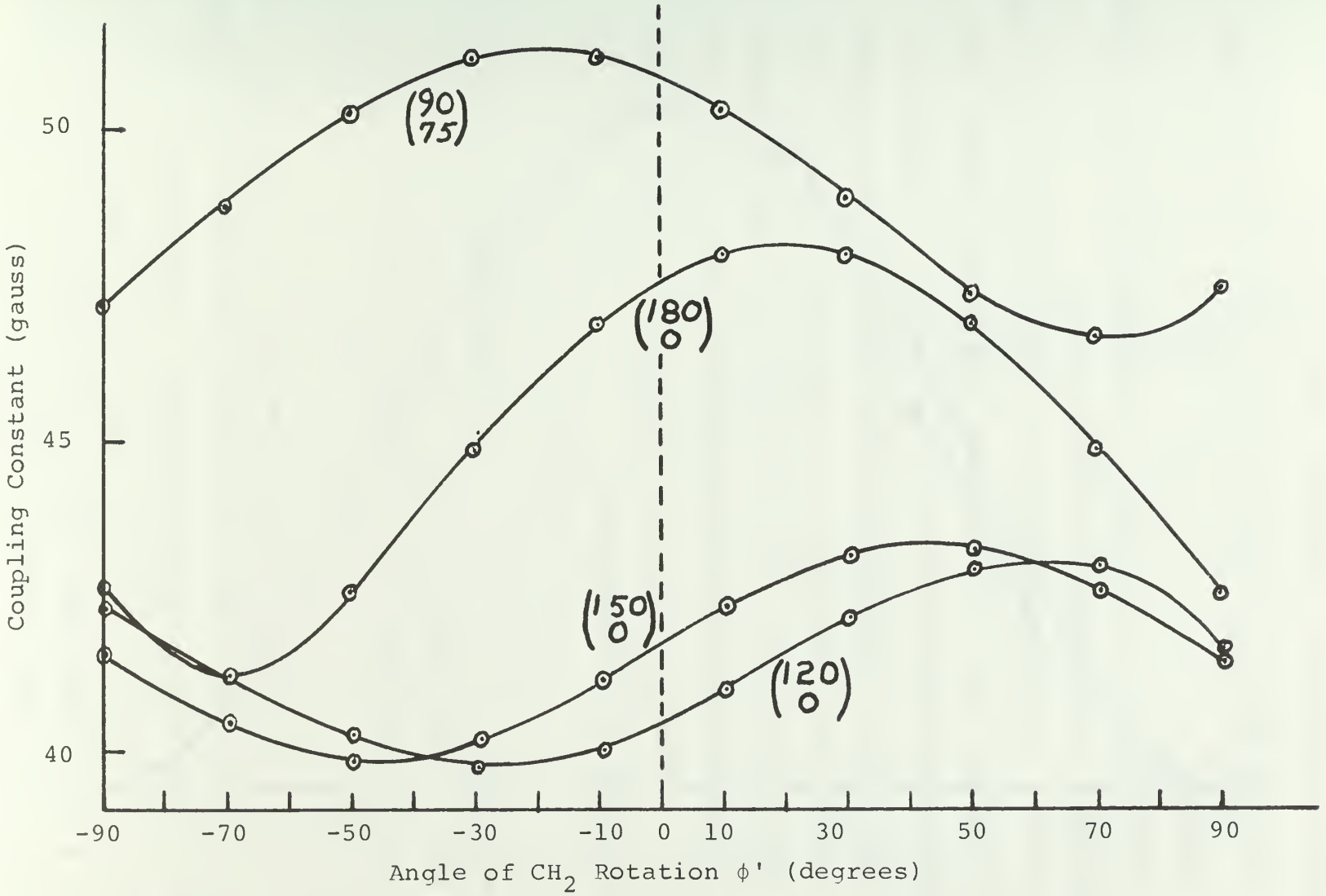

Figure 15. Calculated coupling constants due to dipolar interaction as a function of ϕ'.

It was of note that although the calculated shift was small, the magnitude was the same order as that observed for the methyl radical by Zlochower et.al [Ref. 23].

D. SHIFT OF COUPLING CONSTANTS DUE TO FERMI CONTACT INTERACTION

The theory of hyperconjugation and resulting Fermi contact interaction was discussed in Section III-B.

Using a computerized orbital calculation based on the CNDO approximation [Ref. 19] the proton 2S molecular orbital coefficients were calculated for various angles of rotation, ϕ'. The coefficients squared yielded the amount of free electron spin density that was imparted to the proton 2S orbitals for any angle of rotation. The solid curve of Figure 16 shows a plot of the resulting spin densities versus the angle of rotation, ϕ', which upon examination appeared to closely approximate a function represented by

$$f_{(\phi')} = A\sin^2 2\phi'$$

of amplitude $A = 0.273 \times 10^{-2}$. The dotted curve of Figure 16 is a plot of this function to show that, in fact, the hyperconjugation effect did very closely approximate the $\sin^2 2\phi'$ relationship.

If the entire electron (spin density = 1.0) were found in a proton 2S orbital, then the coupling constants of the planar radical (where due to orbital symmetry, no spin density appears in the proton 2s orbital) would be increased by the factor B = 1,420.4058 MHz, the hyperfine coupling constant of a hydrogen atom with a complete electron in the 2s orbital.

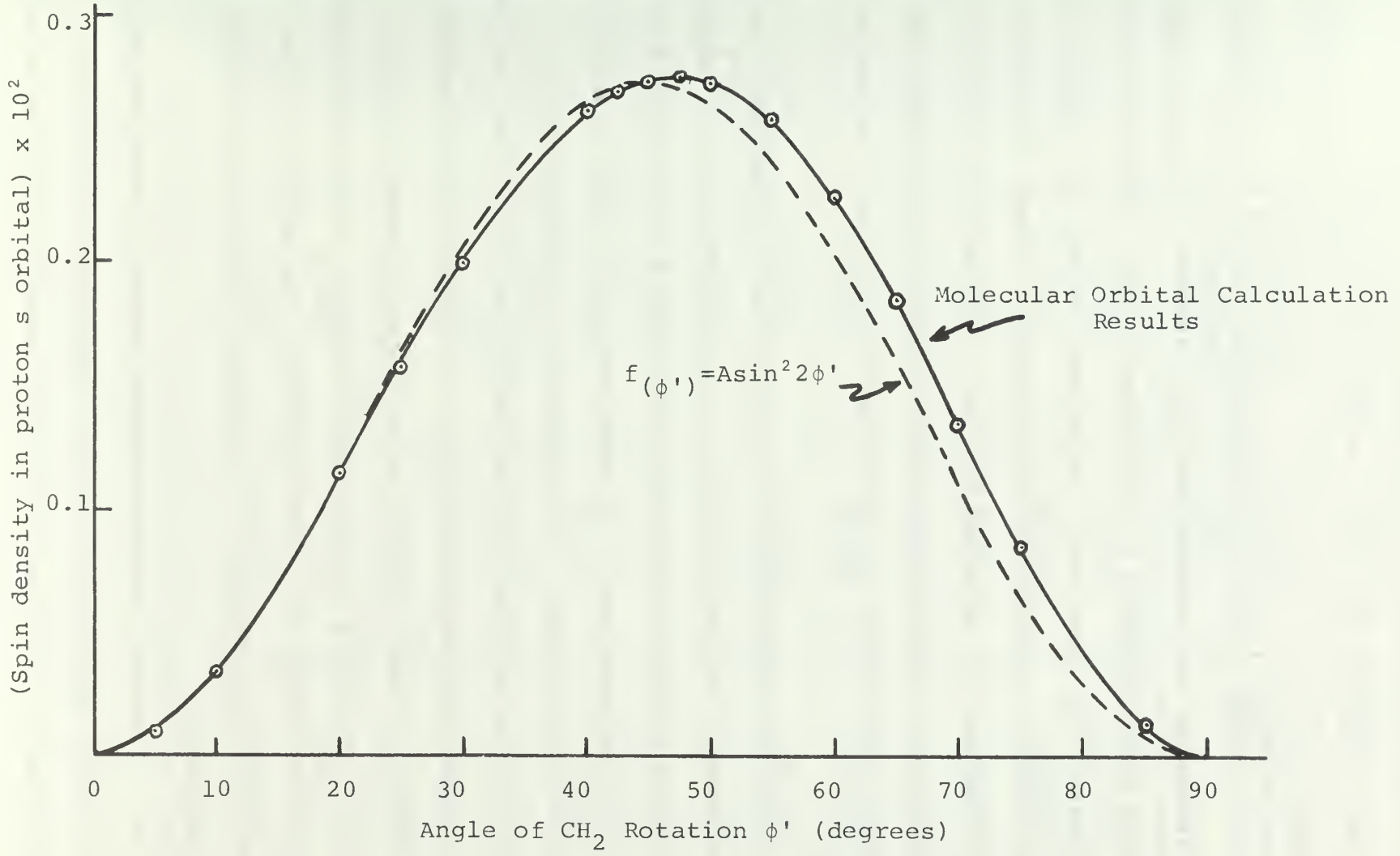

Figure 16. Results of molecular orbital calculation for Fermi contact (hyperconjugation) interaction compared to $f_{(\phi')}A\sin^2 2\phi'$.

Hence, the input coupling constants for the planar radical, A_i, were adjusted for Fermi contact interaction through the relation

$$A_{\phi'} = A_i + B(0.273 \times 10^{-2} \sin^2 2\phi') \ .$$

This relation was incorporated into PREDICT II through subroutine CCCA (Appendix A) and values of the average coupling constants $\langle A \rangle_T$, were again calculated having both dipolar and Fermi contact interaction incorporated. Column 2 of Table VII shows the results obtained for the total shift in coupling constants over temperature range -150°C to +90°C which can be compared with column 3, the values for dipolar interaction only.

Since the hyperconjugation effect has no dependence on orientation of magnetic field but only on angle of rotation, ϕ', it was expected that the effect should be constant for all field orientations. By subtracting the dipolar effect from the total effect, the magnitude of hyperconjugation effect on the coupling constant shift was determined, the results being tabulated in column 4 of Table VII. As expected, the effect is essentially constant for all magnetic field orientations having a value equal to about -0.19 gauss over a temperature range of -150°C to +90°C. The negative value corresponds to a decrease in coupling constant with increasing temperature.

The calculated average coupling constants incorporating both effects were plotted versus temperature giving plots characteristic of Figure 17 for all magnetic field orientations

TABLE VII. Calculated hyperconjugation effect (Fermi contact interaction) on coupling constant shift.[1]

Field Orientation	Shift with Dipolar and Fermi Contact Interaction (gauss)	Shift with Dipolar Interaction Only (gauss)	Shift Due to Hyperconjugation (Fermi Contact) (gauss)
$\binom{45}{30}$	-0.209	-0.013	-0.196
$\binom{45}{60}$	-0.189	-0.006	-0.195
$\binom{60}{60}$	-0.196	0.00	-0.196
$\binom{75}{30}$	-0.158	+0.033	-0.191
$\binom{75}{60}$	-0.220	-0.035	-0.185
$\binom{90}{45}$	-0.245	-0.054	-0.191
$\binom{90}{-45}$	-0.128	+0.045	-0.173
$\binom{90}{75}$	-0.283	-0.091	-0.192
$\binom{90}{90}$	-0.264	-0.079	-0.185
$\binom{120}{0}$	-0.128	+0.048	-0.176
$\binom{135}{0}$	-0.167	+0.013	-0.180
$\binom{150}{0}$	-0.198	-0.013	-0.185
$\binom{165}{0}$	-0.268	-0.079	-0.189
$\binom{180}{0}$	-0.311	+0.119	-0.192

[1]All shifts are determined by subtracting the coupling constant at -150°C from that at +90°C.

studied. Examination of these plots and the data of Table VII led to several conclusions regarding the model as calculated to this point.

First there appeared to be a definite effect on the coupling constants when both dipolar and Fermi contact interaction were considered. The overall effect led to an increase in coupling constants with decrease in temperature as observed experimentally, the primary effect arising from Fermi contact interaction. The plots of Figure 17 indicate a decrease in the temperature coefficient as lower temperatures were approached indicative of quenching of the rotational motion. This observation agreed with experiment but it was of note that no such temperature coefficient decrease occurred at higher temperatures in the calculated effects. Of greatest significance, however, was the magnitude of the calculated effects which was seen to be only about 0.1 to 0.3 gauss, not nearly that observed experimentally (1-6 gauss).

Figure 18 compares a typical experimental result with that calculated on the basis of dipolar and Fermi contact interaction.

Based upon the foregoing observations, it was concluded that although the calculated model showed an overall effect generally of the form observed experimentally, and although dipolar and Fermi contact interaction can be expected to contribute to the shift in coupling constants, these were only a small part of some larger effect which was yet to be established.

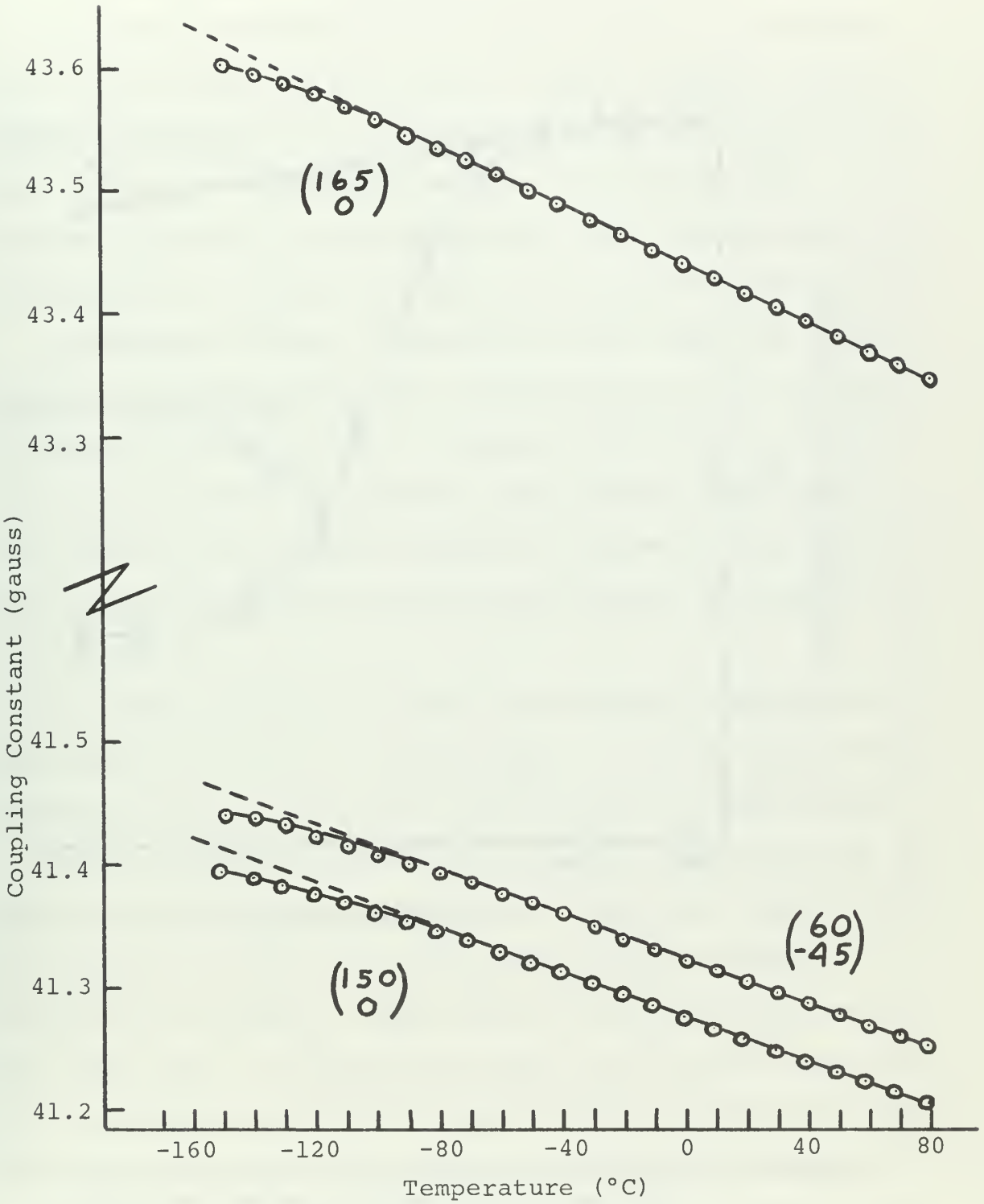

Figure 17. Dependence of coupling constants on temperature due to dipolar and hyperconjugation effects calculated.

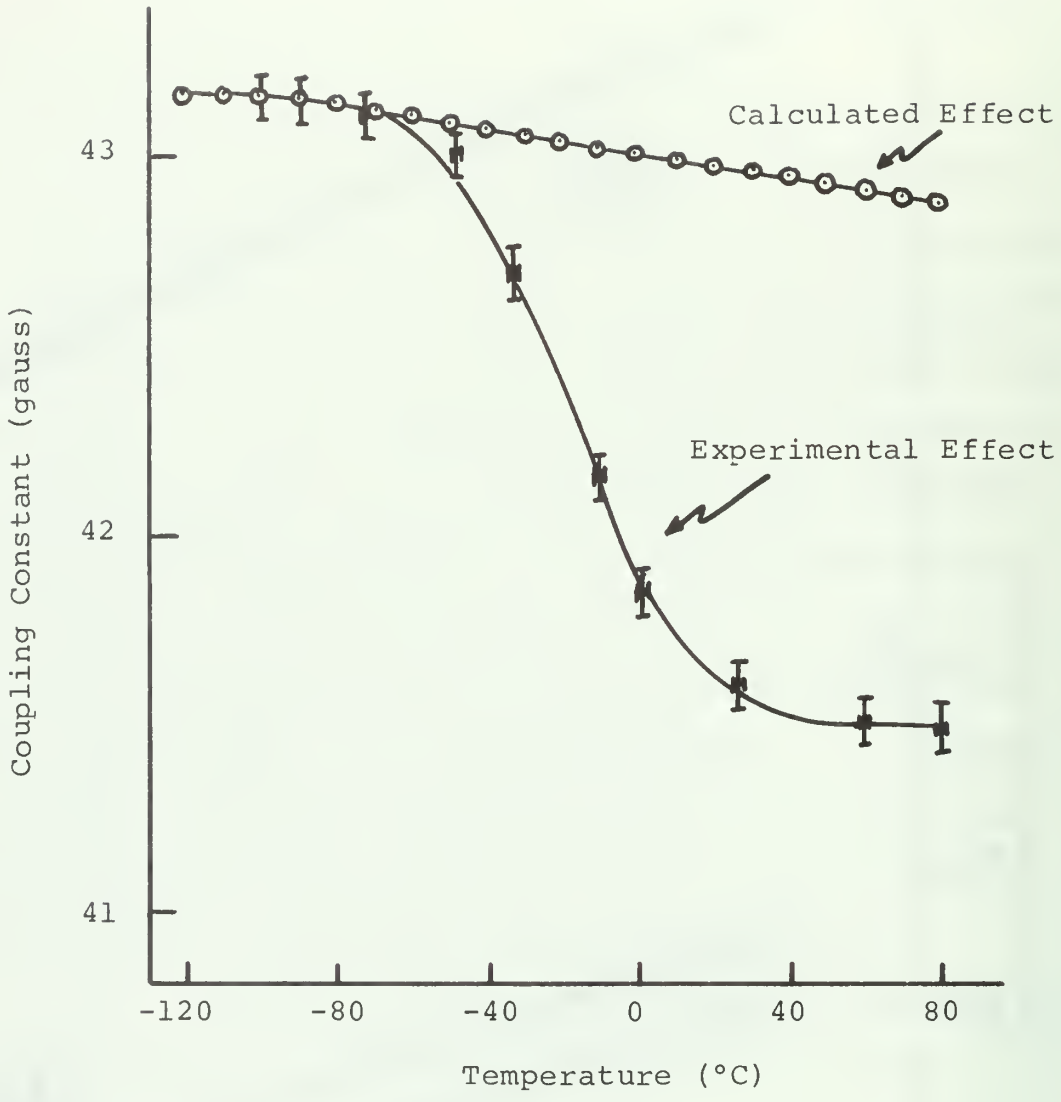

Figure 18. Calculated dependence of coupling constants on temperature due to dipolar and hyperconjugation effects compared to experimentally observed temperature dependence.

E. SHIFT OF COUPLING CONSTANTS DUE TO FLAP MOTION

Out-of-plane flapping motion was discussed in Section III-C and was seen to be a type of hyperconjugation effect leading to Fermi contact interaction as with the rotational model but under a different mathematical relationship. An attempt was made to determine if this type vibration was occurring in the $CH_2CO_2^-$ radical and the magnitude thereof.

A molecular orbital calculation of the same type used for the rotational model [Ref. 19] but with various angles of flap led to the proton 2S orbital spin densities tabulated in Table VIII. In addition, the relative energies of the radical at the various angles of flap were also determined from the molecular orbital calculation and appear in Table VIII.

No simple function relating the coupling constants to angle of flap could be obtained from the data of Table VIII. However, a plot of the energy versus angle of flap as seen in Figure 19 showed a double minimum which indicated that indeed, a flapping vibrational type of motion may exist within the system. The fact that the energy of the radical decreases to a minimum at about ±20° of flap indicated that if flap does exist, then the most stable form of the radical may not be planar as reported by other workers. [Refs. 15 and 21].

A means by which this possibility could be tested would be to lower the temperature of the crystal to liquid helium values in an attempt to freeze out the two stable forms, one with an angle of flap of about + 20° the other of - 20°. An esr spectrum would then be expected to disclose four

TABLE VIII. Results of molecular orbital calculations for flap vibrational motion.

Angle of Flap[1] (degrees)	H_{2s} Spin Density[2] x 10^3	Relative Energy of Radical (aeu)
0	0.000	-52.10978
1	0.004	-52.10980
3	0.049	-52.10990
5	0.090	-52.11006
10	0.182	-52.11058
15	0.181	-52.11097
20	0.133	-52.11110
22	0.118	-52.11106
24	0.096	-52.11097
26	0.071	-52.11081
28	0.054	-52.11059
30	0.040	-52.11030
32	0.030	-52.10994
40	0.003	-52.10773
50	0.001	-52.10301
60	0.002	-52.09578
70	0.000	-52.08570
80	0.020	-52.07244
90	0.129	-52.05565

[1]Negative angles of flap yield nearly identical results.

[2]Values reported to three significant figures.

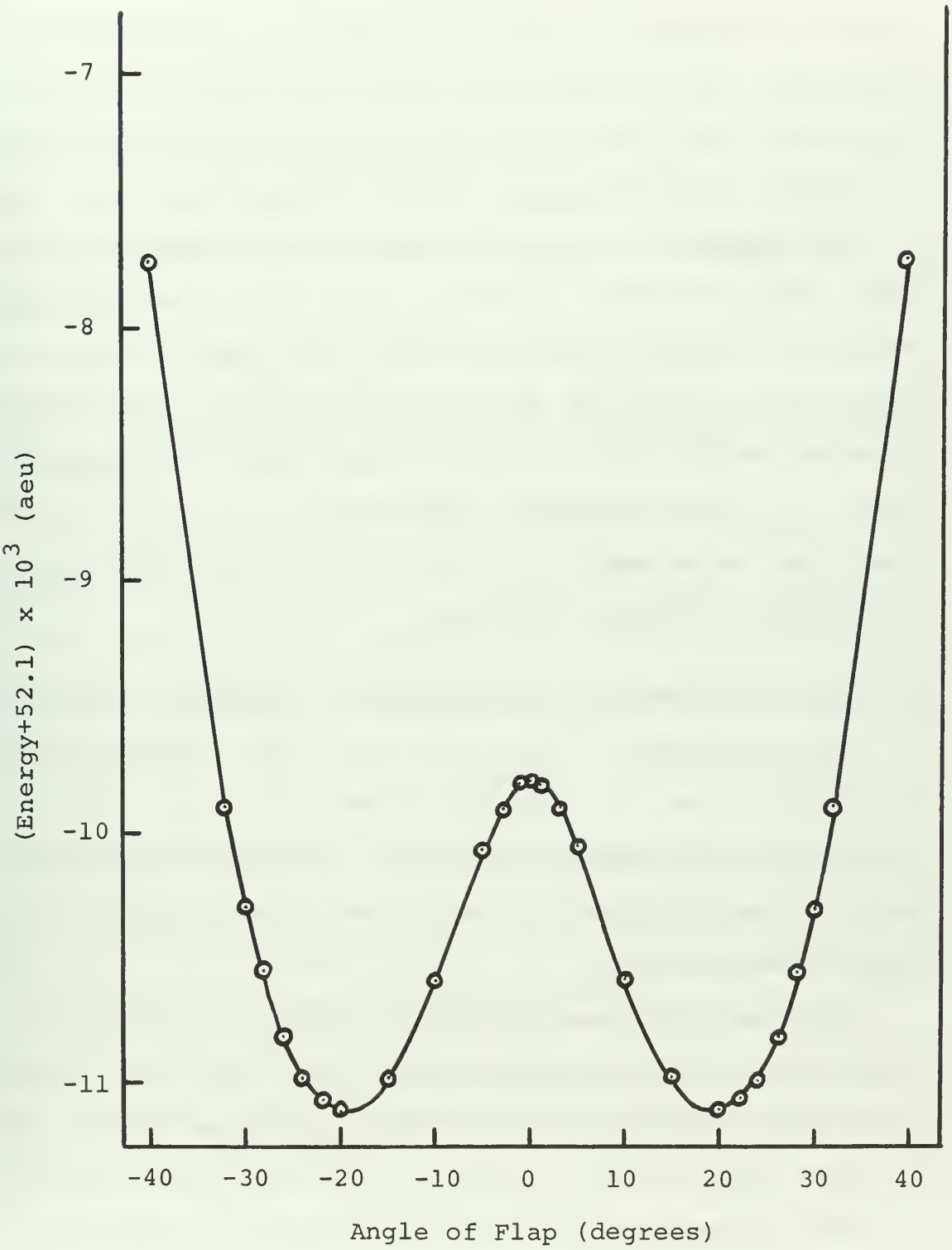

Figure 19. Relative energy of the $CH_2CO_2^-$ radical at configurations caused by CH_2 group out-of-plane flapping motion.

inequivalent sites rather than the two observed at the temperatures studied in this work. If the four sites were to be identified, then raising the temperature through increments would yield data from which, via Arrhenius plots, a barrier to internal flapping motion could be determined.

Flap vibration is not the most likely mechanism to expect. No experimental evidence of the effect was observed over the temperature range of -150°C to +100°C. Based on the more obvious rotational mechanism which can be substantiated by experimental data, it was concluded that if flapping does occur, it is most probably characterized by a very low frequency and large amplitude with insignificant effect upon the system's coupling constants.

F. SHIFT OF COUPLING CONSTANTS DUE TO RELAXATION EFFECTS

The development of the relaxation model and methods of calculation were discussed in Section III-D. It should be noted that the development was based again on the original model of the CH_2 group rotating about the C-C bond of the $CH_2CO_2^-$ radical.

The first step in making the calculation was determination of the limiting conditions and hence the overall shift in coupling constants between these conditions. SSESR with a slight modification was used to calculate the limits.

For a given magnetic field orientation, the relative coupling constants at the low temperature limit (low flip probability) were obtained through solution of Box's [Ref. 2] relation,

$$-|h_{1(+)}| - |h_{2(+)}| + |h_{1(-)}| + |h_{2(-)}|$$

the results of which appear in Table IX column 2.

The high temperature limit was based on the approximation that at high temperature conditions, the rate of flip is so rapid that the effective field experienced by each proton will be an average of the two fields $\vec{h}_1$ and $\vec{h}_2$ as expressed by the relation

$$-|h_{1(+)}+h_{2(+)}| + |h_{1(-)}+h_{2(-)}| \quad .$$

Results from solution of this relation are seen in column 3 of Table IX.

The difference between the two limiting coupling constants yielded the overall shift Δ_c (calculated shift). Since the program calculated the values in units of megahertz it was necessary to divide the resulting overall shift by the conversion factor

2.80 MHz/gauss

in order to compare the results with experimental overall shifts (Δ_e). Column 4 of Table IX shows the final calculated shift and column 5 the overall shift observed experimentally.

The values of Δ_e were plotted versus the values of Δ_c. As seen in Figure 20, the points cluster about a straight line, deviations being assessed to other effects which have not been isolated.

Each point on Figure 20 represents a different magnetic field as tabulated in Table IX. It is of note that approximately ten hours of experimental work and computations were required to establish one point. It was noted, in Section V-A

TABLE IX. Comparison of overall calculated coupling constant shift with experimentally observed shift.

Field Orien.	Low T Limit[1] (MHz)	High T Limit[1] (MHz)	Δ_c (gauss)	Δ_e (gauss)
$\binom{190}{0}$[2]	113.4231	111.3107	0.745	0.40
$\binom{120}{0}$	113.0746	98.9371	5.049	4.25
$\binom{135}{0}$	113.9912	101.2032	4.567	4.48
$\binom{150}{0}$	116.3903	180.6752	2.755	2.90
$\binom{165}{0}$	122.9638	118.3930	1.632	1.60
$\binom{180}{0}$[3]	132.6437	127.5343	1.825	1.86
$\binom{45}{30}$	157.8302	146.4922	4.049	4.61
$\binom{45}{-30}$	127.5728	122.4376	1.834	1.80
$\binom{55.3}{48.2}$[4]	161.8221	149.7523	4.311	3.95
$\binom{55.3}{-48.2}$[4]	118.4243	112.6443	2.064	2.34
$\binom{60}{45}$	161.2777	149.2828	4.284	4.28
$\binom{60}{-45}$	117.4068	110.2377	2.560	2.50
$\binom{90}{45}$	147.5643	138.9060	3.092	3.70
$\binom{90}{-45}$	113.6078	96.3793	6.153	5.69
$\binom{90}{90}$[5]	133.2189	128.0851	1.834	2.70

[1]Calculated limiting conditions

[2]Orientation of magnetic field along the c crystal axis

[3]Orientation of magnetic field along the a* crystal axis

[4]Orientation of magnetic field along the C-C bond

[5]Orientation of magnetic field along the b crystal axis

that experimental plots of coupling constant versus temperature for those cases where $\phi \neq 0$ ($^{\theta}_{\phi}$), showed drift in the coupling constants with lower temperatures after they leveled off at about -60°C. The values of Δ_e used in Table IX and Figure 20 were, for these cases, measured between the high and low leveling off points, and as seen in Figure 20 agree well with the calculated shifts. Initially, the deviations from linearity of Figure 20 were thought perhaps to be due to the drift observed experimentally. However, examination of the data showed no general correlation to confirm this fact.

Based on the linearity of Figure 20 it was felt that the method of calculation for the limiting conditions was representative of the system. Having determined the limiting conditions and hence the overall shift in coupling constants, the calculation of coupling constants for intermediate flip probability (intermediate temperature) was undertaken using the Monte Carlo technique discussed in Section III-D.

The Monte Carlo technique is based upon random statistics, hence the more points on a given curve that are calculated and the more times each point is calculated, the more reliable the final results are expected to be. Numerous calculations of the damped cosine function (Equation III-D4-1, Page 52) approximating the M_x component of magnetic moment and the resulting frequency were made by varying the input parameters of flip probability, d, (from 2 to 100), precession increment, Δ, (from 2 to 10), number of cycles calculated (1 or 2), random number input, and the number of times a particular set of parameters was recalculated (100 to 400 times). The angle α

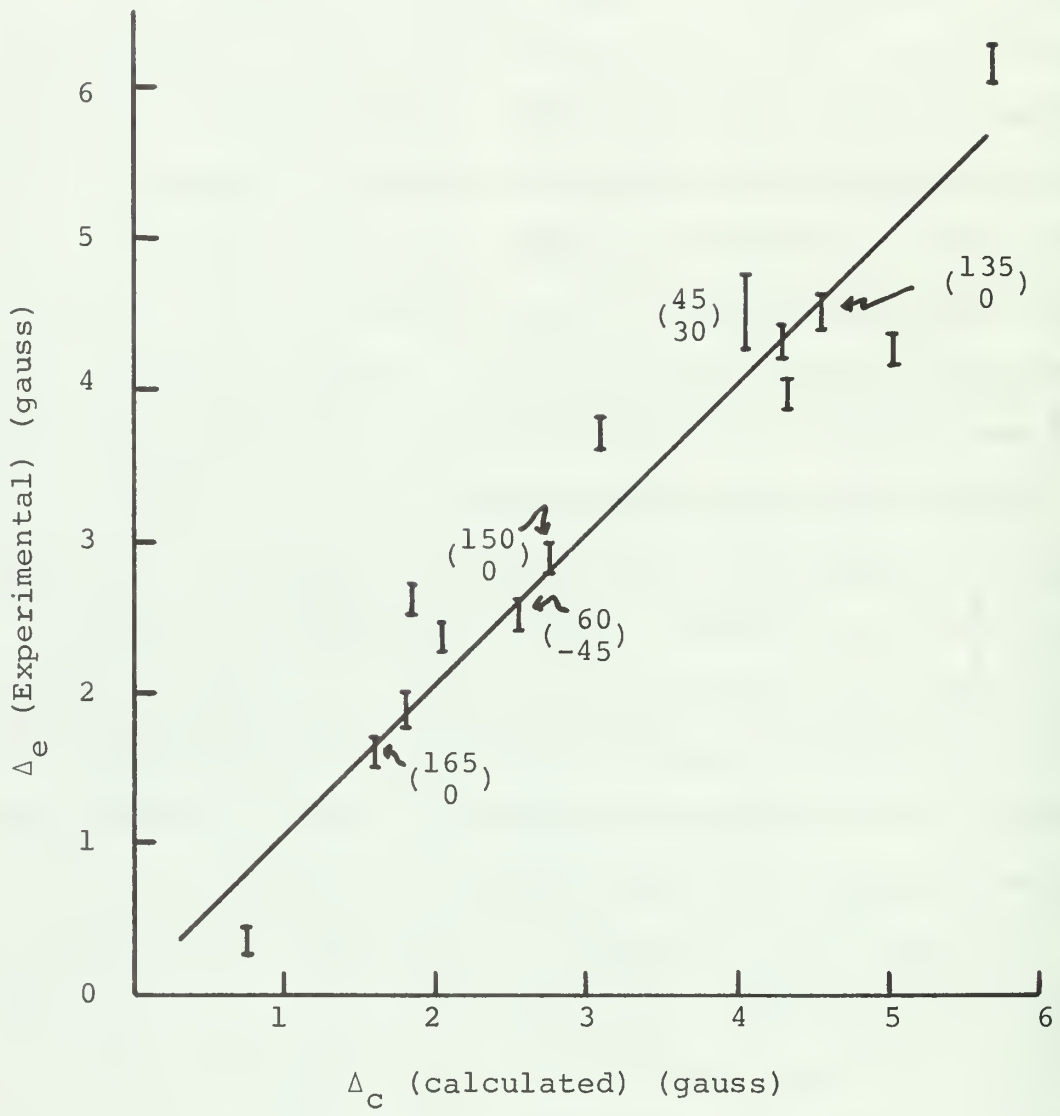

Figure 20. Comparison of total coupling constant shift calculated (Δ_c) with that observed experimentally (Δ_e).

between the Z axis and the effective magnetic field was chosen as 25.84° which permitted frequency to be represented as relative values between 0.90 and 1.00 for a given flip probability. The magnitude of the results were independent of α, but the specific value was chosen for ease in converting the frequency data to increments of overall shift in the coupling constants.

For each value of d and Δ used to determine the best fitting damped cosine function, values of correlation time, τ_c, were calculated by equation III-D6-4 based on a frequency of precession, ν, of one hertz. The values of τ_c calculated thusly were plotted against the frequency of the best fitting damped cosine curve with the results shown in Figure 21. There is a considerable scattering of points in Figure 21 due to the random statistical method of calculation. However, it was not difficult to describe a curve most representative of the greatest majority of points. The "S" shaped curve was noted to be most characteristic of that type function observed experimentally.

For further calculations, only those points lying on or close to the curve described in Figure 21 were used, these conditions being considered as most representative of the relaxation model. Examination of the spectra calculated by PREDICT II for given temperatures and magnetic field orientation showed that the average frequency of precession experienced by the system was about 30.28 MHz. Hence, each

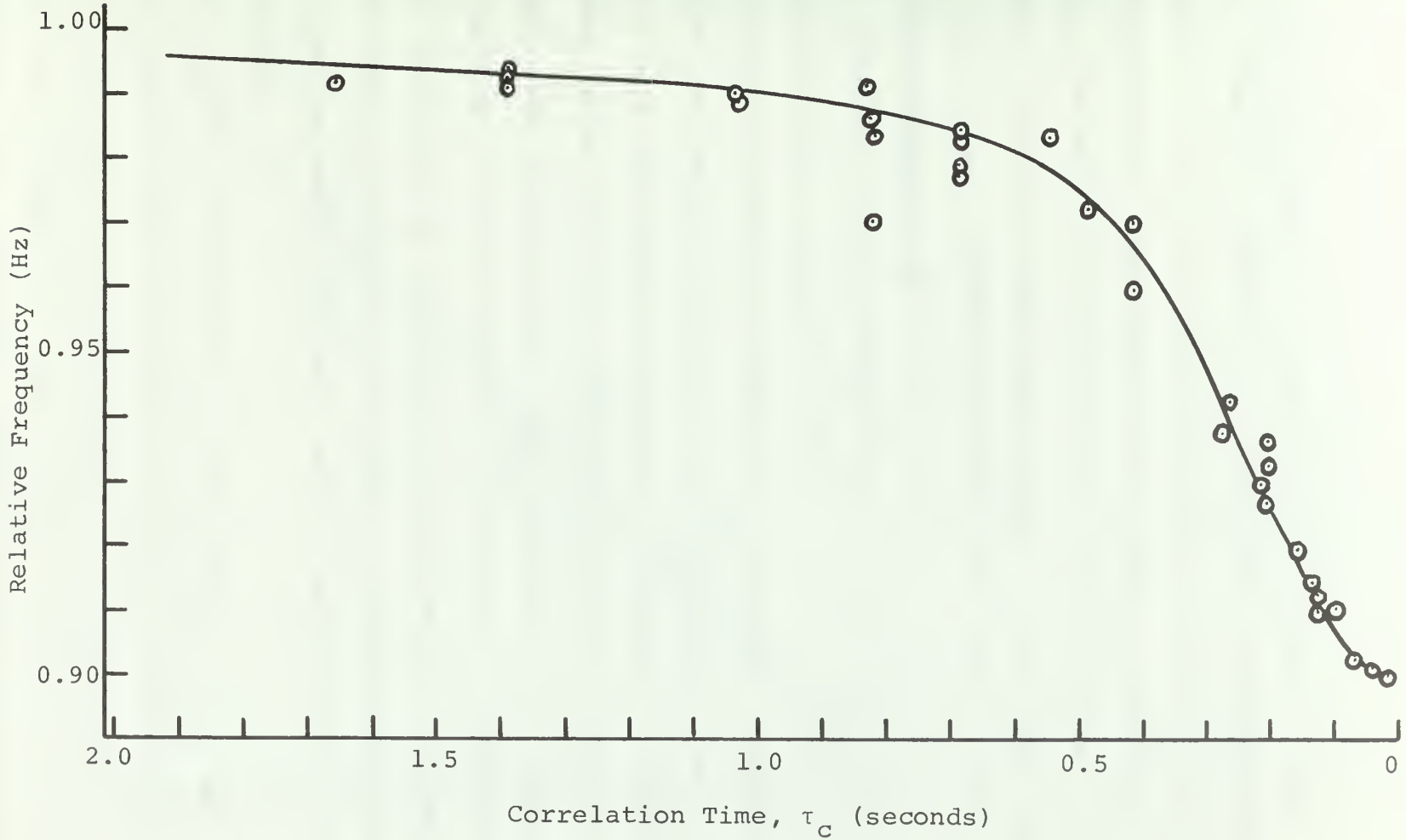

Figure 21. Relative frequency as a function of correlation time based on correlation time calculated on a 1 Hz basis.

correlation time as calculated based on one hertz was adjusted to a τ_{real} consistent with the real system where

$$\tau_{real} = \tau_c/30.28 \times 10^6 \ .$$

Using equation III-D6-5 (Page 57) and τ_{real}, values of temperature were calculated to correspond to the frequency for a given probability d, the results of which are tabulated in Table X.

The plot of relative frequency versus temperature in Figure 22 shows that the "S" shaped function characteristic of the observed experimental function was retained.

The final step was to convert the data of Figure 22 or Table X to coupling constant shift for specific magnetic field orientations. As seen in Figure 22 the frequency was represented as a relative frequency shift between 0.90 and 1.00 where at any given temperature the percentage of total shift between the limiting frequencies and hence coupling constants could be readily determined. For example, at a temperature of 0°C, 43% (0.943) of the total shift in coupling constants is expected to have taken place. Since very good agreement was obtained between the experimental and calculated low temperature limits and overall shift of coupling constants, the percentage shift at a given temperature was applied to observed overall shifts and curves were plotted based on the calculations just discussed, the results being compared with experimental curves as seen in Figures 23a through 23c.

TABLE X. Results of Monte Carlo calculations correlated to temperature.

Probability Factor (d)	Relative Frequency Shift	Temperature (°C)
2	0.9010	+64
2	0.9007	+93
3	0.9021	+44
5	0.9107	+25
6	0.9195	+19
8	0.9327	+10
10	0.9423	+ 4
15	0.9600	- 7
18	0.9725	-12
25	0.9840	-19
30	0.9863	-23
32	0.9352	+ 9
50	0.9794	-19
60	0.9915	-37
75	0.9899	-28
100	0.9914	-34

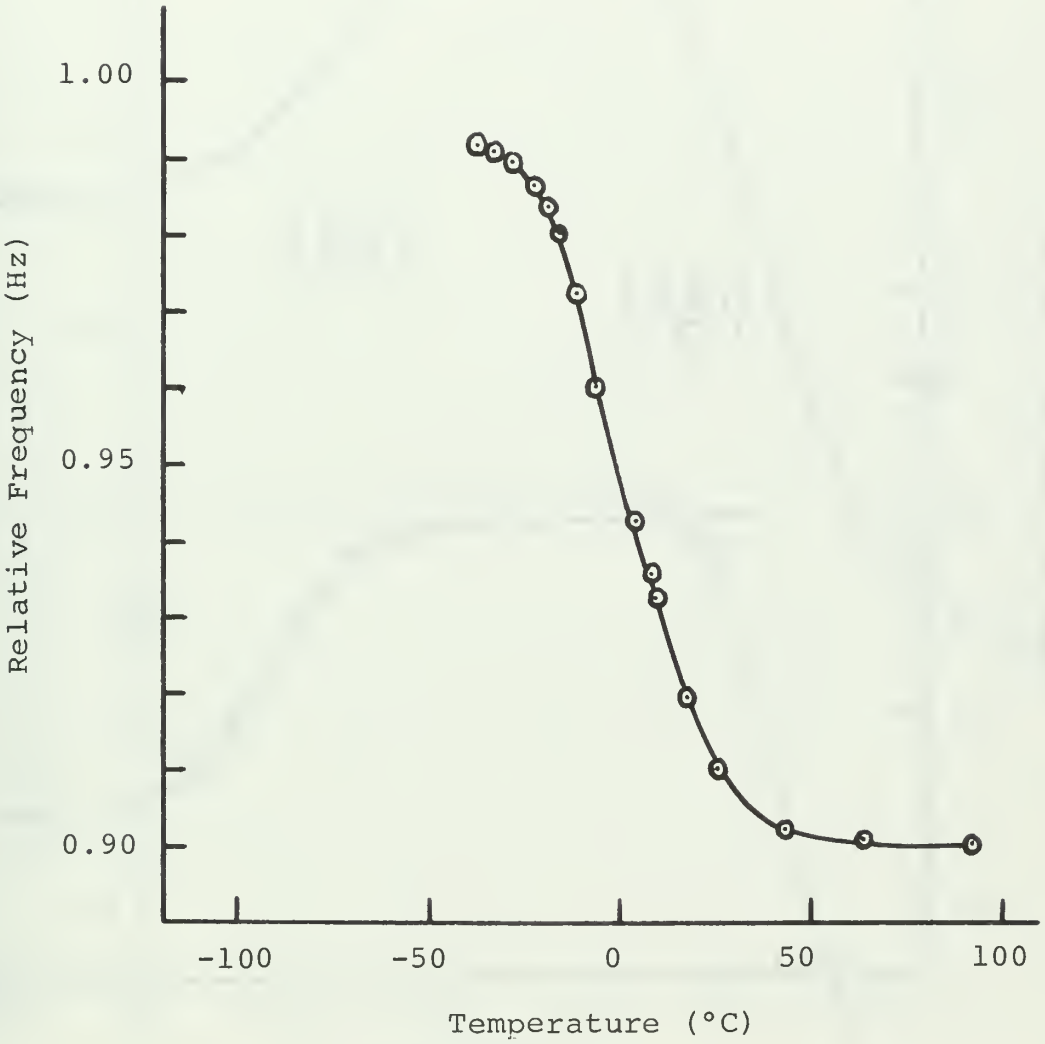

Figure 22. Relative frequency as a function of temperature based on an average precession frequency of 30.28 MHz.

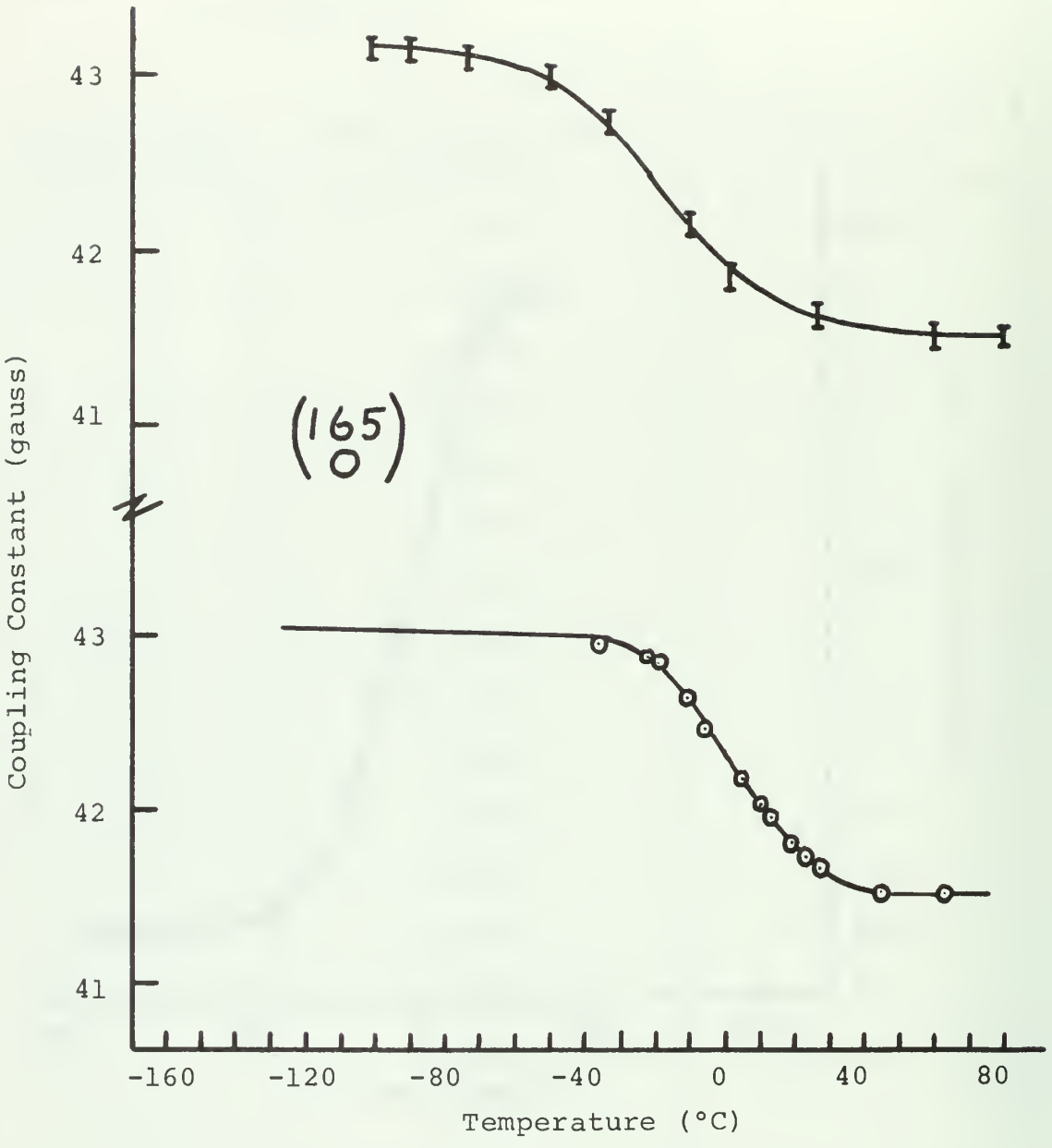

Figure 23a. Comparison of calculated dependence of coupling constants upon temperature due to relaxation effects with experimentally observed dependence for a magnetic field of $\binom{165}{0}$.

I Experimental; ⊙ Calculated.

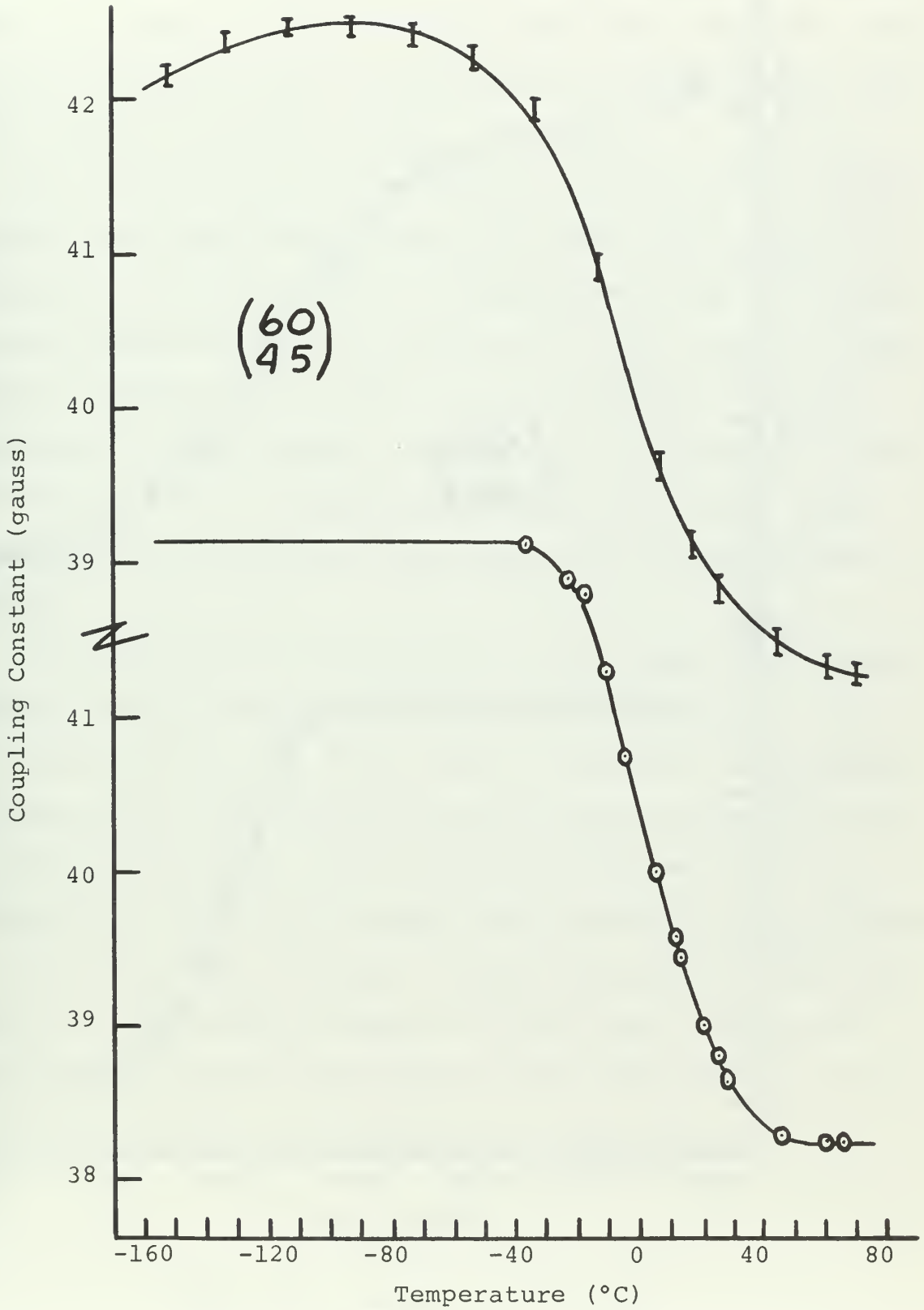

Figure 23b. Magnetic Field $\binom{60}{45}$. I Experiental; ⊙ Calculated

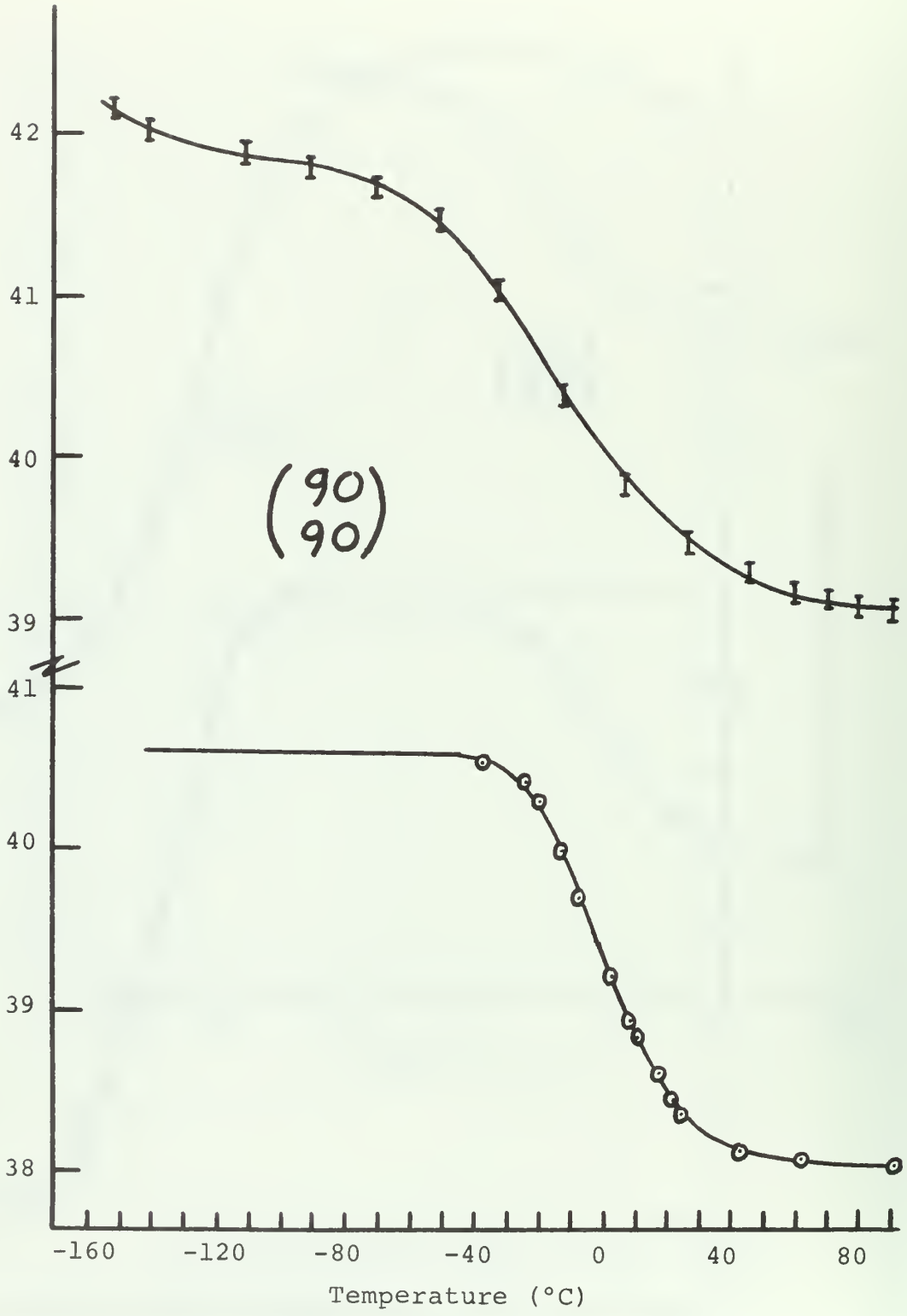

Figure 23c. Magnetic Field $\binom{90}{90}$.
I Experimental; ⊙ Calculated.

Comparison of the calculated and experimental curves was made by noting the temperatures at which the temperature coefficients changed sharply (temperatures where the curves level off) and the inflection points.

The calculated curves followed a function closely approximating the experimental curves, but with a shift upward in temperature of 10°C to 20°C. The position of the calculated curves depended heavily on the value of τ_{real}, shifting downward in temperature for lower values of average frequency experienced by the system. However, this fact was of minimal value in that from calculated spectra results, the average frequency of 30.28 MHz was the proper value to use for the system.

Although the calculated curves did not agree with experimental curves as well as would have been desired, based on the random statistical method used in making the calculation, it was felt that the results obtained were in fact very good in that it was shown that the relation observed could be essentially constructed entirely from theoretical calculations.

Of greatest significance, however, was the fact that the temperature dependence observed in the $CH_2CO_2^-$ radical esr spectrum could now be explained as being due primarily to a relaxation effect as was developed in this work.

VI. CONCLUSIONS

As originally noted by Crawford [Ref. 4] a marked temperature effect upon the esr spectrum of the $CH_2CO_2^-$ radical formed in X-irradiated zinc acetate dihydrate was verified. Decrease in temperature corresponded to increase of coupling constants extracted directly from the spectra of a given magnetic field orientation. The total shift in coupling constants does not spread over the entire temperature range of -150° to +90° studied but was observed to occur between the rather limited range of -60°C to +30°C.

Development of a mathematical model to describe the observed effect led to considerations of several phenomena expected to take place in molecular systems, the results of which indicated that the effect was due to a combination of factors.

Dipolar interaction due to rotation of the CH_2 group about the C-C bond agrees closely with that observed by other workers for a rotating methyl group but does not account for the observed experimental effect. Fermi contact interaction due to hyperconjugation effects in the rotational model shows coupling constant shifts with temperature of the general nature observed experimentally, but again, the magnitude of the effect accounts for only a very small portion of the observed shift.

Flap vibrational motion, although perhaps taking place in the system as indicated by molecular orbital calculations, is

not observed experimentally and is not expected to be a factor of any great importance on the coupling constants.

The primary effect causing the observed temperature dependence is due to a relaxation mechanism within the molecular system. This effect is confirmed experimentally and a model has been developed using random statistical calculations. It is felt at this time, that given an orientation of external magnetic field, and a temperature at which the $CH_2CO_2^-$ radical is stable, the coupling constant can be calculated to within ±1.0 gauss.

The procedures used to study the temperature effect are not restricted solely to the zinc acetate system but could be applied to other systems in which similar relaxation processes are expected to occur.

Although it appears that this work combined with the work of Tolles et.al [Ref. 21] and Ohigashi and Kurita [Ref. 15] nearly exhausts the $CH_2CO_2^-$ radical system, there are yet a few remaining studies which would be worthwhile to undertake. Flapping motion has not been confirmed nor proved to be non-existant. The drift in coupling constants at low temperatures in some orientations of magnetic field has not been explained. Each of these two factors deserves an explanation but of most value to this work as well as to a general contribution to the field of molecular studies would be the development of a rigorous mathematical model by which the coupling constants could be calculated over the entire range of temperature.

This is a challenge yet to be met in the field and it is the hope of this author, that this work may be a major step in that direction.

APPENDIX A

A computer program, PREDICT II, for calculating the average coupling constants of the $CH_2CO_2^-$ radical as a function of temperature. Various combinations of the subroutines may be used to calculate intermediate results as was discussed in the foregoing thesis.

```
C   NN IS THE NUMBER OF SPIN = .5 NUCLEI TO BE INCLUDED IN THE CALCULATION
C   IFRPT IS ZERO FOR INITIAL SET OF DIRECTION COSINES, THEN NOT ZERO FOR EACH
C     REPEATED CALCULATION TO BE DONE BY JUST CHANGING THE DIRECTION COSINES
C     OF THE MAGNETIC FIELD
C   IFNT IS ZERO FOR INITIAL TEMPERATURE, THEN NOT ZERO FOR EACH REPEATED
C     CALCULATION DONE BY CHANGING ONLY TEMPERATURE
C   H IS THE MAGNITUDE OF THE MAGNETIC FIELD, MEASURED IN MEGACYCLES OF THE
C     NUCLEAR ZEEMAN FREQUENCY
C   DCOSB IS THE DIRECTION COSINES MATRIX. ELEMENT I,J,K IS FOR NUCLEUS I
C     RELATING THE J-TH PRINCIPAL AXIS WITH THE K-TH CRYSTAL AXIS BEFORE ROTATION
C   ACOS IS THE NEW DIRECTION COSINES AFTER ROTATION OF HCH ABOUT CC AXIS
C   A(I,J) IS THE J-TH PRINCIPAL VALUE OF THE COUPLING TENSOR FOR ATOM I
C   AA(I,J) IS  A(I,J) AS A FUNCTION OF ANGLE OF ROTATION
C   UH(I) IS THE I-TH COMPONENT OF THE UNIT VECTOR POINTING ALONG THE
C       DIRECTION OF THE MAGNETIC FIELD
C   DE IS THE ARRAY OF TRANSITION FREQUENCIES CALCULATED
C   FINT IS THE CORRESPONDING ARRAY OF INTENSITIES
C   IC IS THE NUMBER OF TRANSITIONS CALCULATED
C   CC(I) IS THE ORIENTATION OF THE C-C BOND AXIS WITH RESPECT TO THE
C     CRYSTAL AXIS
C   ANGLE IS THE ANGLE OF ROTATION OF HCH GROUP ABOUT THE C-C BOND AXIS
C   THETA IS THE ANGLE OF ROTATION OF CRYSTAL ABOUT THE B AXIS
C   PHI IS THE ANGLE OF ROTATION ABOUT THE A* AXIS
C   ROTINC IS HCH ANGLE OF ROTATION ABOUT THE C-C AXIS
C   R2M IS THE MOMENT OF INERTIA
C   BP IS THE BARRIER POTENTIAL
C   AF IS AMPLITUDE FACTOR OF COEFF**2 = AF*SIN**2(2*ANGLE) WHICH
C     REPRESENTS DISTRIBUTION OF FREE ELECTRON IN 2S H ORBITAL AT ANGLE
C   T IS THE TEMPERATURE IN DDEGREES KELVIN
C   EN(I) ARE THE ENERGIES OF TRANSITION, EN(0) BEING TO FIRST EXCITED
C       STATE, EN(1) TO SECOND STATE, ETC.
C   BOT AND TOP ARE LIMITS OF INTEGRATION
C   AAVGT IS THE AVERAGE COUPLING CONSTANT AS FUNCTION OF TEMPERATURE
      IMPLICIT REAL*8(A-H,O-Z)
      DIMENSION DCOSB(10,3,3), A(10,3), UH(3), DE(1000), FINT(1000)
     1,ACOS(10,3,3),CC(3),EN(5),AAVTO1(5),AAVTO2(5),AAVGT1(5)
     2,AAVGT2(5),FAVB(2),AA(10,3)
    1 READ(5,100) NN,IFRPT,H,IFNT
      IF(IFRPT) 2,2,804
    2 IF(IFNT) 5,5,806
    5 IF(NN) 1000,1000,10
   10 DO 15 I = 1,NN
   15 READ(5,101) ((DCOSB(I,J,K), K = 1,3), J = 1,3)
      CALL REFH(DCOSB)
```

```
      DO 16 I = 1,NN
   16 READ(5,102) (A(I,J), J = 1,3)
   45 CALL AXROT(DCOSB,CC)
      READ(5,850) RCTINC
      READ(5,905) R2M,BP
      READ(5,906) (EN(I), I = 1,5)
      READ(5,910) IN,JN,KN,LN
      READ(5,907) BCT,TOP
      READ(5,916) AF
  806 READ(5,908) T
      WRITE(6,915) T
      IF(IENT) 804,804,820
  804 READ(5,902) (THETA,PHI)
      WRITE(6,914) THETA,PHI
  805 CALL HDCOS(THETA,PHI,UH)
      IF(IERPT) 25,25,40
   25 WRITE (6,111) H
      WRITE(6,106)
      DO 31 I = 1,NN
   31 WRITE(6,107) (A(I,J), J = 1,3)
   40 WRITE(6,108) (UH(I), I = 1,3)
  820 DO 41 J = 1,5
      AAVTO1(J) = 0.0
      AAVTO2(J) = 0.0
      AAVGT1(J) = 0.0
   41 AAVGT2(J) = 0.0
  802 ANGLE = BCT
      GO TO 811
  810 ANGLE=ANGLE+RCTINC
  811 CONTINUE
      CALL CCCA(AF,ANGLE,A,AA)
  803 CALL AXR(CC,DCOSB,ANGLE,ACOS)
  830 CALL SSESR(NN,ACOS,AA,UH,H,DE,FINT,IC)
      DO 50 I = 1,IC
   50 DE(I) = DE(I)/2.80246
  890 CALL AVGCC(ANGLE,AAVTO1,AAVTO2,AAVGT1,AAVGT2,ROTINC,DE,IN,JN,
     1KN,LN,R2M,BP)
  831 IF(ANGLE.LT.TOP)GO TO 810
      IF(ANGLE.GE.TOP)GO TO 840
  840 WRITE(6,911) (AAVGT1(J), J = 1,5)
  860 WRITE(6,912) (AAVGT2(J), J = 1,5)
  895 CALL AVBZM(AAVGT1,AAVGT2,EN,T,FAVB)
  870 WRITE(6,913) (FAVB(I), I = 1,2)
      GO TO 1
 1000 STOP
  100 FORMAT (I2,I3,F10.5,I3)
  101 FORMAT (9F7.5)
  102 FORMAT (3F7.3)
```

```
  902 FORMAT (2F9.2)
  901 FORMAT (3F7.4)
  850 FORMAT (F9.2)
  104 FORMAT (1X,//' DIRECTION COSINES'//)
  105 FORMAT (1X,9F12.7)
  106 FORMAT (1X,//' COUPLING CONSTANTS'//)
  107 FORMAT (1X,3F10.5)
  108 FORMAT (1X,/////' DIRECTION COSINES FOR H',//(3F12.7)//)
  109 FORMAT (1X,' TRANSITION FREQUENCIES',/(10F11.5))
  110 FORMAT (1X,' TRANSITION INTENSITIES',/(10F11.5))
  111 FORMAT ((1H1,'NUCLEAR ZEEMAN FREQUENCY = 'F11.5)//)
  112 FORMAT (//' TRANSITIONS, IN GAUSS FROM CENTER, ASSUMING G = 2.0023
     1',/(10F11.5))
  903 FORMAT (1X,' ANGLE OF ROTATION',/(F10.2)//)
  905 FORMAT (2F12.7)
  906 FORMAT (5F12.7)
  907 FORMAT (2F10.5)
  908 FORMAT (F10.3)
  910 FORMAT (4I3)
  911 FORMAT (1X,'AVG COUP CONST(1),EN LEVELS 1-5',/(3D20.9)/)
  912 FORMAT (1X,'AVG COUP CONST(2),EN LEVELS 1-5',/(3D20.9)/)
  913 FORMAT (1X,'AVERAGE COUPLING CONSTANTS',/(D20.9)//)
  914 FORMAT (1X,'THETA AND PHI',/(2F12.7)//)
  915 FORMAT(1X,'TEMPERATURE',/(F12.7)//)
  916 FORMAT (D20.9)
      END



      SUBROUTINE REFH(DCOSB)
C
C   THIS ROUTINE ORTHONORMALIZES THE H TENSORS AND WILL INCLUDE
C     ANY OTHER REFINEMENTS DEEMED NECESSARY
      IMPLICIT REAL*8(A-H,O-Z)
      DIMENSION DCOSB(10,3,3),TERM(3),FN(3)
      DO 5 I = 1,2
      DCOSB(I,3,1)=DCOSB(I,1,2)*DCOSB(I,2,3)-DCOSB(I,1,3)*DCOSB(I,2,2)
      DCOSB(I,3,2)=DCOSB(I,1,3)*DCOSB(I,2,1)-DCOSB(I,1,1)*DCOSB(I,2,3)
      DCOSB(I,3,3)=DCOSB(I,1,1)*DCOSB(I,2,2)-DCOSB(I,1,2)*DCOSB(I,2,1)
      DCOSB(I,1,1)=DCOSB(I,2,2)*DCOSB(I,3,3)-DCOSB(I,2,3)*DCOSB(I,3,2)
      DCOSB(I,1,2)=DCOSB(I,2,3)*DCOSB(I,3,1)-DCOSB(I,2,1)*DCOSB(I,3,3)
    5 DCOSB(I,1,3)=DCOSB(I,2,1)*DCOSB(I,3,2)-DCOSB(I,2,2)*DCOSB(I,3,1)
    1 I = 1
      GO TO 3
    2 I = 2
    3 DO 10 J = 1,3
      TERM(J) = 0.0
```

```
      DO 20 K = 1,3
   20 TERM(J) = TERM(J) + DCOSB(I,J,K)**2
   10 CONTINUE
      DO 30 J = 1,3
   30 FN(J) = DSQRT(1.0/TERM(J))
      DO 40 J = 1,3
      DO 40 K = 1,3
   40 DCOSB(I,J,K) = FN(J)*DCOSB(I,J,K)
   50 WRITE (6,201) ((DCOSB(I,J,K), K = 1,3), J = 1,3)
  201 FORMAT (1X,'NORMALIZED DCOSB',/(3D20.9)//)
      IF(I.GE.2)GO TO 60
      GO TO 2
   60 CONTINUE
      RETURN
      END



      SUBROUTINE HDCOS(THETA,PHI,UH)
C
C  THIS SUBROUTINE COMPUTES THE I-TH COMPONENT OF THE UNIT VECTOR POINTING
C    ALONG THE DIRECTION OF THE MAGNETIC FIELD FOR ANY GIVEN CRYSTAL
C    ORIENTATION OF THETA AND PHI
      IMPLICIT REAL*8(A-H,O-Z)
      DIMENSION UH(3)
      THETA = THETA*3.14159265/180.
      PHI = PHI*3.14159265/180.
      UH(1) = -DCOS(THETA)
      UH(2) = -DSIN(THETA)*DSIN(PHI)
      UH(3) = DSIN(THETA)*DCOS(PHI)
      RETURN
      END



      SUBROUTINE AXROT(DCOSB,CC)
C
C  THIS SUBROUTINE CALCULATES THE DIRECTION COSINES OF THE CC BOND AXIS
C  FN IS A NORMALIZATION FACTOR FOR THE CC(I) VALUES
      IMPLICIT REAL*8(A-H,O-Z)
      DIMENSION DCOSB(10,3,3),CC(3)
      CC(1) = DCOSB(1,1,1) + DCOSB(2,1,1)
      CC(2) = DCOSB(1,1,2) + DCOSB(2,1,2)
      CC(3) = DCOSB(1,1,3) + DCOSB(2,1,3)
      FN = DSQRT(1.0/(CC(1)**2 + CC(2)**2 + CC(3)**2))
      DO 20 I = 1,3
```

```
   20 CC(I) = CC(I)*FN
      RETURN
      END



      SUBROUTINE AXR(CC,DCOSB,ANGLE,ACOS)
C
C   THIS PROGRAM CHANGES THE DIRECTION COSINES FOR EACH TENSOR FOR A CHANGE
C     IN THE ANGLE OF ROTATION OF HCH ABOUT THE C-C BOND AXIS, THE NEW
C     COSINES BEING CALLED ACOS
       IMPLICIT REAL*8(A-H,O-Z)
       DIMENSION CC(3),ACOS(10,3,3),ROTM(3,3),ROTMT(3,3),AR(3,3),S(3,3)
      1,S1(3,3),DCOS1(3,3),DCOS2(3,3),DCOS3(3,3),DCOS4(3,3)
      2,DCOSB(10,3,3)
       E = DSQRT(1.0-CC(3)**2)
       DO 10 I=1,3
       DO 10 J=1,3
   10  ROTM(I,J)=0.0
       ROTM(1,1)=CC(2)/E
       ROTM(1,2)=-CC(1)/E
       ROTM(2,1)=CC(1)*CC(3)/E
       ROTM(2,2)=CC(2)*CC(3)/E
       ROTM(2,3)=-E
       ROTM(3,1)=CC(1)
       ROTM(3,2)=CC(2)
       ROTM(3,3)=CC(3)
       CALL GMTRA(ROTM,ROTMT,3,3)
       ANGN = ANGLE*3.14159265/180.
       F=DCOS(ANGN)
       G=DSIN(ANGN)
       DO 20 I=1,3
       DO 20 J=1,3
   20  AR(I,J)=0.0
       AR(1,1)=F
       AR(1,2)=G
       AR(2,1)=-G
       AR(2,2)=F
       AR(3,3)=1.0
       CALL GMPRD(AR,ROTM,S,3,3,3)
       CALL GMPRD(ROTMT,S,S1,3,3,3)
       I=1
       L=2
       DO 30 J=1,3
       DO 30 K=1,3
       DCOS1(K,J)=DCOSB(I,J,K)
   30  DCOS2(K,J)=DCOSB(L,J,K)
```

```
      CALL GMPRD(S1,DCOS1,DCOS3,3,3,3)
      CALL GMPRD(S1,DCOS2,DCOS4,3,3,3)
      DO 40 J=1,3
      DO 40 K=1,3
      ACOS(I,J,K)=DCOS3(K,J)
   40 ACOS(L,J,K)=DCOS4(K,J)
      RETURN
      END



      SUBROUTINE GMTRA(A,R,N,M)
C
C   THIS PROGRAM TRANSPOSES A GENERAL MATRIX
C
      IMPLICIT REAL*8(A-H,O-Z)
      DIMENSION A(1),R(1)
      IR=0
      DO 10 I=1,N
      IJ=I-N
      DO 10 J=1,M
      IJ=IJ+N
      IR=IR+1
   10 R(IR)=A(IJ)
      RETURN
      END



      SUBROUTINE GMPRD(A,B,R,M,N,L)
C
C   THIS PROGRAM CALCULATES THE PRODUCT OF TWO MATRICES
      IMPLICIT REAL*8(A-H,O-Z)
      DIMENSION A(1),B(1),R(1)
C
      IR=0
      IK=-M
      DO 10 K=1,L
      IK=IK+M
      DO 10 J=1,N
      IR=IR+1
      JI=J-N
      IB=IK
      R(IR)=0.
      DO 10 I=1,M
      JI=JI+N
```

```
      IB=IB+1
   10 R(IR)=R(IR)+A(JI)*B(IB)
      RETURN
      END



      SUBROUTINE SSESR(NN,ACOS,AA,UH,H,DE,FINT,IC)
C
C  VARIABLE DEFINITIONS ARE THE SAME AS IN THE MAIN PROGRAM
C
      IMPLICIT REAL*8(A-H,O-Z)
      DIMENSION ACOS(10,3,3),AA(10,3),UH(3),DE(1000),FINT(1000),
     1HV(10,3),HVP(10,2,3),CE(10),HCOS(10,3),ABH(10,2),S(2),IQ(20)
      S(1) = 1.0
      S(2) = -1.0
      DO 10 I = 1,NN
      DO 10 J = 1,3
      HCOS(I,J) = 0.0
      DO 10 K = 1,3
   10 HCOS(I,J)=HCOS(I,J)+UH(K)*ACOS(I,J,K)
      DO 15 I = 1,NN
      DO 15 J = 1,3
   15 HV(I,J) = 0.0
      DO 20 I = 1,NN
      DO 20 J = 1,3
      CAS=HCOS(I,J)*AA(I,J)
      DO 20 K = 1,3
   20 HV(I,K) = HV(I,K) + CAS*ACOS(I,J,K)
      DO 30 I = 1,NN
      DO 30 J = 1,2
      DO 30 K = 1,3
   30 HVP(I,J,K) = H*UH(K)-0.5*S(J)*HV(I,K)
      DO 40 I = 1,NN
      DO 40 J = 1,2
      ABH(I,J) = 0.0
      DO 35 K = 1,3
   35 ABH(I,J) = ABH(I,J) + HVP(I,J,K)**2
   40 ABH(I,J) = DSQRT(ABH(I,J))
      DO 50 I = 1,NN
      CE(I) = 0.0
      DO 45 J = 1,3
   45 CE(I) = CE(I) + HVP(I,1,J)*HVP(I,2,J)
   50 CE(I) = CE(I)/(ABH(I,1)*ABH(I,2))
      NN2 = 2*NN
      NNTT = 2**(2*NN)
      HNNT = 2**NN
```

```
      DO 55 I = 1,NN2
   55 IQ(I) = 1
      IC = 0
      DO 70 I = 1,NNTT
      IC = IC+1
      DE(IC) = 0.0
      FINT(IC) = 1.0
      DO 60 J = 1,NN
      J1 = IQ(J)
      J2 = IQ(NN+J)
      FINT(IC) = FINT(IC)*(1.0-S(J1)*S(J2)*CE(J))
   60 DE(IC) = DE(IC) + S(J1)*ABH(J,1) + S(J2)*ABH(J,2)
      DE(IC) = 0.5*DE(IC)
      FINT(IC) = FINT(IC)/HNNT
      J = 1
   64 IF(IQ(J)-2) 66,65,66
   65 IQ(J) = 1
      J = J+1
      GO TO 64
   66 IQ(J) = 2
   70 CONTINUE
      RETURN
      END


      SUBROUTINE AVGCC(ANGLE,AAVTC1,AAVTC2,AAVGT1,AAVGT2,ROTINC,DE,
     1IN,JN,KN,LN,R2M,BP)
C
C   BP IS THE BARRIER POTENTIAL
C   R2M IS THE MOMENT OF INERTIA
C   W IS A CONVERSION FACTOR FOR ERGS TO KCAL/MOL
C   X IS A VALUE FOR (PLANCKS CONST)/8*PI**2 IN AMU-AUNITS**2/SEC
C   Y IS PLANCKS CONSTANT IN ERG SEC
C   PROB(I) IS THE NORMALIZED PROBABILITY FUNCTION FOR THE VARIOUS ENERGY
C     LEVELS. PROB(1) IS GROUND STATE. PROB=WAVE FUNCTION SQUARED AND
C     NORMALIZED
C   ACC(I) ARE  COUPLING CONSTANTS DETERMINED FROM RESULTS OF SSESR
C   AAVGT IS THE AVERAGE COUPLING CONSTANT AS FUNCTION OF ANGLE PHI'
      IMPLICIT REAL*8(A-H,O-Z)
      DIMENSION PROB(5),ACC(2),AAVTO1(5),AAVTC2(5),AAVGT1(5),
     1AAVGT2(5),AAVTN1(5),AAVTN2(5),DE(1000),RF(5)
      ANGN = ANGLE*3.14159265/180.0
      ROT = ROTINC*3.14159265/180.0
      W = 6.9446D-14
      X = 5.055D+11
      Y = 6.6250-27
```

```
     1 ZSQD = DSQRT((R2M*BP*W)/(X*Y))*ANGN**2
     2 Z = DSQRT(ZSQD)
       U = DSQRT((R2M*BP*W)/(X*Y))
       V = DSQRT(U)
C   COMPUTE THE NORMALIZATION FACTORS, RF, FOR EACH LEVEL. I=1 REFERS TO
C      GROUND STATE, WHERE THE THEORETICAL VALUE OF N IS ZERO
C   SP IS THE SQUARE ROOT OF 'PI'
       SP = DSQRT(3.14159265D0)
       RF(1) = V*1.0/(1.0*1.0*SP)
       RF(2) = V*1.0/(2.0*1.0*SP)
       RF(3) = V*1.0/(4.0*2.0*SP)
       RF(4) = V*1.0/(8.0*6.0*SP)
       RF(5) = V*1.0/(16.0*24.0*SP)
C   CALCULATE THE NORMALIZED PROBANILITY, PROB(I)  FOR EACH LEVEL.
C      THIS IS WAVE FUNCTION SQUARED X HERMITE POLYNOMIAL SQUARED X RF.
     4 PROB(1) = RF(1)*DEXP(-Z**2)
       PROB(2)=RF(2)*4.*(Z**2)*DEXP(-Z**2)
       PROB(3)=RF(3)*4.*(4.*Z**4-4.*Z**2+1.)*DEXP(-Z**2)
       PROB(4)=RF(4)*16.*(Z**2)*(4.*Z**4-12.*Z**2+9.)*DEXP(-Z**2)
       PPRT=RF(5)*16.*(16.*Z**8-96.*Z**6+168.*Z**4-72.*Z**2+9.)
       PROB(5)=PPRT*DEXP(-Z**2)
C   INCORPORATE COUPLING CONSTANTS FROM DATA OF SSESR SUBROUTINE
C   IN,JN,KN,LN ARE IDENTIFICATION NUMBERS OF TRANSITIONS IN GAUSS
C     FROM CENTER TO BE USED..THOSE WITH SIGNIFICANT INTENSITIES.
       ACC(1) = DE(JN)-DE(LN)
       ACC(2) = DE(KN)-DE(LN)
C   COMPUTE THE SUB AVERAGE VALUE OF COUPLING CONSTANT FOR EACH ENERGY
C     LEVEL,ASSUMING 100 PER CENT POPULATION IN EACH LEVEL
     5 DO 10 J = 1,5
       AAVTN1(J) = PROB(J)*ACC(1)
       AAVGT1(J) = AAVGT1(J) + ((AAVTN1(J)+AAVTO1(J))/2.0)*DROT
    10 AAVTO1(J) = AAVTN1(J)
     6 DO 20 J = 1,5
       AAVTN2(J) = PROB(J)*ACC(2)
       AAVGT2(J) = AAVGT2(J)+((AAVTN2(J)+AAVTO2(J))/2.0)*DROT
    20 AAVTO2(J) = AAVTN2(J)
       RETURN
       END
```

```
      SUBROUTINE AVBZM(AAVGT1,AAVGT2,EN,T,FAVB)
C
C   THIS SUBPROGRAM COMPUTES THE AVERAGE COUPLING CONSTANTS SEEN
C     EXPERIMENTALLY BY INTRODUCING BOLTZMAN STATISTICS TO ENERGY LEVELS
C   T IS THE TEMPERATURE IN DEGREES KELVIN
C   PFCT IS THE PARTITION FUNCTION
C   CT IS THE ENERGY KT IN TERRACYCLES
C   EN(I) ARE THE ENERGIES OF STATES, EN(1) BEING GROUND STATE
C      EN(2) FIRST EXCITED STATE, ETC
       IMPLICIT REAL*8(A-H,O-Z)
       DIMENSION AAVGT1(5),AAVGT2(5),EN(5),FAVB(2)
C   COMPUTE THE PARTITION FUNCTION, PFCT
     1 CT = 0.20753D-01*T
     2 PFCT = 0.0
     3 DO 10 I = 1,5
       TERM = DEXP(-EN(I)/CT)
    10 PFCT = PFCT + TERM
       FAVB(1) = 0.0
       FAVB(2) = 0.0
     4 DO 20 J = 1,5
       FAVB(1) = FAVB(1)+AAVGT1(J)*(DEXP(-EN(J)/CT))/PFCT
    20 FAVB(2) = FAVB(2)+ AAVGT2(J)*(DEXP(-EN(J)/CT))/PFCT
       RETURN
       END



      SUBROUTINE CCCA(AF,ANGLE,A,AA)
C
C   THIS SUBROUTINE COMPUTES THE COUPLING CONSTANTS (PRINCIPAL VALUES OF
C     H TENSORS) AS A FUNCTION OF ANGLE OF ROTATION
       IMPLICIT REAL*8(A-H,O-Z)
       DIMENSION A(10,3),AA(10,3)
       ANGN = ANGLE*3.14159265/180.0
       DO 10 I = 1,2
       DO 20 J = 1,3
    20 AA(I,J)=A(I,J)+1420.4058*AF*(DSIN(2.0*ANGN))**2
    10 CONTINUE
       RETURN
       END
```

A sample of output for PREDICT II

```
NUCLEAR ZEEMAN FREQUENCY = 13.80000


COUPLING CONSTANTS
    -26.80000   -59.59000   -92.15000
    -26.41000   -58.98000   -92.78000


THETA AND PHI
     45.0000000  30.0000000


DIRECTION COSINES FOR H
    -0.7071068  -0.3535534   0.6123724

TEMPERATURE
363.0000000

AVG COUP CONST(1), EN LEVELS 1-5
    0.261480556D  02  0.259451835D  02  0.258136737D  02
    0.257394931D  02  0.257109819D  02
AV COUP CONST(2), EN LEVELS 1-5
    0.298049993D  02  0.294510057D  02  0.291776688D  02
    0.289694564D  02  0.288132342D  02
AVERAGE COUPLING CONSTANTS
    0.260673688D  02

    0.296566194D  02
```

APPENDIX B

A computer program to calculate spin relaxation effects using a Monte Carlo technique.

COMPUTER PROGRAM FOR MONTE CARLO CALCULATION

```
C   NP IS NO OF POINTS CALCULATED
C   NT IS NO OF TIMES EACH POINT IS CALCULATED
C   IX IS RANDOM NUMBER INPUT
C   IP IS PROBABILITY
C   AL DESCRIBES ANGLE ALPHA OF EFFECTIVE FIELD
C   DEL IS INCREMENT OF PRECESSION
C   TH AND PH ARE ANGLES GIVING INITIAL MOMENT POSITION
C
      DIMENSION A(500), IA(500)
      DIMENSION X(3), XP(3), RM(3,3)
    1 READ 100, NP,NT,IX,IP,AL,DEL,TH,PH
  100 FORMAT (2I5,2I10,4F5.2)
      IF(NP) 1000,1000,5
 1000 STOP
    5 CONTINUE
      WRITE(8,103) NP,NT,IX,IP,AL,DEL,TH,PH
      TP = 180.0/3.1415927
      AL = AL/TP
      DEL = DEL/TP
      TH = TH/TP
      PH = PH/TP
      THS = TH
      PHS = PH
      CD = COS(DEL)
      SD = SIN(DEL)
      CA = COS(AL)
      SA = SIN(AL)
      RM(1,1) = CD
      RM(1,2) = -SD*CA
      RM(1,3) = SD*SA
      RM(2,1) = SD*CA
      RM(2,2) = CD*CA**2+SA**2
      RM(2,3) = (-CD+1.0)*SA*CA
      RM(3,1) = -SD*SA
      RM(3,2) = (-CD+1.0)*SA*CA
      RM(3,3) = CD*SA**2+CA**2
      DO 10 I = 1,NP
   10 A(I) = 0.0
      PRINT 102, NP,NT,IX,IP,AL,DEL,TH,PH
  102 FORMAT (1X,2I5,2I10,4F5.2)
  103 FORMAT (//,1X,2I5,2I10,4F5.2)
      DO 51 IC = 1,NT
      X(1) = SIN(THS)*COS(PHS)
      X(2) = SIN(THS)*SIN(PHS)
      X(3) = COS(THS)
      DO 50 JA = 1,NP
      DO 20 I = 1,3
      XP(I) = 0.0
      DO 20 J = 1,3
   20 XP(I) = XP(I)+RM(I,J)*X(J)
      DO 21 I = 1,3
   21 X(I) = XP(I)
      A(JA) = A(JA) + X(1)
      CALL RANDU(IX,IY,RS)
      IYT = 1000*RS
      IX = IY
      IF(IYT-(IYT/IP)*IP) 30,29,30
   29 RM(1,3) = -RM(1,3)
      RM(2,3) = -RM(2,3)
      RM(3,1) = -RM(3,1)
      RM(3,2) = -RM(3,2)
   30 CONTINUE
   50 CONTINUE
   51 CONTINUE
      DO 60 I = 1,NP
   60 A(I) = A(I)/NT
      DO 61 I = 1,NP
   61 IA(I) = A(I)*100
```

```
      WRITE(8,110) (IA(I), I = 1,NP)
  110 FORMAT (1X,36I3)
      CALL DAMP(NP,A,DEL)
      GO TO 1
  120 FORMAT (' FLAG 1')
  121 FORMAT (' FLAG 2')
  122 FORMAT (' FLAG 3')
  123 FORMAT (' FLAG 4')
      END


      SUBROUTINE DAMP(NP,A,DEL)
C
      IMPLICIT REAL*8 (A-H,C-Z)
      REAL*4 A,DEL
      DIMENSION P(10), FINCR(10), R(200), E(200), IR(200)
      DIMENSION PX(200), DA(200), A(200)
  202 FORMAT (' FLAG 0')
  500 FORMAT (I5,5G15.5)
      S = 0.0
      DO 10 I = 1,NP
      S = S+DEL
   10 PX(I) = S
      P(1) = 1.0
      P(2) = 0.0
      FINCR(1) = .0001
      FINCR(2) = .0001
      EPSIL = 1.00D-06
      DO 11 I = 1,NP
   11 DA(I) = A(I)
      CALL LEAST(2,NP,P,PX,PP,PPP,DA,FINCR,EPSIL,NOITR,
     1RRQ,NOF,R,E)
      PRINT 100, NOITR, RRQ
      WRITE(8,100) NOITR,RRQ
  100 FORMAT (I5,G12.5)
      PRINT 101, ((P(I),E(I)), I = 1,2)
      WRITE(8,101) ((P(I),E(I)), I = 1,2)
  101 FORMAT (1X,10G11.4)
      DO 20 I = 1,NP
   20 IR(I) = 1000*R(I)
      WRITE(8,102) (IR(I), I = 1,NP)
  102 FORMAT (30I4)
      RETURN
      END


      SUBROUTINE LEAST(IR,IS,A,X,XB,XC,Z,FINCR,EPSIL,NOITR,
     1RRQ,NOF,R,E)
C
      IMPLICIT REAL*8 (A-H,C-Z)
C IR = NO.OF PARAMETERS, IS = NO. OF POINTS, A IS ARRAY OF
C  PARAMETERS, X IS INDEPENDENT VARIABLE(Z DEPENDENT).FINCR
C  IS ARRAY OF INCREMENT PARAMETERS. EPSIL IS -FRACTIONAL-
C  ERROR CRITERION. NOITR IS NO. OF ITERATIONS REQUIRED (UP
C  TO 10). RRQ IS = SUM OF SQUARES OF RESIDUALS. NOF IS
C  NUMBER OF THE FUNCTION USED IN -EQN-. E IS THE ARRAY OF
C  ESTIMATED ERRORS IN THE PARAMETERS.
C
      DIMENSION A(10), X(200), XB(200), XC(200), Z(200), FIN
     10), D(200,10), DT(10,200), DEL(10), DS(10), DPI(10,10)
     2E(10)
      NOITR = 0
      DO 20 I = 1,IS
   20 R(I) = Z(I) - EQN(A,X(I),XB(I),XC(I),NOF)
   25 IF (NOITR-9) 130,130,4
  130 NOITR = NOITR + 1
      DO 220 J = 1, IR
      A(J) = A(J)+FINCR(J)
      DO 15 I = 1,IS
   15 D(I,J) = EQN(A,X(I),XB(I),XC(I),NOF)
      A(J) = A(J)-FINCR(J)
  220 CONTINUE
```

```
      DO 30 I = 1,IS
      CONST = EQN(A,X(I),XB(I),XC(I),NCF)
      DO 30 J = 1,IR
   30 D(I,J) = (D(I,J)-CONST)/FINCR(J)
      DO 35 I = 1,IS
      DO 35 J = 1,IR
   35 DT(J,I) = D(I,J)
      DO 36 I = 1,IR
      DO 36 J = 1,IR
      DP(I,J) = 0.0
      DO 36 K = 1,IS
   36 DP(I,J) = DP(I,J)+DT(I,K)*D(K,J)
       CALL GAUSS3 (IR,1.0CE-30,DP,DPI,KER)
      IF(KER-1) 120,37,120
   37 DO 40 I = 1,IS
      DO 38 J = 1,IR
      DS(J) = 0.0
      DO 38 K = 1,IR
   38 DS(J) = DS(J)+DPI(J,K)*DT(K,I)
      DO 39 L = 1,IR
   39 DT(L,I) = DS(L)
   40 CONTINUE
      DO 110 I = 1, IR
      DEL(I) = 0.0
      DO 110 J = 1, IS
  110 DEL(I) = DEL(I)+DT(I,J)*R(J)
      DO 10 I = 1,IR
   10 A(I) = A(I)+DEL(I)
      DO320 I = 1,IS
  320 R(I) = Z(I) - EQN(A,X(I),XB(I),XC(I),NCF)
      RRQ = 0.0
      DO 50 I = 1,IS
   50 RRQ = RRQ+R(I)**2
      CRES = DABS(RRQ-RRP) - EPSIL*RRP
      RRP = RRQ
      IF(CRES) 100,100,25
  101 FORMAT (20H CONVERGENCE FAILURE)
    4 PRINT 101
      GO TO 100
  120 PRINT 1001
 1001 FORMAT (16H MATRIX SINGULAR)
  100 FIS1 = IS-IR
      DO 150 I = 1,IR
  150 E(I) = DSQRT(RRQ*DPI(I,I))
      RETURN
      END
C


      SUBROUTINE   GAUSS3(N,EP,A,X,KER)
C
      IMPLICIT REAL*8 (A-H,C-Z)
      DIMENSION A(10,10), X(10,10)
      DO 1 I=1,N
      DO 1 J=1,N
    1 X(I,J)=0.0
      DO 2 K=1,N
    2 X(K,K)=1.0
   10 DO 34 L=1,N
      KP=0
      Z=0.0
      DO 12 K=L,N
      IF(Z-DABS(A(K,L)))11,12,12
   11 Z=DABS(A(K,L))
      KP=K
   12 CONTINUE
      IF(L-KP)13,20,20
   13 DO 14 J=L,N
      Z=A(L,J)
      A(L,J)=A(KP,J)
   14 A(KP,J)=Z
      DO 15 J=1,N
```

```
      Z=X(L,J)
      X(L,J)=X(KP,J)
   15 X(KP,J)=Z
   20 IF(DABS(A(L,L))-EP)50,50,30
   30 IF(L-N)31,34,34
   31 LP1=L+1
      DO 36 K=LP1,N
      IF(A(K,L))32,36,32
   32 RATIO=A(K,L)/A(L,L)
      DO 33 J=LP1,N
   33 A(K,J)=A(K,J)-RATIO*A(L,J)
      DO 35 J=1,N
   35 X(K,J)=X(K,J)-RATIO*X(L,J)
   36 CONTINUE
   34 CONTINUE
   40 DO 43 I=1,N
      II=N+1-I
      DO 43 J=1,N
      S=0.0
      IF(II-N)41,43,43
   41 IIP1=II+1
      DO 42 K=IIP1,N
   42 S=S+A(II,K)*X(K,J)
   43 X(II,J)=(X(II,J)-S)/A(II,II)
      KER=1
      RETURN
   50 KER=2
      RETURN
      END
C
      REAL FUNCTION EQN*8(A,X,XB,XC,NCF)
      IMPLICIT REAL*8 (A-H,C-Z)
      DIMENSION A(10)
      EQN = DEXP(-A(2)*X)*DCOS(A(1)*X)
      RETURN
      END
```

BIBLIOGRAPHY

1. Anderson, P. W., "A Mathematical Model for the Narrowing of Spectral Lines by Exchange or Motion," Journal of the Physical Society of Japan, v.9, p.316-339, May-June 1954.

2. Box, H. C., Freund, H. G., and Budzinski, E. E., "Paramagnetic Absorption of Irradiated Glycine," Journal of the American Chemical Society, v.88, p.658-661, 20 February 1966.

3. Carrington, A., and McLachlan, A. D., Introduction to Magnetic Resonance, p.176-203, Harper and Row, 1967.

4. Crawford, L. P., Electron Paramagnetic Resonance of the $CH_2CO_2^-$ Radical in Irradiated Zinc Acetate, M.S. Thesis, U.S. Naval Postgraduate School, Monterey, California, June 1968.

5. Eisberg, R. M., Fundamentals of Modern Physics, p.256-266, Wiley, 1963.

6. Eyring, H. W. Walter, J., and Kimball, G. E., Quantum Chemistry, p.358-360, Wiley, 1964.

7. Falle, H. R., "Temperature Dependence of the Electron Resonance Spectrum of the Hydrazine Positive Ion," Canadian Journal of Chemistry, v.45 p.1703-1706, 15 May 1968.

8. Griffith, O. H., "Electron Spin Resonance and Molecular Motion of the RCH_2CHOOR' Radicals in X-Irradiated Ester-Urea Inclusion Compounds," The Journal of Chemical Physics, v.41, p. 1093-1105, 15 August 1964.

9. Freed, J. H. and Fraenkel, G. K., "Theory of Linewidths in Electron Spin Resonance Spectra," The Journal of Chemical Physics, v.39, p. 326-348, 15 July 1963.

10. Heller, C. "Electron Spin Resonance and Internal Rotation of the Methyl Group in the $CH_3(COOH)_2$ Radical," The Journal of Chemical Physics, v.36, p. 175-181, 1 January 1962.

11. Heller, C., and McConnell, H. M., "Radiation Damage in Organic Crystals. II Electron Spin Resonance of $(CO_2H)CH_2CH(CO_2H)$ in β-Succinic Acid," The Journal of Chemical Physics, v.32 p. 1535-1539, May 1960.

12. Horsfield, A., Morton, J. R., and Whiffen, D. H., "The Electron Spin Resonance Spectrum of $CH_3CH(CO_2H)$ Between 100°K and 200°K," Molecular Physics, v.5, p. 115-120, 1962.

13. Morton, J. R., "Electron Spin Resonance Spectra of Oriented Radicals," Chemical Reviews, v.453, p. 453-471, August 1964.

14. Moss, R. E., "Vibrational Effects on Electron Resonance Spectra," Molecular Physics, v.10, p. 339-347, 1966.

15. Ohigashi, H. and Kurita, Y., "Electron Spin Resonance of X-Irradiated Single Crystals of Zinc Acetate Dihydrate. Hindered Rotation of Methylene Group in a Free Radical CH_2COO^-," The Bulletin of the Chemical Society of Japan, v. 41, p. 275-284, February 1968.

16. Pople, J. A., Santry, D. P., and Segal, G. A., "Approximate Self-Consistent Molecular Orbital Theory. I. Invariant Procedures," The Journal of Chemical Physics, v. 43, p. S129-S135, 15 November 1965.

17. Schrader, D. M., "Theory of the Temperature Dependences of the Hyperfine Interactions in the Methyl Radical," The Journal of Chemical Physics, v. 46, p. 3895-3904, 15 May 1967.

18. Schrader, D. M. and Karplus, M., "Orbital Following in the Methyl Radical," The Journal of Chemical Physics, v. 40, p. 1593-1601, 15 March 1964.

19. Tolles, W. M., "A Computer Program for Molecular Orbital Calculations Using the CNDO Approximation," Unpublished.

20. Tolles, W. M., "A Computer Program for Spin Relaxation Calculations Using Monte Carlo Techniques," Unpublished.

21. Tolles, W. M., Crawford, L. P., and Valenti, J. L., "EPR Study of Irradiated Zinc Acetate Dihydrate in Crystals," The Journal of Chemical Physics, v. 49, p. 4745-4749, 1 December 1968.

22. Valenti, J. L., Electron Spin Resonance Study of Free Radical Formation in Irradiated Zinc Acetate Dihydrate, M.S. Thesis, U.S. Naval Postgraduate School, Monterey, California, 1967.

23. Zlochower, I. A., Miller, W. R., and Fraenkel, G. L., "Temperature Dependence of Hyperfine Splitting of the Methyl Radical," The Journal of Chemical Physics, v. 42, p. 3339-3340, 1 May 1965.

INITIAL DISTRIBUTION LIST

		No. Copies
1.	Defense Documentation Center Cameron Station Alexandria, Virginia 22314	20
2.	Library, Code 0212 Naval Postgraduate School Monterey, California 93940	2
3.	Defense Atomic Support Agency Department of Defense Washington, D. C. 20305	1
4.	Professor William M. Tolles Department of Material Science and Chemistry Naval Postgraduate School Monterey, California 93940	3
5.	Department of Material Science and Chemistry Naval Postgraduate School Monterey, California 93940	2
6.	Major John W. Hunt, U.S. Army Department of Chemistry United States Military Academy West Point, New York 10996	1
7.	Lt. L. P. Crawford, U.S. Navy USS Springfield (CLG-7) FPO New York, New York 09501	1

DOCUMENT CONTROL DATA - R & D

(Security classification of title, body of abstract and indexing annotation must be entered when the overall report is classified)

1. ORIGINATING ACTIVITY *(Corporate author)*
Naval Postgraduate School
Monterey, California 93940

2a. REPORT SECURITY CLASSIFICATION
Unclassified

2b. GROUP

3. REPORT TITLE
Temperature Dependence of the Electron Spin Resonance Spectrum of the $CH_2CO_2^-$ Radical Formed in X-Irradiated Zinc Acetate Dihydrate

4. DESCRIPTIVE NOTES *(Type of report and, inclusive dates)*
Master's Thesis; (June 1969)

5. AUTHOR(S) *(First name, middle initial, last name)*
John Woodrow Hunt

6. REPORT DATE
June 1969

7a. TOTAL NO. OF PAGES
134

7b. NO. OF REFS
23

8a. CONTRACT OR GRANT NO.

b. PROJECT NO.

c.

d.

9a. ORIGINATOR'S REPORT NUMBER(S)

9b. OTHER REPORT NO(S) *(Any other numbers that may be assigned this report)*

10. DISTRIBUTION STATEMENT
Distribution of this document is unlimited.

11. SUPPLEMENTARY NOTES

12. SPONSORING MILITARY ACTIVITY
Naval Postgraduate School
Monterey, California 93940

13. ABSTRACT

A decrease of one to six gauss (depending on magnetic field orientation) in the coupling constants of the $CH_2CO_2^-$ radical formed in X-irradiated zinc acetate dihydrate has been observed over a temperature range of about -60°C to +30°C. Calculations of dipolar and Fermi contact interaction based on a model of internal rotation of the methylene group about the C-C bond have shown a small coupling constant decrease on the order of 0.19 gauss over a temperature range of -150°C to +90°C. The major effect has been shown to be due to a spin relaxation mechanism. The effect was calculated using Monte Carlo techniques, the results of which were confirmed by experimental data.

14 KEY WORDS	LINK A		LINK B		LINK C	
	ROLE	WT	ROLE	WT	ROLE	WT
Electron spin resonance						
Zinc acetate dihydrate						
Coupling constants						
Temperature effect						
Fermi contact interaction						
Hyperconjugation						
Dipolar interaction						
Spin relaxation						
Monte Carlo calculation						
Magnetic field						

Gaylord
SHELF BINDER
Syracuse, N. Y.
Stockton, Calif.

thesH945
Temperature dependence of the electron s
3 2768 002 13268 0
DUDLEY KNOX LIBRARY